

Biophysical Characterisation of Polymer-Bounded Nanodiscs as *In Vitro* Tools for Membrane-Protein Research

vom Fachbereich Biologie der Technischen Universität Kaiserslautern

zur Verleihung des akademischen Grades

Doktor der Naturwissenschaften

(Doctor rerum naturalium)

– genehmigte Dissertation –

von

Frau Dipl.-Biophys. Anne Grethen

geboren am 23.12.1989 in Luxemburg

Erstgutachter: Prof. Dr. Sandro Keller

Zweitgutachter: Prof. Dr. Martin van der Laan

Drittgutachterin: Prof. Dr. Nicole Frankenberg-Dinkel

Vorsitzender: Prof. Dr. Stefan Kins

Wissenschaftliche Aussprache: 22. April 2021

Index

Abstract	3
List of included publications.....	5
1. Introduction	7
1.1. The biological membrane.....	7
1.2. The challenge of studying membrane proteins	8
1.3. An overview of membrane-mimetic systems	8
1.4. Polymer-bounded nanodiscs	11
1.5. Objectives.....	17
2. Biophysical characterisation of SMA(2:1) nanodiscs	18
2.1. Manuscript 1	20
2.2. Associated results:	36
The composition of SMA(2:1) nanodiscs.....	36
2.2.1. Experimental section	36
2.2.2. The SMA(2:1) nanodisc elution profile.....	36
2.2.3. pH-dependent SMA(2:1) nanodisc composition	38
3. Lipid transfer behaviour and effective charge of SMA(2:1) nanodiscs	42
3.1. Manuscript 2	44
3.2. Associated results:	54
Effective SMA(2:1) nanodisc charge numbers by ζ -potentials.....	54
3.2.1. Experimental section	54
3.2.2. Theoretical background.....	54
3.2.3. Results.....	57
4. Electroneutral polymers for membrane-protein research.....	60
4.1. Manuscript 3	62
5. Discussion.....	98
5.1. Paving the way of polymer nanodiscs for membrane-protein applications.....	98
5.2. Polymer concentration determination by refractometry and UV absorption	98
5.3. The equilibrium solubilisation efficiency of amphiphilic copolymers	99
A comparison of solubilisation efficiencies at similar conditions.....	99
Effects of solvent properties on solubilisation efficiency.....	100
Effects of membrane properties on solubilisation efficiency.....	102
5.4. The nanodisc size	103

5.5. The nanodisc charge	104
5.6. The colloidal stability of polymer nanodiscs.....	106
5.7. The lipid transfer among polymer nanodiscs.....	108
5.8. The nanodisc lipid-bilayer architecture	109
5.9. “Free” or excess polymer after nanodisc formation.....	110
5.10. Membrane protein solubilisation and stabilisation in polymer nanodiscs.....	111
5.11. Future directions	113
6. Conclusions	115
References.....	117
Abbreviations and Variables	125
Acknowledgements	127
Curriculum Vitae.....	129
List of Publications.....	131
Zusammenfassung.....	132
Eidesstattliche Erklärung.....	133

Abstract

To render membrane proteins amenable to *in vitro* functional and structural studies, they need to be extracted from cellular membranes and stabilised using membrane-mimetic systems. Amphiphilic copolymers gain considerable interest, because they are able to co-extract membrane proteins and their surrounding lipids from complex cellular membranes to form polymer-bounded nanodiscs. The latter harbour a native-like lipid-bilayer core stabilised by a copolymer rim. Accordingly, these membrane mimics are supposed to provide superior stability to embedded membrane proteins as compared with conventional detergent micelles.

Herein, the formation of nanodiscs by the most commonly used styrene/maleic acid (SMA) copolymer, termed SMA(2:1), was elucidated in detail. To this end, the equilibrium solubilisation efficiencies towards model and cellular membranes were quantified and compared with those of the more hydrophobic SMA(3:1) and the more hydrophilic diisobutylene/maleic acid (DIBMA) copolymers. It was shown that, from a thermodynamic viewpoint, SMA(2:1) is the most efficient membrane solubiliser in terms of lipid- and protein-extraction yields. Solvent properties (pH, ionic strength) or membrane characteristics (lateral pressure, charge, or thickness) can affect the polymers' solubilisation efficiency to a certain extent. In addition, the lipid transfer behaviour of SMA(2:1) nanodiscs was studied. Notwithstanding their high effective negative charge, SMA(2:1) nanodiscs exchange phospholipids more rapidly among each other than vesicles or protein-bounded nanodiscs, thus rendering them highly dynamic nano-assemblies.

Two alternative electroneutral polymers, namely SMA(2:1)-SB and DIBMA-SB, were introduced in this thesis. They were generated by polymer backbone modifications of SMA(2:1) and DIBMA, respectively. The derivatised polymers were shown to quantitatively solubilise model and biological membranes and, like DIBMA, only had a mild effect on lipid-bilayer integrity. Along these lines, DIBMA-SB preserved membrane-protein complexes of distinct structural classes and extracted them from various cellular membranes. Importantly, the electroneutral polymers were amenable to protein/lipid interaction studies otherwise masked by unspecific interactions of their anionic counterparts with target lipids or proteins. Taken together, the in-depth characterisation of nanodiscs formed by anionic and electroneutral polymers allows for adjusting the nanodisc properties to specifically suit experimental requirements or address membrane-protein research questions.

List of included publications

Manuscript 1

Thermodynamics of nanodisc formation mediated by styrene/maleic acid (2:1) copolymer

Anne Grethen, Abraham Olusegun Oluwole, Bartholomäus Danielczak, Carolyn Vargas, and Sandro Keller

Sci Rep, **2017**, 7, 11517

Manuscript 2

Role of Coulombic repulsion in collisional lipid transfer among SMA(2:1)-bounded nanodiscs

Anne Grethen, David Glueck, and Sandro Keller

J Membr Biol, **2018**, 251, 443

Manuscript 3

Neutral amphiphilic copolymers forming lipid-bilayer nanodiscs for investigating membrane proteins

Anne Grethen,* David Glueck,* Manabendra Das,* Ogochukwu Patricia Mmeka, Eugenio Pérez Patallo, Annette Meister, Ritu Rajender, Jana Strate, Stefan Kins, Markus Räschle, Julian Victor, Manuel Etzkorn, Zoe Köck, Frank Bernhard, Jonathan Oyebamiji Babalola, Carolyn Vargas, and Sandro Keller

2021, in preparation

*shared first authorship

1. Introduction

1.1. The biological membrane

The biological membrane is the natural barrier of cells and organelles, forming discrete compartments to prevent random mixing of their content.^{1,2} It is composed of a complex mixture of lipids and membrane proteins. The dominant lipid class are phospholipids, carrying a phosphorylated hydrophilic head group and two hydrophobic acyl chains. Driven mainly by the hydrophobic effect, these amphiphilic molecules spontaneously form separated phases in aqueous solutions in the form of lipid bilayers.³ In general, the protein and lipid composition varies among different species and cellular membranes, affecting the chemical and physical properties and, thus, rendering biological membranes highly heterogeneous.^{4,5}

Furthermore, biological membranes are particularly dynamic structures. The membrane fluidity typically increases from the interface to the hydrophobic core, because the bulky lipid head groups are more densely packed than the acyl chains, enabling conformational changes within the acyl-chain region.⁶ Lipids and many membrane proteins are additionally able to rapidly diffuse in the translational direction within one leaflet. This is because, under physiological conditions, the natural lipid bilayer generally exists in a liquid-crystalline phase rather than a solid, so-called “gel” phase in which the lipid motility is constrained. The transport of membrane components from one leaflet to another, called “flip-flop”, is however energetically unfavourable and only possible under slow kinetics with the aid of transfer proteins.⁷

Membrane proteins fulfil various vital functions such as the regulatory transport of metabolites and nutrients among different cellular compartments, enzymatic reactions, signal transduction within the cell, cell–cell signalling, or cell motility.⁸ They can be classified in two broad categories, integral and peripheral membrane proteins. The latter interact with lipid head groups by their lipid-binding domains,⁹ whereas integral membrane proteins are partly or completely embedded in the phospholipid bilayer.¹⁰ The hydrophobic effect forces these integral membrane proteins to expose their hydrophobic residues to the lipid acyl chain core, whereas polar residues are localised outside the membrane and are in contact with the aqueous environment. The organisation of proteins and lipids within cellular membranes is governed by the interaction potential among these constituents. Specific protein–lipid

interactions have been shown to be essential for the proper function of certain integral membrane proteins such as voltage-gated ion channels^{11,12} or G-protein coupled receptors (GPCRs).¹³

1.2. The challenge of studying membrane proteins

Given their key functions as transporters and signal transducers, many diseases are directly linked to membrane proteins and, thus, they represent more than 50% of all drug targets.¹⁴ Notwithstanding the biological and pharmacological significance of membrane proteins, structural and functional studies are still immensely lagging behind in comparison with soluble proteins: Currently, >1100 membrane protein structures are available, making up ~3% of >35'000 total protein structures known thus far (<https://blanco.biomol.uci.edu/mpstruc/>).

In order to study specific membrane proteins, they need to be extracted from their complex biological membranes and subsequently isolated from other proteins. However, due to their hydrophobic surface residues, they typically lose their stability and are prone to aggregation in aqueous environments.¹⁵ To overcome the water insolubility of these membrane proteins, membrane-mimetic systems are required to imitate the stabilising lipid-bilayer environment of the parent membrane.

1.3. An overview of membrane-mimetic systems

This chapter provides a summary of common membrane mimics such as conventional detergent micelles, liposomes, bicelles, amphipols, and protein-bounded nanodiscs.

Conventional detergent micelles

Conventional head-and-tail detergents are a class of amphiphilic surface-active agents, so-called surfactants, with a hydrophilic head group and typically one hydrophobic hydrocarbon chain. Due to their conical shape, they generally aggregate into spherical detergent micelles in aqueous environments (Figure 1.1.a). These molecules are able to disrupt the membrane lipid-bilayer, and, thus, extract and solubilise membrane proteins providing a stabilising hydrophobic environment. Because of their small size and unimodal distribution, these protein/detergent complexes enable spectroscopic studies on the target protein. The stability of these complexes is governed by cohesion interactions among detergent molecules and detergent–protein interactions.¹⁶ However, they lack key bilayer properties such as typical membrane thickness and, thus, only partially mimic the lipid-bilayer environment, often

leading to membrane protein aggregation and denaturation.¹⁷ Moreover, even if the extracted proteins remain folded, some still lose their functionality due to the disruption of native protein-lipid interactions. A milder, less destructive alternative to conventional head-and-tail detergents are fluorinated surfactants that carry a perfluorinated alkyl chain instead of a fully hydrogenated chain.^{18,19}

Liposomes

Liposomes or vesicles are spherical lipid-bilayer structures generally formed by synthetic phospholipids, thus representing a simplified *in vitro* model membrane. In aqueous environments, phospholipids spontaneously form multilamellar vesicles (MLVs) of various sizes. A narrow size distribution of unilamellar vesicles (Figure 1.1.b) is however often required, which is obtained by extrusion through polycarbonate filters of specific size²⁰ or sonication.²¹ Because of the above-mentioned poor membrane-mimic characteristics of detergent micelles, detergent-purified proteins are often reconstituted in vesicles, thus forming proteoliposomes that are amenable to downstream biophysical or functional studies.²² Spectroscopic techniques using proteoliposomes are, however, often impeded by their fairly large size of 50–400 nm.

Bicelles

Bilayered micelles, termed bicelles (Figure 1.1.c), spontaneously form upon mixture of certain detergents or lipids such as 1,2-dihexanoyl-*sn*-glycero-3-phosphocholine (DHPC) and short-chain lipids such as 1,2-dimyristoyl-*sn*-glycero-3-phosphocholine (DMPC). They bridge the gap between pure detergent micelles and phospholipid bilayers by maintaining key bilayer properties in the form of small monodisperse particles amenable to spectroscopic techniques. They consist of a detergent-rich rim and a lipid-rich bilayer core, thus conserving a bilayer environment in close vicinity to the membrane protein.²³ However, these systems are only stable under specific experimental conditions such as well-defined detergent/lipid ratios, specific temperatures, and pH values, which challenges various purification steps such as size exclusion or affinity chromatography.

Amphipols

Amphipols are short-chained amphipathic polymers that carry hydrophobic and hydrophilic groups. Generally, detergent-solubilised proteins are supplemented with amphipols to form

detergent/amphipol/protein complexes.²⁴ After removal of detergents, amphipols directly interact with hydrophobic protein transmembrane domains and, thus, can act as a membrane protein stabiliser after extraction and purification for downstream analysis.²⁵

Protein-bounded nanodiscs

Amphipathic α -helical proteins synthesised from human apolipoprotein, so-called membrane-scaffold proteins (MSPs), form protein-bounded or, more specifically, MSP nanodiscs (Figure 1.1.d).²⁶ Typically, two MSPs form a belt by wrapping around a phospholipid bilayer, each stabilising one of the hydrophobic cores of each bilayer leaflet.²⁷ These MSP nanodiscs have a unimodal size distribution of 10–20 nm. They proved effective for the study of various membrane proteins such as G-protein-coupled receptors²⁸ or the protein translocon complex SecYEG.²⁹ One specific disadvantage of protein-bounded nanodiscs is that the UV detection of encapsulated target proteins is impeded by the absorbance of MSPs in the same UV range.

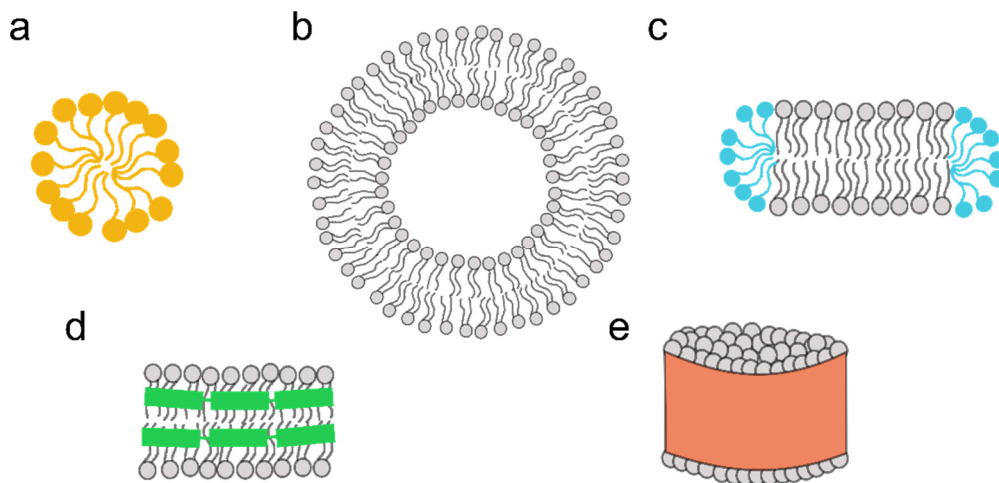


Figure 1.1. Common membrane-mimetic systems used in membrane-protein research. a) Conventional detergent micelles. b) Phospholipid liposomes or vesicles. c) Bicelles with a lipid-rich core and a detergent-rich rim. d) Protein-bounded nanodiscs. e) Polymer-bounded nanodiscs.

The above-mentioned membrane-mimetic systems have a predominant drawback in common: they all crucially depend on conventional head-and-tail detergents to disrupt the biological membrane for the initial extraction of membrane proteins. This often leads to an irreversible protein structure and function loss prior reconstitution into artificial bilayer mimics such as vesicles, bicelles, or protein-bounded nanodiscs. In the next chapter, polymer-bounded nanodiscs (Figure 1.1.e) are introduced as a promising alternative surfactant system that overcomes this bottleneck.

1.4. Polymer-bounded nanodiscs

Amphiphilic copolymers are typically composed of at least two distinct monomeric subunits that carry hydrophobic and hydrophilic groups. Originally used in engineering plastic applications such as the automotive industry, commercially available styrene/maleic acid (SMA)^{30,31} and diisobutylene/maleic acid (DIBMA)³² copolymers are the most prominent representatives at present. They are gaining increasing attention, because they are able to co-extract membrane proteins and annular lipids from model and cellular membranes into nanoscopic, near native-like, and disc-shaped particles.³³ Independent of conventional detergents, they mildly insert into lipid bilayers to form nanodiscs that retain the bilayer architecture of the parent membrane and are stabilised by a copolymer rim.³⁴ They can thus be termed polymer-bounded nanodiscs, lipodisc particles,³⁵ native nanodiscs,^{36,37} or, more specifically, SMA lipid particles (SMALPs)³¹ and DIBMA lipid particles (DIBMALPs)³² (Figure 1.2).

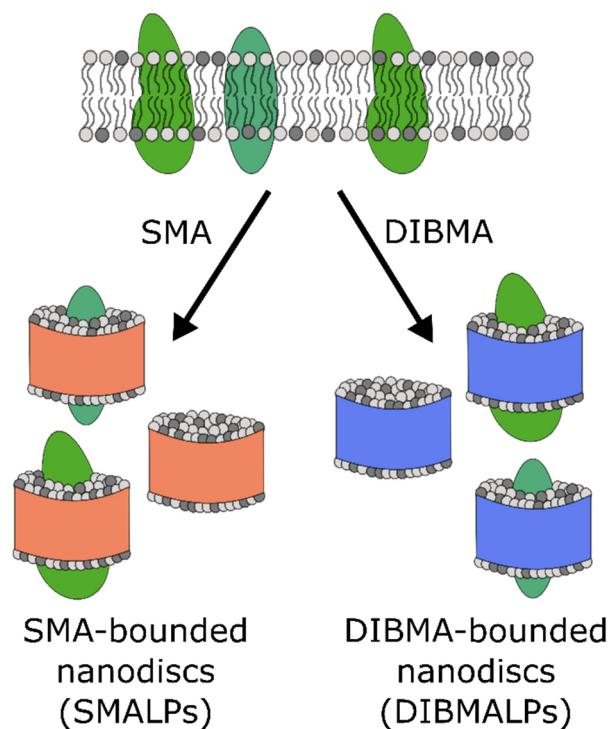


Figure 1.2. Membrane solubilisation as mediated by styrene/maleic acid (SMA) and diisobutylene/maleic acid (DIBMA) copolymers. Both copolymers extract membrane proteins and surrounding lipids directly from their complex cellular membranes to form near-native polymer-bounded nanodiscs or SMALPs/DIBMALPs.

Styrene/maleic acid (SMA) copolymers

SMA carries randomly distributed hydrophobic styrene (S) and hydrophilic maleic acid (MA) moieties, hence defined as a random copolymer (Figure 1.3).³⁸ It is available in different average S/MA molar ratios varying from 1:1 to 4:1, displaying increasing hydrophobicities with elevated styrene content.³⁹ The polymers' hydrophobicity is a crucial property that influences its solubilisation efficiency towards lipid bilayers.³⁰ SMA(2:1) and SMA(3:1) are the variants that have proven capable of membrane solubilisation at near-physiological conditions, thus exhibiting hydrophobicities that enable lipid-bilayer insertion and nanodisc stabilisation.³⁹

The nanodisc formation was first described by a model suggesting that the membrane insertion of SMA is driven by the hydrophobic effect.⁴⁰ Theoretical predictions and experimental data support this model by showing the binding of SMA to the lipid bilayer interface, intercalation of the styrene moieties in the hydrophobic core, the formation of transmembrane pores leading to membrane disruption, and, finally, nanodisc assembly.^{41,42} Using dynamic light scattering (DLS) and ³¹P nuclear magnetic resonance (NMR) spectroscopy, the membrane partitioning and solubilisation efficiency of the polymers can be studied from a thermodynamic viewpoint.⁴³ In accordance with lipid/detergent mixtures, the membrane equilibrium solubilisation by SMA and related polymers follows a three-stage solubilisation scenario that quantifies the minimum polymer concentration required for complete solubilisation.^{44,45} Above this so-called solubilisation threshold, the diameter of SMA-bounded nanodiscs decreases with elevating polymer/lipid ratios and varies between 8–40 nm.^{43,46} In accordance with biological membranes, the bilayer thickness of SMALPs was approximated to 5 nm.⁴⁷

The solubilisation performance of SMA is, to some extent, tuneable by solvent and environmental conditions such as pH, ionic strength, or temperature.^{40,48} In addition, the physicochemical membrane characteristics such as the lateral membrane pressure caused by lipid unsaturation or protein packing density,^{49,50} membrane thickness, charge of lipid bilayer interface, or membrane thermotropic phases^{49,51} also influence the solubilisation behaviour of SMA. In a homogeneous membrane that harbours various lipid types, SMA shows, however, no solubilisation preference towards specific lipid species.^{40,51}

Membrane protein solubilisation and stabilisation in SMALPs was first reported in 2009.³¹ Since then, SMA copolymers have proven effective in solubilising a large variety of membrane

proteins from, among others, bacterial cells,^{52–56} yeast,^{57–60} insect cells,^{61–63} mammalian cells,^{57,58} or plant thylakoid membranes.^{64,65} A solubilisation study of human cells showed non-preferential equilibrium solubilisation of the plasma membrane and the subcellular organelle membranes, even though, on a kinetic scale, the organelle membrane solubilisation was slightly more effective.⁶⁶ These results underline the broad applicability of SMA in terms of membrane protein isolation from various expression systems.

Importantly, despite the above-mentioned wide-range applicability of SMA in terms of extraction power from various membranes, SMA-solubilised proteins show an increased stability over detergent-extracted proteins. More specifically, among others, G-protein coupled receptors (GPCRs),^{57,58} the KcsA potassium ion channel,⁵⁴ or ATP-binding cassette (ABC) transporters,^{62,63} displayed a superior thermostability and storage stability, all while preserving protein conformation and function. SMA-encapsulated nanodiscs even preserve stability and function of noncovalently-bound protein assemblies of up to 48 transmembrane domains.^{52,53,59,67} Furthermore, SMA copolymers render membrane proteins amenable to structural analyses by cryo-electron microscopy,⁶⁷ solid-state NMR,⁶⁸ or X-ray crystallography.⁶⁹ Functional studies such as specific binding assays were also successfully performed on membrane proteins embedded in SMALPs.^{58,63}

At near-neutral pH, the carboxylate groups of SMA are partially charged, thus rendering SMALPs polyanionic structures with a negatively charged rim.³⁹ This high charge density leads to repulsive forces among SMALPs and polymer chains. Notwithstanding this fact, SMA nanodiscs are able to spontaneously and rapidly exchange and transfer their contents. They readily exchange lipids with absorbed lipid monolayers⁷⁰ and among each other through particle collisions.⁷¹ By increasing the lipid concentration in a polymer/lipid mixture, and, thus, shifting the equilibrium towards the formation of liposomes, solubilised lipids re-associate into vesicular assemblies.⁴⁹ Furthermore, polymer transfer was observed among SMALPs^{72,73} and it was even shown that membrane proteins can be reconstituted from SMA nanodiscs into planar lipid bilayers⁵⁴ and in lipidic cubic phases for X-ray crystallography.⁶⁹ This underlines that SMALPs are highly dynamic equilibrium structures rather than static, kinetically trapped assemblies.

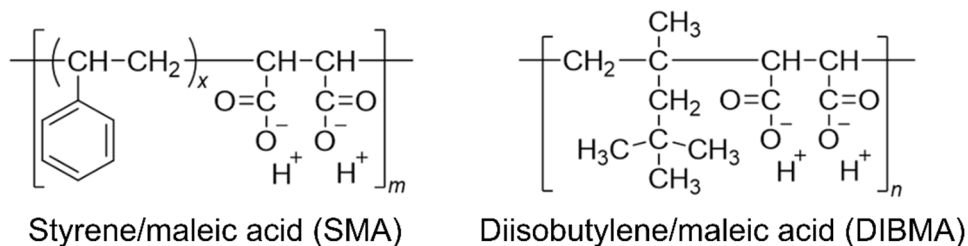


Figure 1.3. Chemical structures of SMA and DIBMA.⁷⁴

Diisobutylene/maleic acid (DIBMA) copolymers

DIBMA is an alternative amphiphilic copolymer displaying distinct polymer properties, and, thus, a different solubilisation behaviour than SMA. DIBMA copolymers lack the aromatic S moieties that characterise SMA polymers but, instead, carry aliphatic diisobutylene (DIB) groups (Figure 1.3). DIB and MA sidechains are strictly alternating in a 1:1 molar ratio, rendering DIBMA less hydrophobic than the efficient SMA variants. Unlike aromatic SMA, DIBMA absorbs substantially less in the far-UV range and, thus, renders membrane proteins directly amenable to optical spectroscopic studies such as UV absorbance or circular dichroism (CD) spectroscopy.^{31,58} At similar conditions, DIBMA nanodiscs are slightly larger than SMALPs and provide an even more native-like environment, as DIBMA has a milder effect on lipid acyl-chain order.^{32,74} Moreover, DIBMA shows a superior stability in the presence of divalent cations and, thus, allows enzymatic activity studies that require high concentrations of these cations.⁶³ Nevertheless, DIBMA is less efficient than SMA in terms of protein extraction yields, which often displays a limiting factor in choosing DIBMA over SMA for membrane-protein studies.³²

Notwithstanding this caveat, DIBMA already proved effective in extracting a wide range of membrane proteins, such as bacterial outer membrane proteins,³² ABC transporters,⁷⁵ or GPCRs.⁷⁵ More specifically, DIBMA stabilised a class B GPCR, representing a notoriously challenging yet pharmacologically relevant GPCR class, with noncovalently-bound ligand and G-protein, thus underlining the even more native-like properties of DIBMALPs. DIBMA nanodiscs were furthermore used to study the membrane binding of soluble α -synuclein, demonstrating their applicability in protein/lipid interaction studies.⁷⁶

Expanding the polymer toolbox

Apart from the most common copolymers described above, the variety of polymers available for membrane-protein solubilisation and stabilisation is continually and rapidly growing.^{36,77} This is to suit specific experimental requirements that are limited by SMA and DIBMA.

For affinity chromatography techniques or fluorescence spectroscopy studies, SMA was thiol-labelled.^{72,78} Reactive SMA-SH can thus be further functionalised by molecular tags or fluorophores to be used for protein purification.

In comparison with negatively charged SMA and DIBMA, positively charged variants of SMA, such as styrene maleimide (SMI) copolymer,⁷⁹ styrene maleimide quaternary ammonium (SMA-QA),⁸⁰ or SMA_d-A,⁸¹ were also shown to efficiently solubilise membranes into nanodiscs. These polymers display a high compatibility with divalent cations and are functional at acidic pH.

The high charge density of commonly used SMA and DIBMA potentially leads to unspecific polymer/protein interactions and, thus, might impede specific protein functional studies. Furthermore, the polymer charge density is not compatible with biochemical and biophysical techniques such as sodium dodecyl sulphate polyacrylamide gel electrophoresis (SDS-PAGE) or surface plasmon resonance (SPR) spectroscopy. This general limitation aroused the interest in finding alternative polymers with a similar amphipathic character and a reduced or neutral net charge in a biologically relevant pH range. Thus far, zwitterionic zSMA, carrying a phosphocholine headgroup attached to the SMA backbone, proved effective in solubilising membranes in a wide range of solvent conditions.^{82,83} It is, however, made through tedious *de novo* polymer synthesis. Furthermore, net neutral SMA variants such as SMA-ED also enable membrane solubilisation, but are not soluble under near-physiological conditions.⁸¹

To overcome this bottlenecks, two new electroneutral copolymers, synthesised from DIBMA and SMA(2:1) backbones, are herein introduced (Figure 1.4). A sulphobetaine side chain was attached to the anhydride form of both polymers, resulting in SMA(2:1)-SB and DIBMA-SB, respectively.

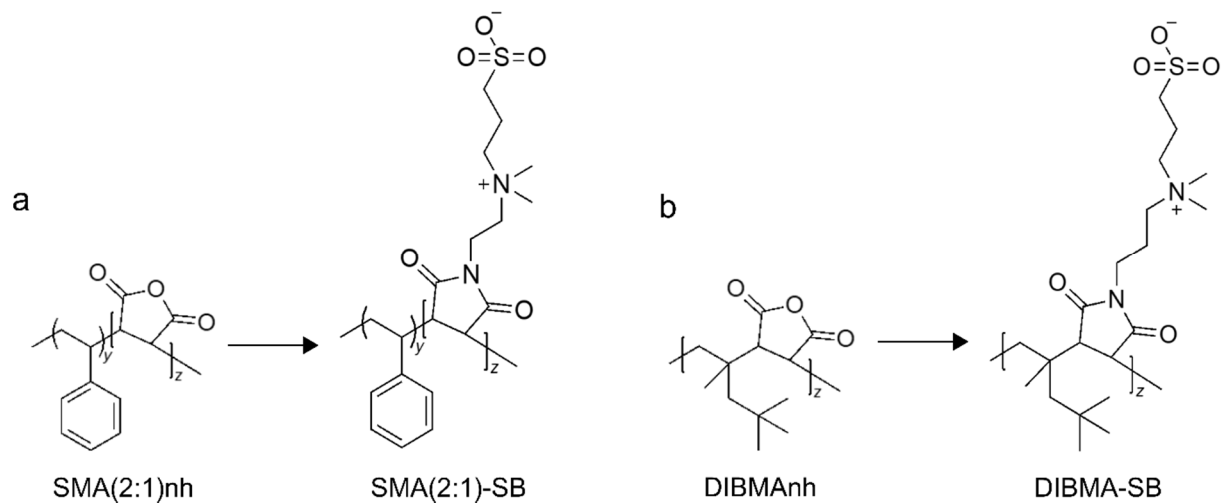


Figure 1.4. Chemical structures of zwitterionic a) SMA(2:1)-SB and b) DIBMA-SB copolymers as obtained from SMA(2:1)nh and DIBMAAnh (nh: anhydride) backbones by attachment of sulphobetaine (SB) side chains, respectively.

1.5. Objectives

The work reported in this thesis focused, on the one hand, on an in-depth biophysical characterisation of SMA(2:1) and its nanodiscs, as it emerged as the most powerful SMA variant from a kinetic viewpoint³⁹ and in terms of specific membrane protein extraction.⁸⁴ On the other hand, two electroneutral copolymers that overcome the bottlenecks of negatively charged SMA and DIBMA were introduced. In more detail, the goals of this thesis can be specified as follows:

- 1) Elucidate the equilibrium solubilisation properties of SMA(2:1) towards model phospholipid vesicles and *Escherichia coli* membranes under various solvent conditions. To this end, nanodisc formation and the solubilisation behaviour was monitored and compared with previous studies on SMA(3:1) and DIBMA.
- 2) Study the dynamic behaviour of SMA(2:1)-bounded nanodiscs. To this end, the lipid transfer kinetics and how it is affected by ionic strength was elucidated. Along this rationale, the effective nanodisc charge was estimated on the basis of theoretical models and determined experimentally.
- 3) Characterise the newly synthesised electroneutral polymers SMA(2:1)-SB and DIBMA-SB and their corresponding nanodiscs. This was addressed by studying the equilibrium solubilisation behaviour towards model phospholipid vesicles and human cell membranes in terms of total protein extraction and specific membrane proteins.

2. Biophysical characterisation of SMA(2:1) nanodiscs

Summary (Manuscript 1)

In this work, the thermodynamics of nanodisc formation by the most commonly used SMA(2:1) copolymer were scrutinised using model and *Escherichia coli* membranes and compared with those of SMA(3:1) and DIBMA.

The polymer refractive index increments, dn/dc , of SMA(2:1), SMA(3:1), and DIBMA were determined to allow for the concentration determination of dialysed polymers. Subsequently, the equilibrium solubilisation efficiency, that is, the solubilisation capacity from a thermodynamic viewpoint, of SMA(2:1) was studied using vesicles of different phospholipid compositions. Employed phospholipids were the saturated, short-chained 1,2-dimyristoyl-*sn*-glycero-3-phosphocholine (DMPC) and the unsaturated, long-chained 1-palmitoyl-2-oleoyl-*sn*-3-phosphocholine (POPC). To this end, SMA(2:1) nanodisc formation was monitored by DLS. The corresponding saturation (SAT) (i.e., first nanodisc formation) and solubilisation (SOL) (i.e., completion of nanodisc formation) boundaries were determined by ^{31}P NMR. On a mass concentration scale and under identical conditions, SMA(2:1) most efficiently extracted phospholipids from model membranes, as indicated by low saturating and solubilising polymer/lipid ratios and the corresponding vesicle-to-nanodisc transfer Gibbs free energies.

The ionic strength had no or little effect on the solubilisation efficiency of SMA(2:1) for DMPC and POPC vesicles, respectively. However, varying the pH value had a pronounced influence on the solubilisation of both phospholipids: at an acidic pH value of 6.4, a substantially higher concentration of SMA(2:1) was needed to completely solubilise DMPC vesicles followed by neutral (pH 7.4) and moderately alkaline pH values (pH 8.3). These findings are in stark contrast to the kinetic solubilisation of DMPC, which slows down with alkaline pH.³⁹ It is suggested that the decreased hydrophobicity of SMA(2:1) at alkaline pH slows down the solubilisation of vesicles, but that, in equilibrium, less polymer with an extended conformation is needed to stabilise the nanodiscs.

Furthermore, the influence of SMA(2:1) on thermotropic lipid phase transitions was studied by differential scanning calorimetry (DSC) and compared with SMA(3:1) and DIBMA. On a mass concentration scale, SMA(3:1) reduced the gel-to-fluid phase-transition temperature T_m of DMPC most drastically with increasing polymer concentrations, followed by SMA(2:1) and

DIBMA. These results demonstrated that the perturbation of the lipid acyl-chain packing is most drastic with SMA(3:1), suggesting the penetration of phenyl moieties being the major cause. Hence, SMA(2:1) with a low styrene content had a relatively mild effect, followed by DIBMA, which contains no styrene moieties at all.

Finally, the performance of SMA(2:1) towards complex, native *E. coli* membranes was elucidated. To this end, the solubilising power of SMA(2:1) was determined in terms of protein extraction quantities and compared to results of SMA(3:1), DIBMA, and a standard conventional head-and-tail detergent *n*-dodecyl- β -D-maltoside (DDM).³² Relative to DDM, the protein extraction yield of SMA(2:1) amounted to over 90 %. SMA(2:1) extracted 10 % more membrane proteins at pH 8.3 than at pH 7.4, correlating with the findings on pH-dependence using model membranes. Importantly, under identical conditions, SMA(2:1) extracted 10–30 % more membrane proteins compared with SMA(3:1) and DIBMA. It can be thus concluded that, among studied polymers, SMA(2:1) is the most efficient solubiliser of both model and cellular membranes.

2.1. Manuscript 1

Thermodynamics of nanodisc formation mediated by styrene/maleic acid (2:1) copolymer

Anne Grethen, Abraham Olusegun Oluwole, Bartholomäus Danielczak, Carolyn Vargas, and Sandro Keller

Scientific Reports, **2017**, 7, 11517

Contribution

For this work, I designed, performed, and analysed all refractometry, DLS, and ³¹P NMR experiments. I created Figures 1–5 and wrote the original draft of the manuscript.

Reprinted by permission given under the terms of the Creative Commons CC BY license.

SCIENTIFIC REPORTS

OPEN

Thermodynamics of nanodisc formation mediated by styrene/maleic acid (2:1) copolymer

Anne Grethen¹, Abraham Olusegun Oluwole^{1,2}, Bartholomäus Danielczak¹, Carolyn Vargas¹ & Sandro Keller¹

Styrene/maleic acid copolymers (SMA) have recently attracted great interest for *in vitro* studies of membrane proteins, as they self-insert into and fragment biological membranes to form polymer-bounded nanodiscs that provide a native-like lipid-bilayer environment. SMA copolymers are available in different styrene/maleic acid ratios and chain lengths and, thus, possess different charge densities, hydrophobicities, and solubilisation properties. Here, we studied the equilibrium solubilisation properties of the most commonly used copolymer, SMA(2:1), by monitoring the formation of nanodiscs from phospholipid vesicles using ³¹P nuclear magnetic resonance spectroscopy, dynamic light scattering, and differential scanning calorimetry. Comparison of SMA(2:1) phase diagrams with those of SMA(3:1) and diisobutylene/maleic acid (DIBMA) revealed that, on a mass concentration scale, SMA(2:1) is the most efficient membrane solubiliser, despite its relatively mild effects on the thermotropic phase behaviour of solubilised lipids. In contrast with previous kinetic studies, our equilibrium experiments demonstrate that the solubilisation of phospholipid bilayers by SMA(2:1) is most efficient at moderately alkaline pH values. This pH dependence was also observed for the solubilisation of native *Escherichia coli* membranes, for which SMA(2:1) again turned out to be the most powerful solubiliser in terms of the total amounts of membrane proteins extracted.

Amphiphilic copolymers—in particular, styrene/maleic acid (SMA) copolymers—have gained considerable attention over the past few years because of their ability to solubilise biological membranes into SMA-bounded nanodiscs containing membrane proteins and lipids^{1–3}. This approach is independent of conventional detergents and results in nanosized membrane mimics that retain the bilayer architecture of the parent membrane^{4,5}. Polymer-mediated solubilisation renders membrane proteins amenable to functional^{6–8} and biophysical^{7,9} studies as well as structural analysis by nuclear magnetic resonance (NMR) spectroscopy^{10,11}. Furthermore, SMA-bounded nanodiscs have recently been used to transfer membrane proteins into lipidic cubic phases for structure determination by X-ray crystallography¹².

SMA is a random copolymer that is commercially available in different average styrene/maleic acid ratios and chain lengths and, consequently, different charge densities, hydrophobicities, and solubilisation properties. The most hydrophilic variant SMA(1:1) and the most hydrophobic variant SMA(4:1), which have average styrene/maleic acid molar ratios of 1:1 and 4:1, respectively, are of limited use for solubilising lipid vesicles because of the narrow pH windows within which these copolymers are sufficiently soluble and hydrophobic. By contrast, SMA(2:1) and SMA(3:1) are capable of forming lipid-bilayer nanodiscs over a broader range of pH values and have become the two most popular amphiphilic copolymers used for this purpose. SMA(2:1) has been shown to be the most favourable solubiliser of three different membrane proteins¹³ and is emerging as the standard SMA variant for membrane-protein research using polymer-bounded nanodiscs¹⁴. While the structural properties⁵ and the self-association¹⁵ of SMA(2:1) as well as the kinetics of vesicle solubilisation mediated by this copolymer¹⁵ have been studied in great detail, only little is currently known about its solubilisation thermodynamics. One observation from kinetic experiments that remains particularly puzzling is that the solubilisation performance of SMA(2:1) is higher than that of SMA(3:1) but appears to decrease with increasing pH¹⁵, although a higher maleic acid content—as in SMA(2:1) compared with SMA(3:1)—and elevated pH should have similar effects on the charge density and the effective hydrophobicity of the copolymer.

¹Molecular Biophysics, University of Kaiserslautern, 67663 Kaiserslautern, Germany. ²Department of Chemistry, University of Ibadan, 200284 Ibadan, Nigeria. Correspondence and requests for materials should be addressed to S.K. (email: mail@sandrokeller.com)

Herein, we provide a thermodynamic benchmark for a more detailed understanding of the interactions of SMA(2:1) with lipid membranes and, specifically, of the roles of polymer, lipid, and solvent properties. To this end, we present the first account of the equilibrium solubilisation properties of SMA(2:1) against large unilamellar vesicles (LUVs) composed of either 1,2-dimyristoyl-*sn*-glycero-3-phosphocholine (DMPC) or 1-palmitoyl-2-oleoyl-*sn*-glycero-3-phosphocholine (POPC) as monitored by ^{31}P NMR spectroscopy, dynamic light scattering (DLS), and differential scanning calorimetry (DSC). We rationalised the solubilisation equilibrium in terms of a pseudophase concept, constructed phase diagrams, and obtained vesicle-to-nanodisc transfer free energies that enable a thermodynamic comparison with more hydrophobic SMA(3:1)^{16,17} and less hydrophobic diisobutylene/maleic acid (DIBMA)¹⁸ copolymers. We found that, on a mass concentration scale, both the onset and the completion of solubilisation of DMPC and POPC LUVs require less SMA(2:1) than SMA(3:1) or DIBMA, thus showing that SMA(2:1) is the most efficient solubiliser of lipid membranes. Importantly, SMA(2:1)-mediated lipid solubilisation was thermodynamically more efficient at pH 8.3 than at pH 7.4, even though the solubilisation process has been reported to slow down at alkaline pH¹⁵. Our lipid-bilayer studies under equilibrium conditions rather than kinetic control correlate with experiments performed on protein-containing biological membranes, as we found SMA(2:1) to furnish the largest amounts of membrane proteins extracted from native *Escherichia coli* membranes, again with an improvement in solubilisation yield at pH 8.3 as compared with pH 7.4.

Theoretical background

Pseudophases in lipid/surfactant mixtures. We have shown^{16–18} that the solubilisation of DMPC and POPC LUVs by SMA(3:1) or DIBMA can be rationalised in terms of a three-stage model^{19,20} that considers lipid (L) and surfactant (S) molecules in bilayer (b) and micellar (m) phases as well as surfactant monomers in the aqueous (aq) phase. The concentrations of lipid and surfactant, c_L and c_S , respectively, determine the presence and abundance of each of these phases. In a lipid/polymer mixture, where the polymer assumes the role of the surfactant, an increase in c_S at given c_L leads to a transition from the vesicular bilayer range to the coexistence range, within which polymer-saturated bilayer vesicles coexist with lipid-saturated nanodiscs. Upon a further increase in c_S , the vesicles are completely solubilised and transformed into polymer-bounded nanodiscs. In this interpretation of the three-stage model, nanodiscs take the role of mixed micelles found in conventional lipid/surfactant mixtures^{19,20}. The first nanodiscs are formed at a threshold known as the saturation (SAT) boundary, while a second transition designated as the solubilisation (SOL) boundary marks the completion of nanodisc formation and the concomitant disappearance of the last vesicular structures.

Plotting the c_S values at the SAT and SOL boundaries against the corresponding lipid concentrations c_L gives rise to two straight lines described by:

$$c_S^{\text{SAT}} = c_S^{\text{aq},0} + R_S^{\text{b,SAT}} c_L \quad (1)$$

$$c_S^{\text{SOL}} = c_S^{\text{aq},0} + R_S^{\text{m,SOL}} c_L \quad (2)$$

The slopes $R_S^{\text{b,SAT}}$ and $R_S^{\text{m,SOL}}$ denote the polymer/lipid molar ratios in vesicular bilayers and nanodiscs at which the vesicles become saturated with polymer and at which solubilisation is complete, respectively. Ideally, both lines meet at a common ordinate intercept, $c_S^{\text{aq},0}$, which corresponds to the concentration of “free” polymer in the aqueous phase within the coexistence range. In both our previous^{16–18} and present phase diagrams, the ordinate intercepts of the SAT and SOL boundaries are negligibly low, so that the concentration of “active” (i.e., solubilisation-competent) polymer in the aqueous phase can be taken as $c_S^{\text{aq},0} = 0$.

The critical mole fractions of polymer in vesicular bilayers and nanodiscs, $X_S^{\text{b,SAT}}$ and $X_S^{\text{m,SOL}}$, respectively, amount to:

$$X_S^{\text{b,SAT}} = \frac{R_S^{\text{b,SAT}}}{1 + R_S^{\text{b,SAT}}} \quad (3)$$

$$X_S^{\text{m,SOL}} = \frac{R_S^{\text{m,SOL}}}{1 + R_S^{\text{m,SOL}}} \quad (4)$$

The partition coefficients quantifying the transfer of polymer and lipid from vesicles into nanodiscs, $K_S^{\text{b} \rightarrow \text{m}}$ and $K_L^{\text{b} \rightarrow \text{m}}$, are then given by:

$$K_S^{\text{b} \rightarrow \text{m}} \equiv \frac{X_S^{\text{m,SOL}}}{X_S^{\text{b,SAT}}} = \frac{R_S^{\text{m,SOL}}(1 + R_S^{\text{b,SAT}})}{R_S^{\text{b,SAT}}(1 + R_S^{\text{m,SOL}})} > 1 \quad (5)$$

$$K_L^{\text{b} \rightarrow \text{m}} \equiv \frac{X_L^{\text{m,SOL}}}{X_L^{\text{b,SAT}}} = \frac{1 - X_S^{\text{m,SOL}}}{1 - X_S^{\text{b,SAT}}} = \frac{1 + R_S^{\text{b,SAT}}}{1 + R_S^{\text{m,SOL}}} < 1 \quad (6)$$

From these partition coefficients, the corresponding standard molar Gibbs free-energy changes accompanying the transfer of the polymer and the lipid from vesicles into nanodiscs, $\Delta G_S^{\text{b} \rightarrow \text{m},0}$ and $\Delta G_L^{\text{b} \rightarrow \text{m},0}$, respectively, are obtained as:

$$\Delta G_S^{b \rightarrow m, o} = -RT \ln K_S^{b \rightarrow m} < 0 \quad (7)$$

$$\Delta G_L^{b \rightarrow m, o} = -RT \ln K_L^{b \rightarrow m} > 0 \quad (8)$$

Derivation of phase boundaries from ^{31}P NMR. According to the three-stage model, all phospholipid molecules and, thus, all phosphorus nuclei reside in bilayer membranes as long as the surfactant concentration is lower than or equal to c_S^{SAT} according to equation 1. In solution-state NMR experiments, the signal arising from ^{31}P nuclei in large, vesicular structures is broadened beyond detection. Thus, the area of the ^{31}P NMR peak, A , is zero in the absence of solubilised phospholipid:

$$A(c_S \leq c_S^{\text{SAT}}) = 0 \quad (9)$$

Once the polymer concentration exceeds c_S^{SOL} (equation 2), all phospholipid molecules are solubilised, and the area under the ^{31}P NMR peak amounts to:

$$A(c_S^{\text{SOL}} \leq c_S) = f c_L \quad (10)$$

where f is the proportionality factor between the concentration of solubilised lipids and the experimentally determined peak area. In general, f depends on the experimental conditions but is constant for a given NMR spectrometer operated using identical instrument settings and acquisition parameters. Within the coexistence range, the peak area is expected to be proportional to the extent of solubilisation:

$$A(c_S^{\text{SAT}} \leq c_S \leq c_S^{\text{SOL}}) = f c_L \frac{c_S - c_S^{\text{SAT}}}{c_S^{\text{SOL}} - c_S^{\text{SAT}}} \quad (11)$$

Here, the last term on the right-hand side reflects the fraction of solubilised lipid as given by the lever rule^{20,21}.

Pairs of c_S^{SAT} and c_S^{SOL} values at a given lipid concentration were obtained by analysing the areas derived from the corresponding ^{31}P NMR signals in terms of equations 9–11^{16–18}. In addition to such local fits considering only one lipid concentration at a time, peak areas measured at four different lipid concentrations were globally fitted with equations 9–11 in order to obtain the best-fit $R_S^{b, \text{SAT}}$ and $R_S^{m, \text{SOL}}$ values. 95% confidence intervals were derived by nonlinear least-squares fitting in Excel spreadsheets, as detailed elsewhere²².

Experimental Section

Materials. DMPC and POPC were kind gifts from Lipoid (Ludwigshafen, Germany). SMA(2:1) (hydrolysed from styrene/maleic anhydride (2:1), tradename Xiran SZ30010) and SMA(3:1) (Xiran SL25010 S25) copolymer solutions were kind gifts from Polyscope (Geleen, Netherlands). DIBMA (Sokalan CP 9) was kindly provided by BASF (Ludwigshafen, Germany). D_2O was purchased from Deutero (Kastellaun, Germany) and NaCl from VWR (Darmstadt, Germany). 85% (w/v) H_3PO_4 in D_2O and Na_2HPO_4 were from Sigma–Aldrich (Steinheim, Germany), and Coomassie Brilliant Blue G250, NaH_2PO_4 , ethylenediamine tetraacetic acid (EDTA), sodium dodecyl sulphate (SDS), tris(hydroxymethyl)aminomethane (Tris), and Tris–HCl were from Carl Roth (Karlsruhe, Germany). All chemicals were purchased in the highest purity available.

Determination of copolymer refractive index increments. In order to measure copolymer concentrations, we modified a procedure based on a published protocol¹⁴. To this end, we precipitated 5 mL of a commercial SMA(2:1), SMA(3:1), or DIBMA solution by adding 3 mL of 4 M HCl and washed the pellets 4 times with 50 mL triple-distilled water. After each washing step, the polymer was pelleted by centrifugation at 8000 g for 15 min, and the supernatant was discarded. Washed pellets were resuspended in 3 mL of 0.5 M NaOH followed by a second precipitation and washing procedure as described above. Pellets were directly (i.e., without resuspension in NaOH¹⁴) aliquoted and lyophilised for at least 24 h using an Alpha 2–4 LSCplus (Martin Christ, Osterode am Harz, Germany). After lyophilisation, dried polymer powders were resuspended in 100 mM NaOH to yield polymer concentrations of 1% (w/v). Refractive index (RI) values were measured on an Abbemat 500 refractometer (Anton Paar, Graz, Austria) for dilution series comprising 5–10 polymer concentrations to determine RI increments (cf. Table 1).

Preparation of SMA(2:1) stock solutions. SMA(2:1) has a styrene/maleic acid molar ratio of 2.2:1, a mass-average molar mass of $M_w = 7.0 \text{ kg mol}^{-1}$, a number-average molar mass of $M_n = 2.7 \text{ kg mol}^{-1}$, and, thus, a dispersity of $M_w/M_n = 2.6$. Stock solutions of SMA(2:1) for vesicle solubilisation assays were prepared as described previously for SMA(3:1)¹⁷ and DIBMA¹⁸. Briefly, 3-mL aliquots of commercial SMA(2:1) solution were dialysed against 0.5 L Tris (50 mM Tris, 200 mM NaCl, pH 7.4 or 8.3) or phosphate buffer (50 mM $\text{Na}_2\text{HPO}_4/\text{NaH}_2\text{PO}_4$, 200 mM NaCl, pH 6.4) in 5-mL QuixSep dialysers (Membrane Filtration Products, Seguin, USA) using Spectra/Por 3 dialysis membranes with a molar-mass cutoff of 3.5 kg mol^{-1} (Spectrum Laboratories, Rancho Dominguez, California, USA). Dialysis was performed for 36 h at room temperature under gentle stirring with buffer exchange after 16 h. Dialysed stock solutions were sterile-filtered using 0.22- μm poly(vinylidene fluoride) syringe filters (Carl Roth, Karlsruhe, Germany), and final SMA(2:1) concentrations were determined refractometrically using the dn/dc value determined as described above (cf. Table 1). The concentrations of all polymers are reported on the basis of their respective number-average molar masses (cf. Table 1).

	SMA(2:1)	SMA(3:1)*	DIBMA**
dn/dc (L mol ⁻¹)	0.53	0.80	1.35
$dn/d\rho$ (L kg ⁻¹)	0.20	0.20	0.16
M_n (kg mol ⁻¹)	2.7	4.0	8.4
M_w (kg mol ⁻¹)	7.0	10.0	15.3
M_w/M_n	2.60	2.50	1.82
ϵ_{260} (L (mol cm) ⁻¹)	4121	6989**	234
μ_{260} (L (kg cm) ⁻¹)	1526	1747	28

Table 1. Molar RI increments (dn/dc), specific RI increments ($dn/d\rho$), number-average molar masses (M_n), mass-average molar masses (M_w), dispersities (M_w/M_n), molar extinction coefficients at 260 nm, ϵ_{260} , and specific extinction coefficients at 260 nm, μ_{260} , of nanodisc-forming polymers. *Recalculated from Cuevas Arenas *et al.*¹⁷ using the modified protocol described here. **Taken from Oluwole *et al.*¹⁸.

Vesicle preparation. Lipid powders were suspended in either Tris buffer (50 mM Tris, 200 mM NaCl, pH 7.4 or 8.3) or phosphate buffer (50 mM Na₂HPO₄/NaH₂PO₄, 200 mM NaCl, pH 6.4) to final lipid concentrations of 30–45 mM. Lipid suspensions were vortexed for 10 min prior to 35-fold extrusion through two stacked polycarbonate membranes with a nominal pore diameter of 100 nm. DMPC was extruded at 30 °C using a block-heated Mini-Extruder (Avanti, Alabama, USA) and POPC at 20 °C using a LiposoFast extruder (Avestin, Ottawa, Canada). Unimodal particle size distributions were confirmed by DLS (see below), yielding hydrodynamic vesicle diameters of ~150 nm.

³¹P NMR spectroscopy. Samples containing 2.5, 5.0, 7.5, or 10.0 mM lipid and 0–4 mM SMA(2:1) (corresponding to 0–1.1% (w/v) copolymer) were prepared from stock solutions in Tris buffer (pH 7.4). 10% D₂O (v/v) was included in the sample buffer to provide a lock signal. Samples were incubated for at least 16 h at 30 °C for DMPC or room temperature for POPC. NMR measurements were carried out at 30 °C for DMPC or 25 °C for POPC on an Avance 400 spectrometer (Bruker Biospin, Rheinstetten, Germany) operating at a ³¹P resonance frequency of 162 MHz using a 5-mm broadband inverse probe. 256 scans were acquired with an inverse-gated decoupling sequence using an acquisition time of 1.6 s, a sweep width of 9746 Hz, and a relaxation delay of 6 s. Data were multiplied by an exponential function with a line-broadening factor of 1.0 Hz before Fourier transformation. Chemical shifts were referenced to 85% (w/v) H₃PO₄ in D₂O as external standard at 0 ppm. Peaks were integrated using the software Bruker Topspin 3.2.

Dynamic light scattering. Samples containing 6 mM lipid in the form of LUVs and 0–3.1 mM SMA(2:1) (corresponding to 0–0.8% (w/v) copolymer) in either Tris buffer (pH 7.4 or 8.3) or phosphate buffer (pH 6.4) were incubated for at least 16 h at 30 °C for DMPC or room temperature for POPC. DLS measurements were performed on a Zetasizer Nano S90 (Malvern Instruments, Malvern, UK) working with a 633-nm He–Ne laser and a detection angle of 90°. Samples were thermostatted for 2 min at 30 °C for DMPC or 25 °C for POPC before measurements were performed in a 45- μ L quartz glass cuvette with a cross-section of 3 mm \times 3 mm (Hellma Analytics, Müllheim, Germany). Each sample was measured twice: firstly, with the attenuator position automatically optimised for determination of size distributions and, secondly, with the attenuator set to the maximum in order to ensure comparability of total scattering intensities. The effects of different NaCl concentrations and buffer components on the viscosity and RI of the solvent were accounted for during data analysis. Autocorrelation functions were fitted using a non-negatively constrained least-squares function²³ to yield intensity-weighted particle size distributions and by cumulant analysis²⁴ to obtain z -average particle diameters and associated polydispersity indices (PDIs). Distribution widths of z -average diameters, σ , were calculated as $\sigma = \sqrt{\text{PDI}} z$.

Differential scanning calorimetry. Samples containing 5 mM DMPC and 0–5 mM SMA(2:1) (corresponding to 0–1.4% (w/v) copolymer) in Tris buffer (pH 7.4) were incubated at 30 °C for 16 h prior to experiments. The sample and reference cells were filled with buffer and were repeatedly heated and cooled at a rate of 30 °C h⁻¹ before the buffer in the sample cell was replaced with sample. Apart from the first upscan, successive heating and cooling scans, which were also performed at a rate of 30 °C h⁻¹, overlaid very closely. Data were averaged, blank-subtracted, and normalised against the molar amount of DMPC in the sample using the software MicroCal Origin 7.0 (OriginLab, Northampton, USA). The melting temperature, T_m , was taken as the temperature at which the excess molar isobaric heat capacity, ΔC_p , reached a maximum.

Solubilisation of native *E. coli* membranes. *E. coli* BL21(DE3) cells were transformed with an empty pET-24 vector and selected by kanamycin resistance. After incubation in lysogeny broth overnight at 37 °C under permanent agitation, cells were harvested by centrifugation and washed twice with saline (154 mM NaCl). Cell pellets were resuspended in a 10-fold volume of ice-cold buffer (50 mM Tris, 2 mM EDTA, 200 mM NaCl, pH 7.4) and ultrasonicated twice for 10 min in an S-250 A sonifier (Branson Ultrasonics, Danbury, USA). The lysate was further centrifuged for 30 min at 1000 g and 4 °C. The supernatant was ultracentrifuged for 1 h at 100,000 g and 4 °C and subjected to 7 buffer washing steps to remove soluble proteins. Membrane pellets were resuspended in buffer (50 mM Tris, 200 mM NaCl, pH 7.4) to a final concentration of 42.5 mg mL⁻¹ and treated with 10 mM (0.5% (w/v)) DDM, 9.3 mM (2.5% (w/v)) SMA(2:1), 6.3 mM (2.5% (w/v)) SMA(3:1), 3.0 mM (2.5% (w/v)) DIBMA, or

buffer. Polymer-containing samples were incubated for 16 h at 20 °C with gentle agitation and subsequently subjected to ultracentrifugation for 1 h at 100,000 g and 4 °C. The supernatant containing solubilised membrane proteins was analysed by sodium dodecyl sulphate polyacrylamide gel electrophoresis (SDS-PAGE). To avoid band smearing caused by the presence of polymers¹⁴, solubilised fractions were precipitated with CH₃OH/CHCl₃/H₂O in a mixing ratio of 4:1:3 (v/v/v)²⁵. Briefly, to a 100- μ L aliquot of ice-cold sample, we successively added 400 μ L ice-cold CH₃OH, 100 μ L ice-cold CHCl₃, and 300 μ L ice-cold water with thorough vortexing after each addition. The mixture was centrifuged for 2 min at 14,000 g and 4 °C. The upper, aqueous layer was removed, and 400 μ L CH₃OH was added before the sample was vortexed again. Precipitated proteins were pelleted by centrifugation for 1 min at 5000 g and another 5 min at 20,000 g, both at 4 °C. This two-step centrifugation was performed to make sure that the pellet completely sticks to the bottom rather than the sides of the centrifugation tube. CH₃OH was carefully removed using a pipette. Residual organic solvent was allowed to evaporate under a chemical hood and was subsequently removed under high vacuum in a desiccator overnight. The dried pellet was resuspended in SDS buffer (106 mM Tris-HCl, 141 mM Tris, 2% (w/v) SDS, 10% (w/v) glycerol, 0.51 mM EDTA, 0.22 mM Coomassie Brilliant Blue G250, 0.175 mM Phenol Red, pH 8.5), boiled for 10 min under agitation, and subjected to SDS-PAGE.

Results and Discussion

Determination of copolymer concentrations by refractometry. We have recently shown that refractometry is a useful tool for determining the concentrations of SMA(3:1)^{16,17} and DIBMA¹⁸ in aqueous solutions. Refractometry is particularly valuable for DIBMA, which contains no aromatic residues and, thus, no chromophores that would allow a straightforward quantification by UV absorbance¹⁸. Our previous protocols for determining the RI increments of SMA(3:1)^{16,17} and DIBMA¹⁸ differed from one another in that the contribution of NaOH to the RI of the polymer stock solution was accounted for only in the case of DIBMA. Thus, to allow for quantitative comparisons among different polymers, we established a refined and general protocol for the refractometric quantification of polymer concentrations. As described in a recent protocol for preparing SMA(2:1) solutions¹⁴, we first washed and lyophilised the polymer solutions obtained from the manufacturer (cf. Experimental Section for details). The major departure from the standard procedure¹⁴ was that, rather than resuspending the polymer pellets in NaOH for lyophilisation after the last washing step, we directly lyophilised the pelleted polymer. This approach aimed at minimising the Na⁺ and Cl⁻ contents in the lyophilised polymer pellets, which otherwise would be difficult to control or quantify but would also contribute to the measured RI values. We then resuspended the lyophilised polymer in 100 mM NaOH and measured RI values at different concentrations of each polymer. The constant contribution of NaOH to the RI signal was accounted for by subtracting the RI value of a 100 mM NaOH blank. For each polymer, both molar and specific RI increments, dn/dc and $dn/d\rho$, were obtained from the slopes of the plots of RI against molar and mass concentrations, c and ρ , respectively. Table 1 summarises the dn/dc and $dn/d\rho$ values thus determined along with the corresponding number-average molar masses, M_n , mass-average molar masses, M_w , and dispersities, M_w/M_n , of the three polymers. To provide a comprehensive overview of the physicochemical properties of the three polymers that can be used to determine their concentrations, Table 1 lists also their molar extinction coefficients at 260 nm, ϵ_{260} , and specific extinction coefficients at 260 nm, μ_{260} . Note that the extinction coefficients of DIBMA are shown for completeness only, as they are of limited use for concentration determination (see above).

Unsurprisingly, dn/dc increases with increasing molar mass of the polymer, whereas the $dn/d\rho$ values are identical for SMA(2:1) and SMA(3:1) but significantly lower for DIBMA. The dn/dc value of SMA(3:1) reported in Table 1 is 28% lower than the value previously estimated without the above-mentioned correction for the presence of inorganic ions^{16,17}. Thus, use of the dn/dc value determined here results in somewhat higher SMA(3:1) concentrations than those reported previously, which does not, however, affect any of the major conclusions drawn from these earlier studies^{16,17}.

Solubilisation of saturated phospholipids by SMA(2:1). To quantify the solubilisation of lipid-bilayer vesicles by SMA(2:1) under equilibrium rather than kinetically controlled conditions, we used ³¹P NMR spectroscopy to follow the solubilisation of DMPC LUVs at 30 °C. This temperature is well above the main phase-transition temperature, T_m , of DMPC, so that the lipid bilayer was always in the liquid-crystalline (i.e., fluid) state. In the absence of copolymer, the NMR signal of large, slow-tumbling vesicles was broadened beyond detection (Fig. 1A). Addition of SMA(2:1) at concentrations above the saturation (SAT) boundary resulted in the emergence of an isotropic peak, thus indicating the formation of smaller, fast-tumbling lipid particles^{16–18}. Beyond this point, the peak area increased linearly with the concentration of SMA(2:1), until a plateau reflecting the completion of solubilisation was reached at the solubilisation (SOL) boundary. At each lipid concentration tested, the NMR peak area reflected such a three-stage solubilisation behaviour with two breakpoints, namely, the SAT and SOL phase boundaries (Fig. 1B). The concentrations of SMA(2:1) at the SAT and SOL boundaries at four different DMPC concentrations yielded a phase diagram characterised by critical SMA(2:1)/DMPC molar ratios of $R_S^{b,SAT} = 0.087 \pm 0.006$ and $R_S^{m,SOL} = 0.130 \pm 0.004$, respectively (Fig. 1C). These ratios furnished Gibbs free-energy changes accompanying the vesicle-to-nanodisc transfer of $\Delta G_L^{b \rightarrow m,0} = (0.098 \pm 0.023)$ kJ mol⁻¹ and $\Delta G_S^{b \rightarrow m,0} = -(0.91 \pm 0.23)$ kJ mol⁻¹ for the lipid and the polymer, respectively (Fig. 2A).

Comparison of equilibrium solubilisation efficiencies among copolymers. On the basis of the new data (Fig. 1) and earlier results^{16–18}, we compared the equilibrium solubilisation efficiencies of SMA(2:1), SMA(3:1), and DIBMA toward DMPC LUVs in terms of their SAT and SOL phase boundaries and the Gibbs free-energy changes accompanying the vesicle-to-nanodisc transfer of the lipid and the polymers. The critical polymer/lipid molar ratios required for the onset and completion of solubilisation in the case of SMA(2:1) were significantly lower than for SMA(3:1) but higher than for DIBMA (Fig. 2A). Since the average molar masses of the

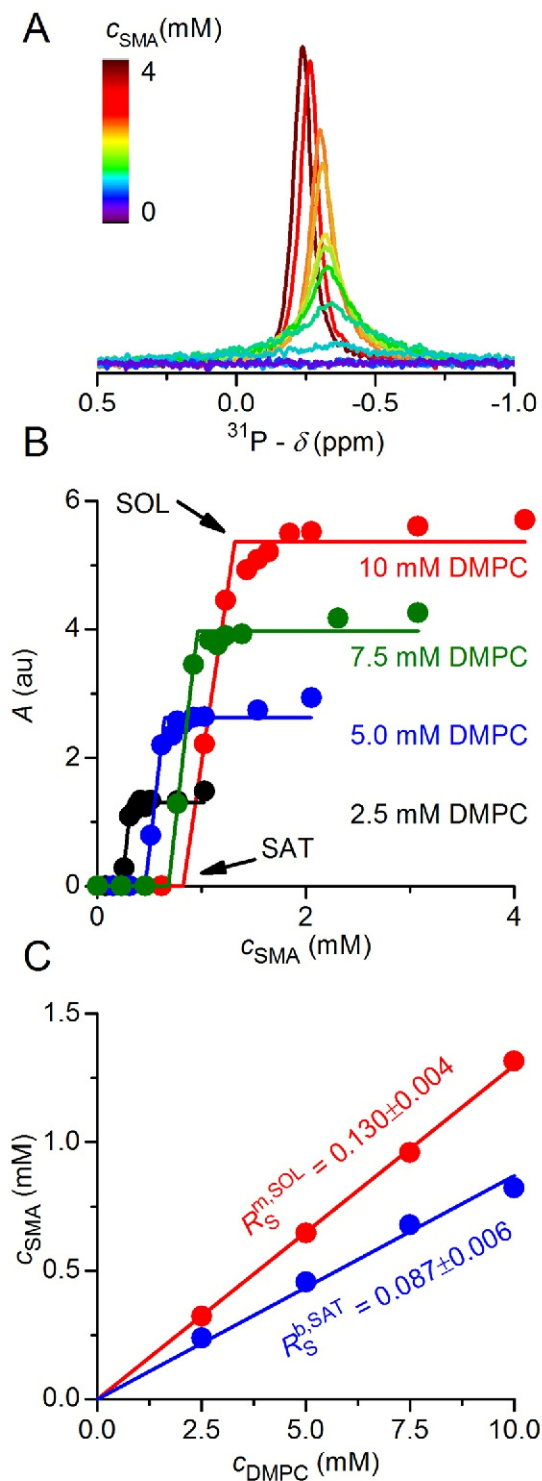


Figure 1. Solubilisation of DMPC vesicles by SMA(2:1) at 30 °C as monitored by ^{31}P NMR. **(A)** NMR spectra of 10 mM DMPC initially present in the form of LUVs upon exposure to increasing concentrations of SMA(2:1). **(B)** Peak areas, A , at four different DMPC concentrations as functions of SMA(2:1) concentration, showing experimental data (circles) and global fits (lines) according to equations 9–11. The slight increase in A upon complete solubilisation is due to a decrease in nanodisc size with increasing SMA(2:1) concentration, thus resulting in sharper peaks that are better resolved from the baseline, as seen in A. **(C)** Phase diagram of DMPC/SMA(2:1) at 30 °C showing the onset (saturation; SAT) and completion (solubilisation; SOL) of solubilisation. Shown are pairs of $c_{\text{S}}^{\text{SAT}}$ and $c_{\text{S}}^{\text{SOL}}$ (circles) obtained from breakpoints derived from local fits in (B) and global fits (solid lines).

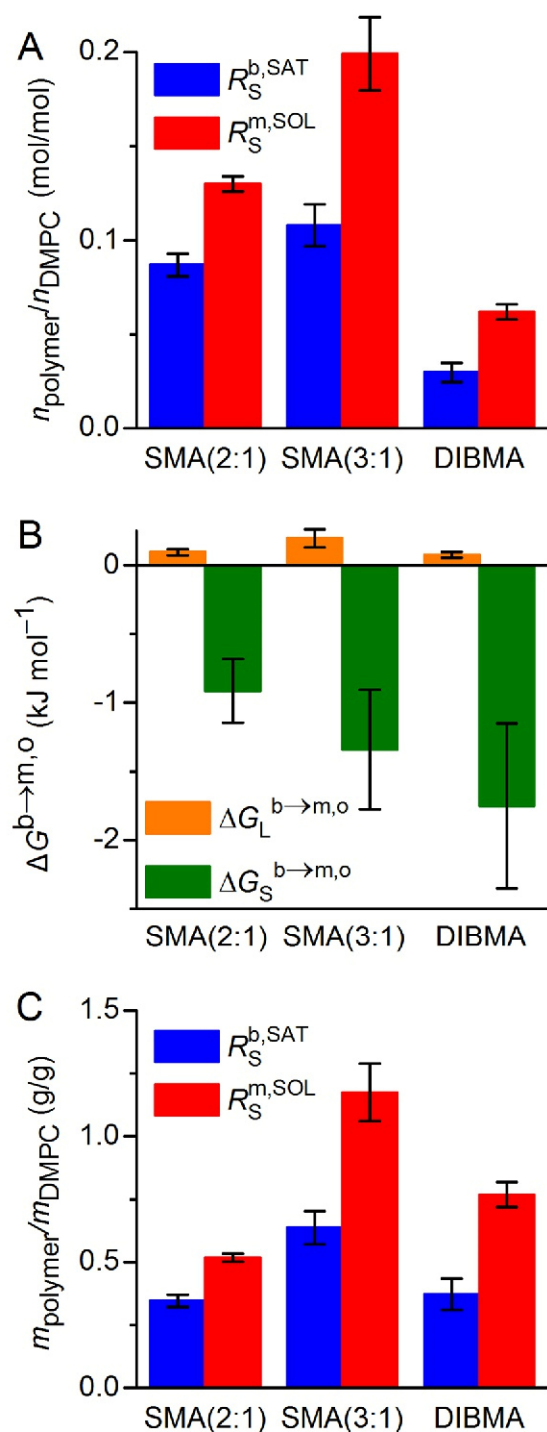


Figure 2. Thermodynamic parameters characterising the solubilisation of DMPC vesicles at 30 °C by the three copolymers compared in this study. **(A)** SAT and SOL phase boundaries of SMA(2:1), SMA(3:1), and DIBMA based on polymer/lipid *molar* ratios. **(B)** Transfer free energies of lipid and copolymers, $\Delta G_L^{b \rightarrow m, o}$ and $\Delta G_S^{b \rightarrow m, o}$, respectively, as derived from phase boundaries in **(A)**. **(C)** SAT and SOL phase boundaries of SMA(2:1), SMA(3:1), and DIBMA based on copolymer/lipid *mass* ratios. Error bars denote 95% confidence intervals, roughly corresponding to ± 2 standard deviations.

copolymers exceed that of the lipid by a factor of 4–12, comparisons based on polymer/lipid *molar* ratios should be taken with caution. Notwithstanding this caveat, knowledge of the polymer/lipid ratio required for solubilising a given amount of lipids is instructive not only for practical purposes but also for thermodynamic considerations relying on the Gibbs free energies deduced from $R_S^{b,SAT}$ and $R_S^{m,SOL}$ (Fig. 2B). We found $\Delta G_S^{b \rightarrow m, o}$, which drives nanodisc formation, to be most favourable for DIBMA and least favourable for SMA(2:1). In the case of the two

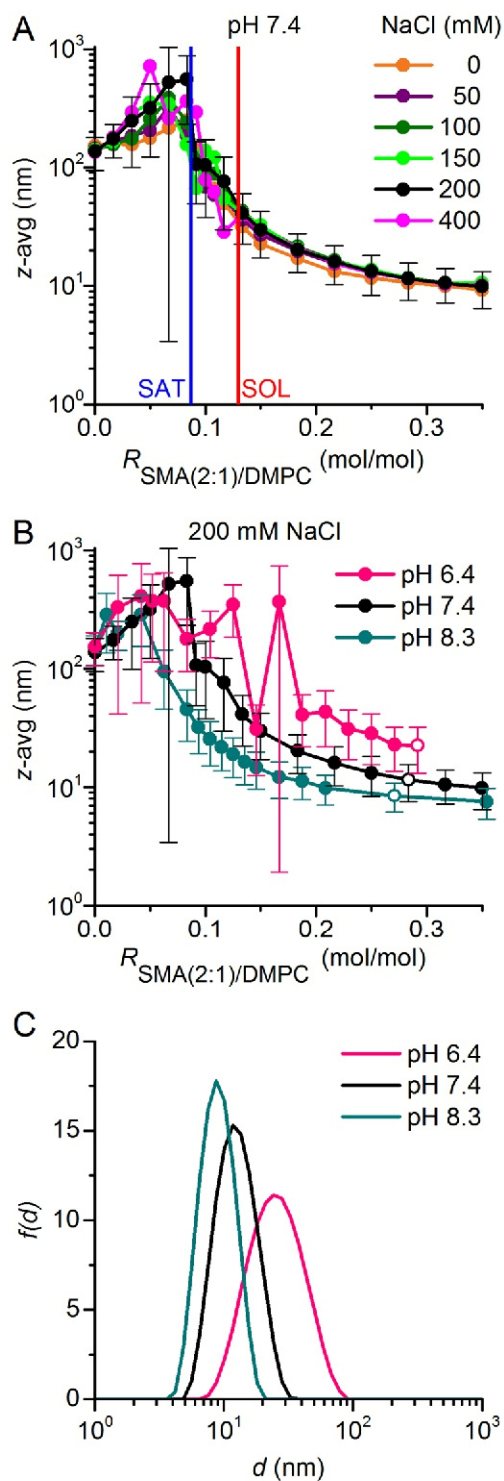


Figure 3. Solubilisation of DMPC vesicles by SMA(2:1) at 30 °C in the presence of different NaCl concentrations and pH values as monitored by DLS. **(A)** z -Average diameters as functions of SMA(2:1)/DMPC molar ratio at pH 7.4 and increasing NaCl concentrations. Vertical lines indicate the SAT and SOL boundaries derived from NMR in the presence of 200 mM NaCl (Fig. 1C). **(B)** z -Average diameters as functions of SMA(2:1)/DMPC molar ratio at 200 mM NaCl and different pH values. Error bars denote peak distribution widths as given by $\sigma = \sqrt{\text{PDI}}$. **(C)** Intensity-weighted particle size distributions, $f(d)$, as functions of pH at similar, completely solubilising SMA(2:1)/DMPC molar ratios as indicated by open circles in **(B)**.

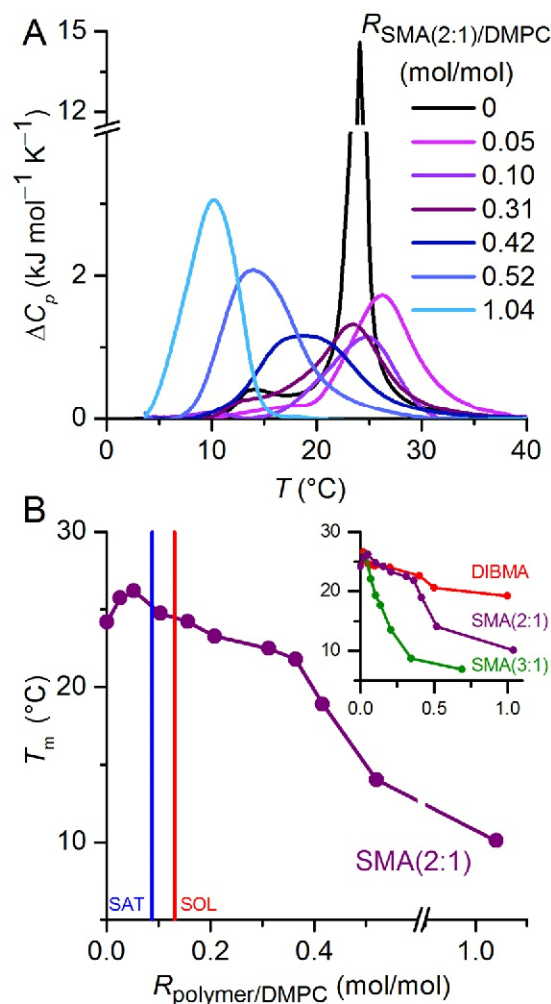


Figure 4. Thermotropic phase behaviour of DMPC upon solubilisation by SMA(2:1) at pH 7.4. **(A)** DSC thermograms showing excess molar isobaric heat capacities, ΔC_p , of 5 mM DMPC initially present in the form of LUVs upon exposure to increasing concentrations of SMA(2:1). **(B)** Gel-to-fluid phase transition temperature, T_m , of 5 mM DMPC in the presence of increasing concentrations of SMA(2:1), SMA(3:1), or DIBMA. SMA(3:1)/DMPC molar ratios were recalculated from Oluwole et al.¹⁸ using the dn/dc value determined in this work (cf. Table 1). Vertical lines in the main panel indicate the SAT and SOL boundaries of SMA(2:1) derived from NMR at 30 °C (Fig. 1C). The same T_m values are shown as functions of polymer/DMPC mass ratios in Supplementary Figure 1.

SMA copolymers, insertion of their planar phenyl moieties into the lipid bilayer is expected to make a substantial contribution to the adsorption of the polymers onto the membrane²⁶. This could render the membrane-adsorbed state of SMA(2:1) relatively stable, thereby reducing the absolute value of $\Delta G_s^{b \rightarrow m, o}$. By contrast, the bulky, branched neopentyl moieties of DIBMA are less easy to intercalate among the lipid acyl chains, which may favour the nanodisc-surrounding over the membrane-adsorbed state.

As noted above, comparisons among the three polymers on a *molar* basis need to be interpreted with caution, since SMA(2:1) ($M_n = 2.7 \text{ kg mol}^{-1}$) is smaller than SMA(3:1) ($M_n = 4.0 \text{ kg mol}^{-1}$) and much smaller than DIBMA ($M_n = 8.4 \text{ kg mol}^{-1}$). To account for these differences in molecular size, we converted the phase boundaries from *molar* ratios (i.e., with units of mol/mol) to *mass* ratios (i.e., g/g). On this *mass* ratio scale, SMA(2:1) is the most efficient solubiliser, followed by DIBMA and SMA(3:1) (Fig. 2C). The observation that SMA(2:1) has a higher equilibrium lipid-solubilisation efficiency than SMA(3:1) is interesting in the light of a recent study¹³ reporting that, among several SMA variants, SMA(2:1) is the preferred choice for solubilising membrane proteins. Specifically, three membrane proteins of different sizes, topologies, and functions have been shown to be most efficiently solubilised by SMA(2:1) in terms of the total amounts, purities, and functionalities of the extracted proteins¹³. Moreover, our equilibrium solubilisation efficiencies correlate with the finding that SMA(2:1) is the most efficient copolymer as regards the solubilisation kinetics of lipid vesicles¹⁵. It should be noted that such a correlation between equilibrium and kinetic results is not trivial, as will be discussed in more detail below (cf. Figures 3B and 5F).

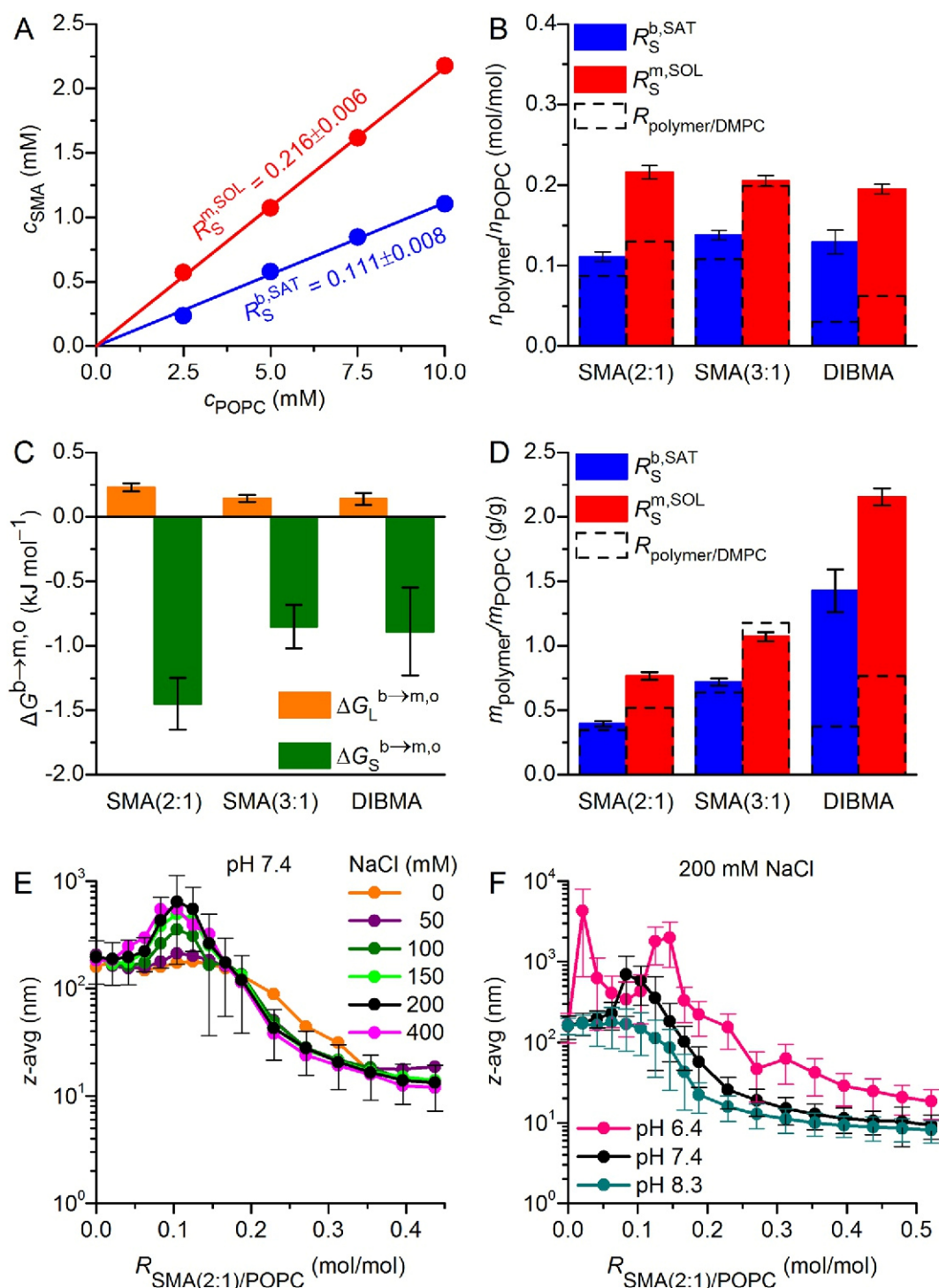


Figure 5. Solubilisation of POPC vesicles by SMA(2:1) at 25 °C as monitored by ^{31}P NMR and DLS. **(A)** Phase diagram of POPC/SMA(2:1) showing the onset (saturation; SAT) and completion (solubilisation; SOL) of solubilisation. Shown are pairs of $c_s^{b,\text{SAT}}$ and $c_s^{m,\text{SOL}}$ (circles) obtained from breakpoints derived from local fits and global fits (solid lines). **(B)** SAT and SOL phase boundaries of SMA(2:1), SMA(3:1), and DIBMA based on copolymer/lipid molar ratios. For comparison, corresponding SAT and SOL phase boundaries determined for DMPC (Fig. 2A) are indicated as dashed bars. **(C)** Transfer free energies of lipid and copolymers, $\Delta G_L^{b \rightarrow m, o}$ and $\Delta G_S^{b \rightarrow m, o}$, respectively, as derived from phase boundaries in (B). **(D)** SAT and SOL phase boundaries of SMA(2:1), SMA(3:1), and DIBMA based on copolymer/lipid mass ratios. For comparison, corresponding SAT and SOL phase boundaries determined for DMPC (Fig. 2C) are indicated as dashed bars. **(E)** z-Average diameters as functions of SMA(2:1)/POPC molar ratio at different NaCl concentrations. **(F)** z-Average diameters as functions of SMA(2:1)/POPC molar ratio at pH values of 6.4, 7.4, and 8.3. Error bars denote peak distribution widths as given by $\sigma = \sqrt{\text{PDI}} z$.

Effects of ionic strength and pH on the equilibrium solubilisation efficiency of SMA(2:1). It has been shown that both ionic strength²⁶ and pH¹⁵ modulate the kinetics of membrane solubilisation by SMA(2:1). However, no data are presently available that report on the effects of these two solution properties on the equilibrium of SMA(2:1)-mediated lipid-bilayer solubilisation. Therefore, we titrated DMPC with SMA(2:1) in the presence of 0–400 mM NaCl at pH 7.4 to study the influence of ionic strength and, in another set of experiments, kept the NaCl concentration at 200 mM and monitored the solubilisation equilibrium at pH values of 6.4, 7.4, and 8.3. Hydrodynamic particle sizes monitored by DLS (Fig. 3A) furnished two major observations when the ionic strength of the buffer was varied: (i) Under subsolubilising conditions, where polymer-coated vesicles tend to aggregate^{16–18}, the apparent particle diameters increased with NaCl concentration. This could be explained by stronger salt screening of the repulsive Coulomb forces that must act among vesicles carrying polyanionic copolymer chains, thus facilitating vesicle aggregation. However, it is important to point out that the increase in particle size with ionic strength suggested by DLS might, at least in part, be only apparent. The calculation of particle sizes from diffusion coefficients is based on the assumption that the particles do not interact with each other. At low ionic strength, this is a poor assumption; in fact, interparticle repulsion then will lead to an overestimation of the diffusion coefficient and an underestimation of the particle size. Hence, the hydrodynamic diameters obtained at elevated ionic strength might reflect the true particle sizes more closely than those determined in the presence of low salt concentrations. (ii) Under conditions of complete solubilisation, there were no differences in nanodisc size among different NaCl concentrations, with a smooth decrease in hydrodynamic diameter¹⁷ down to ~10 nm at SMA(2:1)/DMPC molar ratios in excess of ~0.3. Hence, the solubilisation of DMPC LUVs was not significantly different at low ionic strength as compared with higher salt concentrations. In particular, no shift in the SOL boundary was detected, as one might have expected from the fact that decreasing ionic strength slows down the solubilisation process²⁶.

Contrary to the lack of influence of ionic strength on DMPC solubilisation efficiency and nanodisc size, we observed a pronounced effect upon varying the pH value at a constant salt concentration of 200 mM NaCl (Fig. 3B,C). At pH 6.4, substantially higher concentrations of SMA(2:1) were required for solubilisation than at pH 7.4, where solubilisation was, in turn, less efficient than at pH 8.3. This equilibrium behaviour is in stark contrast with the kinetics of DMPC solubilisation by SMA(2:1), which becomes slower with increasingly alkaline pH¹⁵. The latter observation has been attributed to the effect of pH on the conformation of the copolymer¹⁵; accordingly, SMA(2:1) becomes more charged and less hydrophobic with increasing pH, which results in a more extended chain conformation stabilised by electrostatic repulsion, thereby reducing the driving force for membrane adsorption and solubilisation. The present thermodynamic findings, however, suggest a different, more nuanced picture of the important role of pH-dependent conformational properties of SMA(2:1) in the lipid-solubilisation process: At elevated pH, the reduced effective hydrophobicity of SMA(2:1) appears to slow down the solubilisation of phospholipids from vesicles; once solubilisation has occurred, however, the more extended conformation of the copolymer chains allows for a more efficient encapsulation of solubilised lipids, thereby lowering the minimum amount of SMA(2:1) required for complete solubilisation. In summary, the solubilisation of DMPC LUVs by SMA(2:1) is slower but thermodynamically more efficient at moderately alkaline than at neutral or slightly acidic pH values.

Influence of SMA(2:1) on the gel-to-fluid phase transition of phospholipids. Owing to its main phase-transition temperature of $T_m \approx 24^\circ\text{C}$, DMPC lends itself for analysing thermotropic lipid phase transitions and, thus, membrane-perturbing effects of amphiphilic copolymers with the aid of DSC. Previous DSC studies of DMPC in nanodiscs bounded by SMA(2:1)⁵, SMA(3:1)^{4,18}, or DIBMA¹⁸ have used various buffer conditions and, more critically, different copolymer/lipid ratios, which impedes straightforward comparisons among the three copolymers. Therefore, we investigated the concentration-dependent effects of SMA(2:1) on the thermotropic phase behaviour of DMPC in more detail and compared them with those of SMA(3:1) and DIBMA under identical conditions.

In the absence of copolymer, a highly cooperative gel-to-fluid phase transition typical of DMPC LUVs was observed at 24°C (Fig. 4A). In the presence of SMA(2:1), the thermograms were broadened, and the peak height decreased by a factor of ~10. After a slight increase in T_m at polymer/lipid ratios below $R_S^{b,SAT}$, there was only a marginal downshift in T_m to ~ 23°C upon complete solubilisation of DMPC vesicles by SMA(2:1) (Fig. 4B). Above $R_S^{m,SOL}$, T_m monotonically decreased with increasing SMA(2:1) concentration, with a pronounced kink at an SMA(2:1)/DMPC molar ratio of ~0.4, that is, well within the fully solubilised range. The initial increase in T_m reflects a stabilisation of the gel over the fluid phase, possibly caused by partial dehydration of the membrane surface upon adsorption of the copolymer. Once solubilisation is complete, T_m decreases because the lipid molecules tend to pack more loosely in nanodiscs than in vesicles, which might be due to the intercalation of the copolymer's phenyl moieties^{4,5}. Among the three polymers, SMA(3:1) had the most drastic effect on T_m (Fig. 4B, inset), which suggests a stronger perturbation of lipid acyl-chain packing by this copolymer as compared with SMA(2:1), which has a lower styrene content, and DIBMA, which contains no aromatic groups at all.

The DSC data also highlight two significant differences between polymer-based nanodiscs on the one hand and nanodiscs bounded by membrane scaffold proteins (MSPs) on the other hand: First, lipid-bilayer nanodiscs surrounded by amphiphilic copolymers generally exhibit reduced T_m values indicative of a less densely packed acyl-chain core, whereas MSP nanodiscs have slightly increased T_m values as compared with vesicular membranes²⁷. Second, unlike in the case of MSP-bounded nanodiscs²⁷, repeated DSC scans of the same samples were found to be highly reproducible for all three types of polymer-bounded nanodiscs (data not shown), attesting to their pronounced thermal stability.

In addition to changes in T_m , the transition peak of SMA(2:1)/DMPC nanodiscs monotonously broadened with increasing polymer concentration up to a copolymer/lipid molar ratio of ~0.4 (Fig. 4A). Such broadening

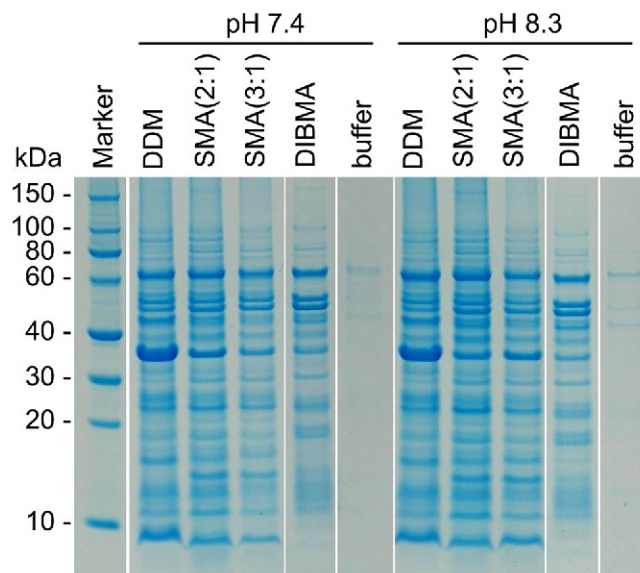


Figure 6. SDS-PAGE showing the solubilisation of *E. coli* BL21(DE3) membranes by 10 mM (0.5% (*w/v*)) DDM, 9.3 mM (2.5% (*w/v*)) SMA(2:1), 6.3 mM (2.5% (*w/v*)) SMA(3:1), or 3.0 mM (2.5% (*w/v*)) DIBMA. Buffer conditions were 50 mM Tris, 200 mM NaCl, 20 °C. Shown are the solubilised membrane-protein fractions after removal of cell debris, intrinsically soluble proteins, and unsolubilised material by serial centrifugation. Data for DDM, SMA(3:1), and DIBMA are reproduced from Oluwole et al.¹⁸ For clarity and conciseness, the gel was cropped as indicated. The full-length gel is presented in Supplementary Figure 2.

has been reported for MSP nanodiscs²⁷ as well as for nanodiscs surrounded by SMA(2:1)⁵, SMA(3:1)^{4,18}, and DIBMA¹⁸ and is readily explained by a decrease in the number of lipid molecules in the “cooperative unit” in nanodiscs as compared with LUVs. In addition to this straightforward explanation, it should be kept in mind that the thermotropic phase behaviour of DMPC molecules that are in close vicinity to the polymer rim most likely differ drastically from that of “bulk” lipids. In an extreme scenario, such lipid molecules could be fluidised even at the lowest experimental temperatures and, then, would be excluded from the observed phase transition. If the thermotropic phase transition of peripheral lipids is not abolished but merely shifted to lower or higher temperatures than that of lipid molecules in the nanodisc centre, the transition peak will be further broadened.

Solubilisation of unsaturated phospholipids by SMA(2:1). To more closely mimic biological membranes containing unsaturated phospholipids, we also investigated the solubilisation of POPC LUVs by SMA(2:1). POPC is an unsaturated zwitterionic phospholipid naturally present in most eukaryotic and some prokaryotic cells²⁸, which therefore is often used as a model membrane lipid for *in vitro* research.

The pseudophase diagram of SMA(2:1) and POPC (Fig. 5A) reveals saturating and solubilising SMA(2:1)/POPC molar ratios of $R_S^{b,SAT} = 0.111 \pm 0.008$ and $R_S^{m,SOL} = 0.216 \pm 0.006$, respectively. Thus, both the SAT and the SOL boundaries of SMA(2:1) are higher for POPC than for DMPC. Comparing these values with those of SMA(3:1) and DIBMA on a *molar* concentration scale unveils only minor differences among their solubilisation efficiencies (Fig. 5B). This is because of compensating differences in the transfer Gibbs free energies of POPC and the three copolymers, as $\Delta G_L^{b \rightarrow m,0}$ is more unfavorable for SMA(2:1) than for SMA(3:1) and DIBMA, whereas $\Delta G_S^{b \rightarrow m,0}$ is more favorable for SMA(2:1) than for SMA(3:1) and DIBMA (Fig. 5C). Again, a different picture emerges when solubilisation efficiencies are compared on a *mass* concentration scale, which may be more relevant for many practical applications: on this scale, it is apparent that SMA(2:1) is the most powerful solubiliser of POPC bilayers, followed by SMA(3:1) and DIBMA (Fig. 5D). The most conspicuous result that emerges from a comparison of POPC and DMPC solubilisation thermodynamics (Fig. 5B,D; dashed) is that the two SMA copolymers are much less susceptible to the effect of chain unsaturation than is DIBMA. Presumably, the increased lateral pressure²⁹ in the acyl-chain region of the lipid bilayer that is due to the presence of a double bond in POPC has a more detrimental effect on the insertion of the bulky aliphatic side chains of DIBMA than on the intercalation of the planar aromatic groups of SMA.

In contrast with the case of DMPC, the solubilisation efficiency of SMA(2:1) toward POPC was slightly impaired at very low ionic strength, that is, in the absence of additional NaCl (Fig. 5E). Under such conditions, the hydrodynamic particle diameter decreased more gradually than in the presence of higher NaCl concentrations. In general, accumulation of a highly negatively charged polymer on or within a membrane will be facilitated by higher ionic strengths because of electrostatic screening²⁶. We hypothesise that, in the case of LUVs composed of the saturated phospholipid DMPC, adsorption and penetration of SMA(2:1) into the lipid bilayer are so strong that a decrease in ionic strength has no significant effect. By contrast, bilayer penetration should be more difficult in the case of POPC because of the increased lateral pressure in the acyl-chain region of the membrane²⁹. Thus, polymer adsorption is weaker at low ionic strengths but becomes stronger as the electrostatic repulsion is

screened at higher salt concentrations. For POPC, we found the same pH dependence as observed for DMPC, that is, the equilibrium solubilisation efficiency was lowest at pH 6.4 and highest at pH 8.3 (Fig. 5F).

Solubilisation of native *E. coli* membranes by SMA(2:1). Both SMA(3:1) and DIBMA solubilise a broad range of membrane proteins directly from *E. coli* membranes but show different pH dependencies¹⁸. After evaluating the equilibrium efficiency of SMA(2:1) in solubilising model lipid vesicles, we were interested in testing its performance on native membranes, which represent chemically heterogeneous, protein-containing targets. While homogenous, well-defined model lipid vesicles enable a quantitative description of the thermodynamics of solubilisation, the extraction of membrane proteins from biological membranes depends not only on their lipid matrix, the composition of which is often poorly defined, but also on the types and contents of the many diverse protein constituents. In general, the solubilisation behaviour of model membranes by detergents is, therefore, not directly transferable to native membranes. This motivated us to extend our previous analysis of SMA(3:1) and DIBMA¹⁸ by determining the protein extraction yields of SMA(2:1) at pH 7.4 and 8.3 and compare them with those of SMA(3:1) and DIBMA under identical conditions (cf. Experimental Section for details). Briefly, we prepared *E. coli* membrane fragments, solubilised proteins, performed SDS-PAGE, and used densitometry to quantify the total amounts of protein extracted by each of the three polymers (Fig. 6).

At both pH values, the protein-solubilisation yield of SMA(2:1) amounted to >90% relative to that of the commonly used detergent *n*-dodecyl- β -D-maltopyranoside (DDM). This underlines the excellent performance of SMA(2:1) in solubilising native membranes, which affords protein yields 10–30% higher than those of SMA(3:1) and DIBMA. Additionally, we found that the solubilisation yield of SMA(2:1) was >10% higher at pH 8.3 than at pH 7.4, which correlates with the above observation that the lipid-solubilisation efficiency of SMA(2:1) under equilibrium conditions is enhanced with increasing pH (Fig. 5F), although solubilisation is slower under such alkaline conditions¹⁵. On a broader note, this highlights the usefulness of *in vitro* lipid-bilayer studies, particularly those performed under equilibrium rather than kinetically controlled conditions, for tuning the solubilisation of more complex, biological membranes containing considerable amounts of proteins. In spite of the overall high protein-extraction yields enabled by all three copolymers, it is also obvious that different copolymers solubilise various proteins to different extents (Fig. 6). In particular, DIBMA tends to preferentially extract larger proteins rather than smaller ones, which could be owed to the fact that this copolymer forms larger nanodiscs than the two SMA variants¹⁸. Finally, it should be noted that these protein-extraction trials were performed at polymer concentrations of 2.5% (*w/v*), which corresponds to the “default” concentration typically used in the literature¹⁴ but is far beyond the SOL boundaries determined using model lipid membranes (cf. Figure 2). Thus, it is conceivable that lower polymer concentrations could be employed for membrane-protein extraction without compromising yield.

Summary and Conclusions

Amphiphilic copolymers that can solubilise proteins and lipids into nanoscale bilayer environments have recently opened new avenues in membrane research. While various types of SMA have been used over the past few years, there is a clear trend in the field to focus on SMA(2:1)¹⁴. This motivated us to undertake a systematic characterisation of the equilibrium membrane-solubilisation behaviour of SMA(2:1) based on approaches previously applied to SMA(3:1)^{16,17} and DIBMA¹⁸. Herein, we showed that

- SMA(2:1) is an efficient solubiliser of lipid membranes, as indicated by low saturating and solubilising polymer/lipid ratios and the corresponding vesicle-to-nanodisc transfer Gibbs free energies;
- experimental conditions are important determinants of solubilisation behaviour, as SMA(2:1) is, from a thermodynamic viewpoint, more efficient at pH 8.3 than at near-neutral pH values, even though the solubilisation process is slower at elevated pH;
- SMA(2:1) represents a milder membrane solubiliser than the more hydrophobic SMA(3:1) variant but is harsher than the more hydrophilic, aliphatic copolymer DIBMA, as gauged from their effects on lipid thermotropic phase behaviour;
- the total amounts of membrane proteins extracted from native *E. coli* membranes are highest for SMA(2:1), although some proteins may be solubilised more efficiently or more mildly by DIBMA or, possibly, other copolymers.

References

1. Tonge, S. R. & Tighe, B. J. Responsive hydrophobically associating polymers: a review of structure and properties. *Adv. Drug Deliv. Rev.* **53**, 109–122 (2001).
2. Knowles, T. J. *et al.* Membrane proteins solubilized intact in lipid containing nanoparticles bounded by styrene maleic acid copolymer. *J. Am. Chem. Soc.* **131**, 7484–7485 (2009).
3. Dörr, J. M. *et al.* The styrene/maleic acid copolymer: a versatile tool in membrane research. *Eur. Biophys. J.* **45**, 3–21 (2016).
4. Orwick, M. C. *et al.* Detergent-free formation and physicochemical characterization of nanosized lipid-polymer complexes: Lipodisq. *Angew. Chem. Int. Ed.* **51**, 4653–4657 (2012).
5. Jamshad, M. *et al.* Structural analysis of a nanoparticle containing a lipid bilayer used for detergent-free extraction of membrane proteins. *Nano Res.* **8**, 774–789 (2015).
6. Gulati, S. *et al.* Detergent-free purification of ABC (ATP-binding-cassette) transporters. *Biochem. J.* **461**, 269–278 (2014).
7. Jamshad, M. *et al.* G-protein coupled receptor solubilization and purification for biophysical analysis and functional studies, in the total absence of detergent. *Biosci. Rep.* **35**, 1–10 (2015).
8. Logez, C. *et al.* Detergent-free isolation of functional G protein-coupled receptors into nanometric lipid particles. *Biochemistry* **55**, 38–48 (2016).
9. Dörr, J. M. *et al.* Detergent-free isolation, characterization, and functional reconstitution of a tetrameric K⁺ channel: the power of native nanodiscs. *Proc. Natl. Acad. Sci. USA.* **111**, 18607–18612 (2014).

Supplementary Information

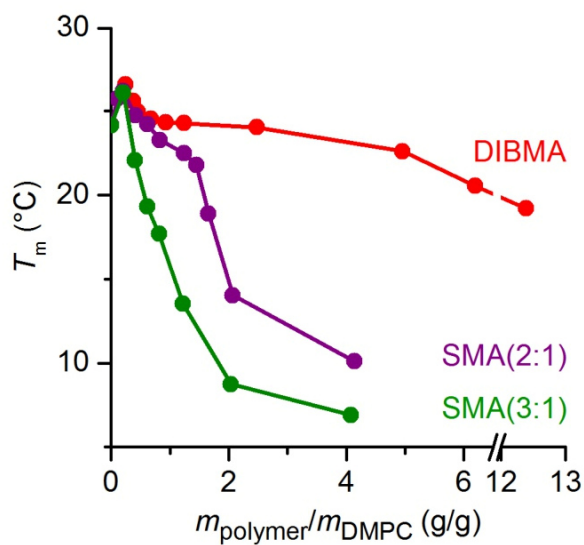
Thermodynamics of nanodisc formation mediated by styrene/maleic acid (2:1) copolymer

Anne Grethen¹, Abraham Olusegun Oluwole^{1,2}, Bartholomäus Danielczak¹, Carolyn Vargas¹ & Sandro Keller^{1,*}

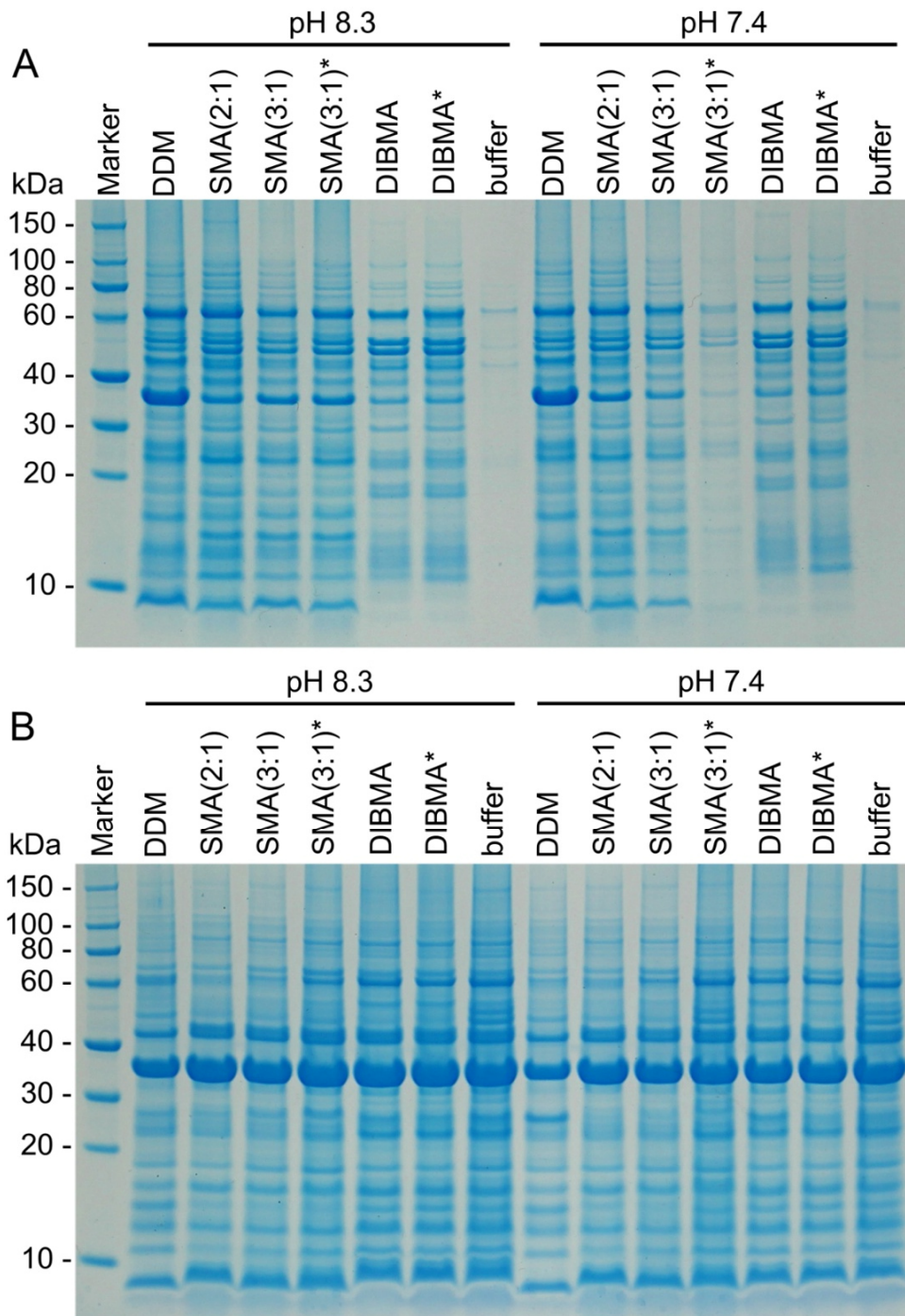
¹ Molecular Biophysics, University of Kaiserslautern, 67663 Kaiserslautern, Germany

² Department of Chemistry, University of Ibadan, 200284 Ibadan, Nigeria

[*mail@sandrokeller.com](mailto:mail@sandrokeller.com)



Supplementary Figure 1. Gel-to-fluid phase transition temperatures, T_m , as functions of polymer/DMPC mass ratios. The same T_m values as functions of polymer/DMPC molar ratios are shown in Fig. 4B in the main text.



Supplementary Figure 2. Full-length SDS-PAGE showing the solubilisation of *E. coli* BL21(DE3) membranes by 10 mM (0.5% (w/v)) DDM, 9.3 mM (2.5% (w/v)) SMA(2:1), 6.3 mM (2.5% (w/v)) SMA(3:1), or 3.0 mM (2.5% (w/v)) DIBMA. (A) Solubilised membrane-protein fractions (i.e., supernatants) after removal of unsolubilised material by ultracentrifugation. Data for DDM, SMA(3:1), and DIBMA are reproduced from Oluwole et al. *Angew. Chem. Int. Ed.* **56**, 1919–1924 (2017). A cropped version of this gel is shown in Figure 6 of the main text. (B) Unsolubilised membrane fragments (i.e., resuspended pellets) after ultracentrifugation for 1 h at 100,000 g. Note that relative solubilisation yields are generally low under these conditions but increase with decreasing amounts of *E. coli* membranes used for extraction. *Solubilisation trials performed at an elevated ionic strength of 500 mM NaCl as compared with standard buffer conditions (i.e., 50 mM Tris, 200 mM NaCl, 20°C). Reduced protein-extraction yields were most likely due to aggregation of SMA(3:1) at 500 mM NaCl (Scheidelaar et al. *Biophys. J.* **111**, 1974–1986 (2016)).

2.2. Associated results:

The composition of SMA(2:1) nanodiscs

In this section, the study of fluorescently labelled SMA(2:1) nanodiscs at near-physiological conditions by size exclusion chromatography (SEC) is reported. In *Manuscript 1*, it was shown that the solubilisation efficiency of SMA(2:1) decreases at acidic pH. Accordingly, herein, the equilibrium composition of SMA(2:1) nanodiscs was elucidated by SEC at different pH values and polymer/lipid molar ratios.

2.2.1. Experimental section

SEC was performed on an Äkta Purifier 10 system equipped with a Superdex 200 Increase 10/300 GL column and a UV detector (both GE Healthcare, Freiburg, Germany) at 8°C. Samples containing 4 mM large unilamellar vesicles (LUVs) formed by DMPC and 0.52–1.56 mM SMA(2:1), corresponding to SMA(2:1)/DMPC molar ratios of 0.13, 0.2, 0.3, and 0.4, were used. Bare SMA(2:1) samples at corresponding concentrations (i.e., in the absence of lipid) were used as control samples. The polymer and respective nanodisc samples were prepared in either Tris buffer (pH 7.4 or 8.3) or phosphate buffer (pH 6.4) and incubated for at least 16 h at 8°C. Fluorescently labelled SMA(2:1) nanodiscs at a DMPC/NBD-PE (*N*-(7-nitrobenz-2-oxa-1,3-diazol-4-yl)-1,2-dihexadecanoyl-*sn*-glycero-3-phosphoethanolamine, $\lambda_{\text{ex}} = 463 \text{ nm}^{85}$) ratio of 98:2 mol% and a SMA(2:1)/lipid molar ratio of 0.3 were prepared as described in *Manuscript 2*. The SEC column was equilibrated with 3 column volumes (CV) precooled buffer, then 100 μL -aliquots of nanodiscs or polymer were injected at a flow rate of 0.5 mL/min. UV absorbance was measured at 260 nm for SMA(2:1) detection and at 463 nm for NBD-PE detection of labelled nanodiscs. Each sample was measured in triplicates. Fluorescently labelled nanodiscs were collected in 250 μL -fractions. Then, the two resulting peaks in the SEC profile were pooled, concentrated using Amicon tubes (Merck, Darmstadt, Germany) with a 10 kDa cut-off, and re-injected at a flow rate of 0.5 mL/min. To quantify the UV absorbance for each sample, respective peaks were integrated.

2.2.2. The SMA(2:1) nanodisc elution profile

To monitor the elution behaviour of SMALPs at near-physiological conditions (50 mM Tris, 200 mM NaCl, pH 7.4) by SEC, SMA(2:1)/DMPC nanodiscs were fluorescently labelled using the phospholipid NBD-PE. This enabled the simultaneous UV detection of the polymer at

260 nm, caused by aromatic styrene moieties, and NBD-PE at 463 nm, corresponding to the excitation wavelength λ_{ex} of NBD. It has to be noted that, herein, the detection of fluorescent lipid was extrapolated to the total phospholipid content of the sample.

The polymer detection in SMA(2:1) nanodiscs (grey line) gave rise to two distinct peaks at 260 nm, a large peak at ~ 13 mL (peak 1) and a small peak at ~ 19 mL (peak 2) (Figure 2.1). At identical conditions and concentrations, SMA(2:1) polymer (i.e., bare polymer without added lipid) showed one large peak with a peak maximum at ~ 18 mL (green line), which is in close agreement with the nanodiscs' peak 2. NBD-PE absorbance at 463 nm showed a peak at the same elution volume than nanodisc peak 1 (blue line). These findings demonstrate that, for SMA(2:1) nanodiscs, peak 1 represents the nanodisc population, containing, under the given conditions, approximately 60% of the polymer concentration and the total concentration of labelled lipids, and, thus, the total phospholipid concentration. Peak 2 corresponds to a fraction that contains excess or "free" SMA(2:1) copolymer, as previously shown.⁷⁸

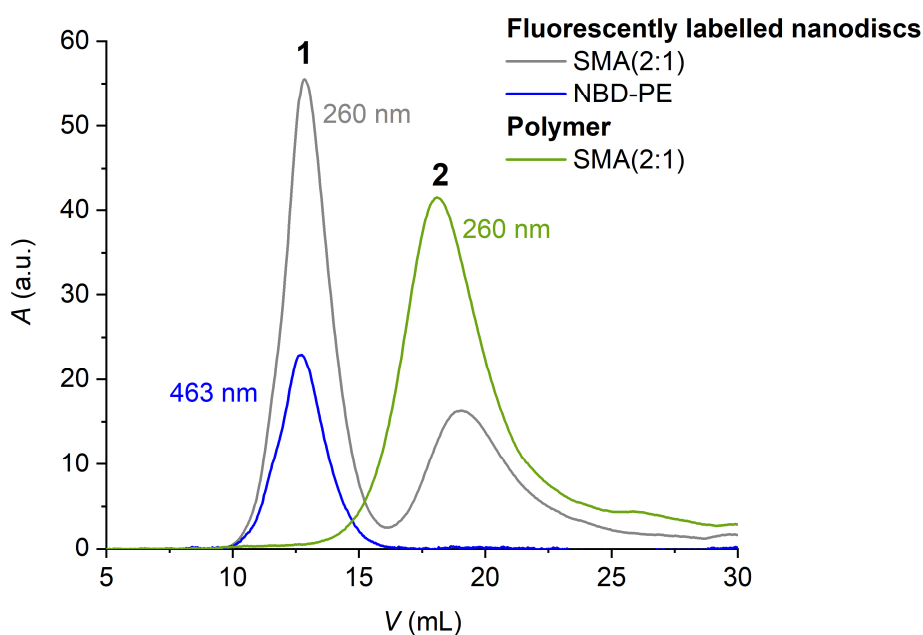


Figure 2.1. SEC elution profiles of fluorescently labelled SMA(2:1) nanodiscs and SMA(2:1) copolymer as monitored by UV absorbance at 260 nm (grey and green line) and 463 nm (blue line) using a Superdex 200 Increase 10/300 GL column at pH 7.4 and 8°C.

To further characterise the elution behaviour of SMA(2:1) nanodiscs, peak 1 and 2 were collected, pooled, concentrated, and re-injected onto the column (Figure 2.2). Normalised elution profiles showed that the re-injected nanodisc fraction (red line) and "free" polymer fraction (purple line) elute at the same volume than the respective peaks of the total nanodisc

sample (grey line). The monomodal size distribution of the re-injected nanodisc fraction is an indicator that the nanodisc population is an inert fraction that is not in equilibrium with the excess polymer fraction. Accordingly, peak 2 possibly represents an inactive polymer fraction, that is, under the given experimental conditions, an SMA(2:1) fraction that does not interact with the phospholipids and, thus, is not involved in the nanodisc formation.

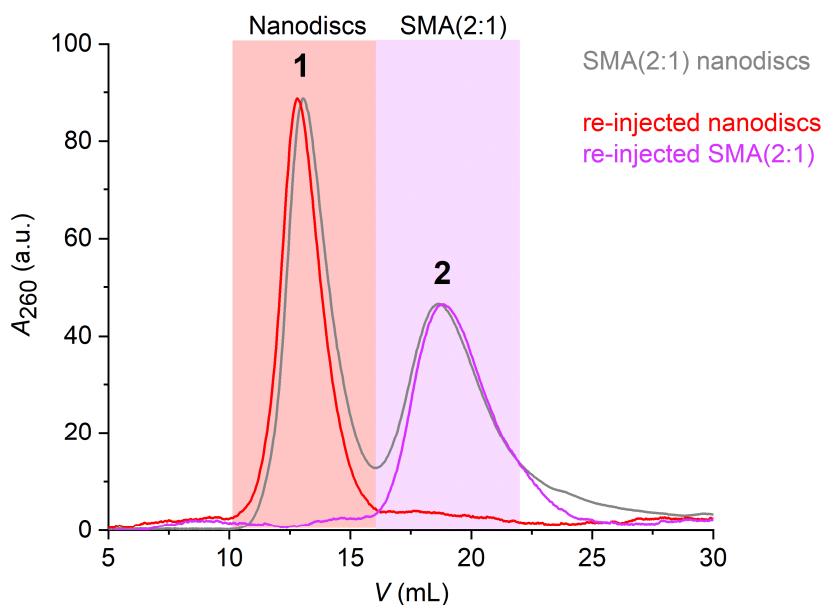


Figure 2.2. Representative and normalised SEC elution profiles at 260 nm of the total SMA(2:1) nanodisc sample (grey line), the re-injected peak 1, corresponding to the nanodisc fraction (red line), and the re-injected peak 2, corresponding to the “free” SMA(2:1) fraction (purple line).

2.2.3. pH-dependent SMA(2:1) nanodisc composition

In *Manuscript 1*, it was shown that the equilibrium solubilisation efficiency is pH-dependent. In particular, a superior solubilising power of SMA(2:1) became apparent at slightly alkaline pH. This finding aroused the interest in elucidating the effect of pH on SMA(2:1)/DMPC nanodisc composition by SEC.

At all pH values, peak 1 shifted to larger elution volumes (V), and thus, to reduced molecular weights (M_w), with increasing SMA(2:1)/DMPC molar ratios R (Figure 2.3.a–c). This demonstrates the expected decrease in nanodisc size with increasing R or polymer concentrations, as shown in *Manuscript 1*. For different R values and at a specific pH value, peak 2 eluted at comparable V . Furthermore, the signal intensity of UV absorbance at 260 nm increased with increasing R , because it is concentration-dependent and predominantly arises from SMA(2:1).

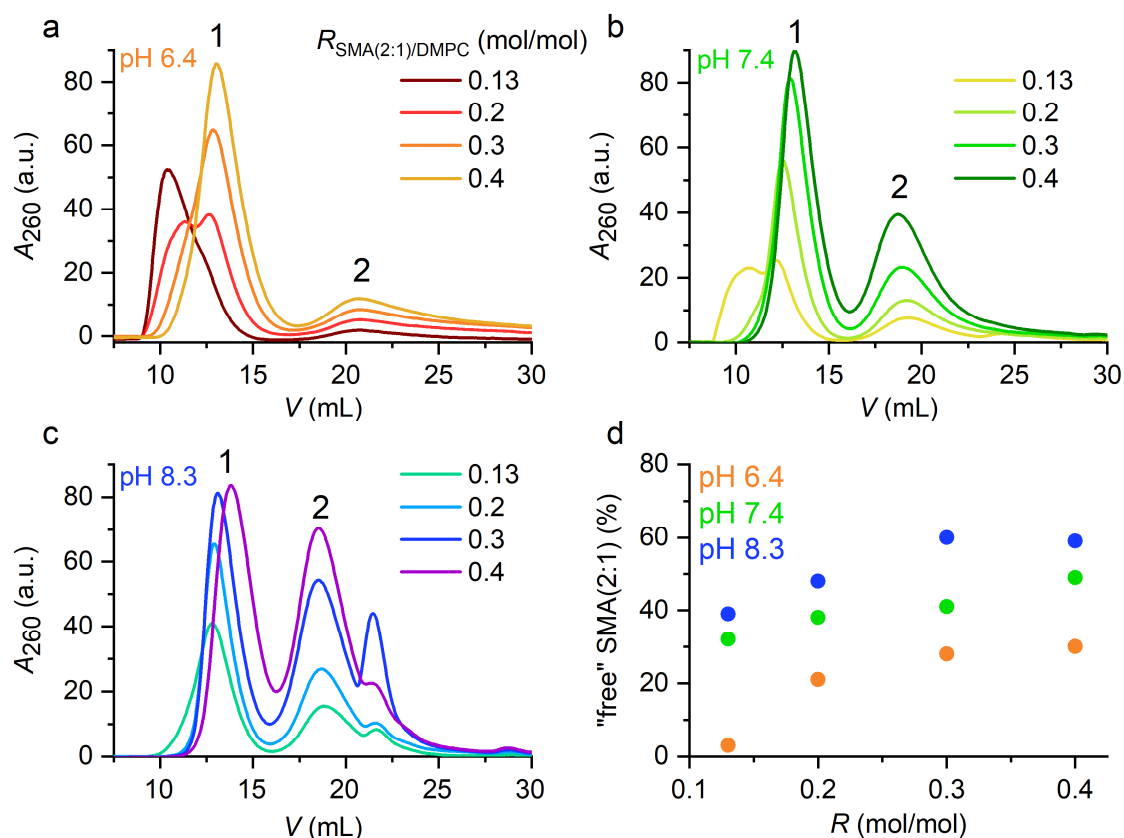


Figure 2.3. SEC elution profiles of SMA(2:1) nanodiscs for different SMA(2:1)/DMPC molar ratios, R , and (a) pH 6.4, (b) pH 7.4, and (c) pH 8.3 as monitored by UV absorbance at 260 nm and 8°C. (d) "Free" or excess SMA(2:1) content (%) compared with the amount of polymer involved in nanodisc formation, as functions of pH and R .

At pH 6.4, the nanodisc sample of $R = 0.13$ eluted at the specific column exclusion volume of ~ 8 mL, indicating the presence of large particles such as vesicles or polymer/lipid aggregates. This suggests that, under these conditions, nanodisc formation was not complete. At $R = 0.2$, a bimodal distribution in the range of 8–15 mL became apparent, indicating the presence of two distinct populations of non-solubilised vesicles and nanodiscs. With further increasing polymer concentrations, the nanodisc peak became more pronounced and was shifted to larger V , underlining the complete solubilisation and decrease in nanodisc size. To compare, at pH 7.4, $R = 0.13$ was the only nanodisc sample showing two peaks at 8–14 mL, whereas at pH 8.3, a unimodal distribution was observed at $R = 0.13$, revealing the complete solubilisation of vesicles at low R . It has to be noted that at pH 7.4 and at 30°C (i.e., above the phase transition temperature, T_m , of DMPC), $R = 0.13$ corresponds to the SOL boundary of liquid-crystalline SMA(2:1)/DMPC mixtures, as determined in *Manuscript 1*. It was previously shown that the solubilisation of gel-phase DMPC by SMA(3:1) is more efficient than at liquid-crystalline DMPC.⁴⁹ Here, SEC experiments were performed below T_m at 8°C, it is thus very

plausible that the SOL boundary was shifted to lower polymer concentrations than at 30 °C. Nevertheless, the findings are in close agreement with DLS data performed at 30°C in the course of the manuscript, showing that at pH 8.3, the solubilisation set in at lower polymer concentrations than at pH 7.4 and 6.4.

At a specific R value, the elution volume of peak 2, corresponding to “free” polymer, was shifted from ~21 mL at pH 6.4 to ~18.5 mL at pH 8.3. At alkaline pH, SMA(2:1) adapts an extended chain conformation due to the repulsive forces of anionic maleic acid moieties, and thus, elutes at a smaller V (i.e., larger M_w) than the collapsed SMA(2:1) polymer chains at acidic pH values.³⁹

A quantitative analysis of the SEC elution profiles was performed by integration of the total UV absorbance and subsequent calculation of the “free” SMA(2:1) content compared with the polymer concentration involved in nanodisc formation (Figure 2.3.d). It was found that, for all pH values, the “free” polymer content increased with elevated R . Furthermore, at identical R , excess SMA(2:1) concentrations increased from acidic to alkaline pH. These findings suggest that more polymer is involved in nanodisc formation at pH 6.4 than at pH 8.3. Again, this can be explained by Coulombic screening of the polymers’ negative charges at acidic pH that leads to a compact conformation and, thus, a reduced membrane affinity. Accordingly, it is suggested that the increased polymer concentration involved in nanodisc formation also causes the increased nanodisc size at acidic pH.

Although the total UV absorbance of nanodiscs was expected to be constant at specific R over the pH range, an increase of 10–30% from pH 6.4 to 8.3 was observed. To exclude polymer concentration differences over the pH range, concentrations of SMA(2:1) stock solutions were, after concentration determination by refractometry, validated by UV/VIS spectrometry (data not shown). There are, however, two plausible explanations for the observed differences. First, absorption spectra are dependent on the chemical environment of the chromophore, which is, in this case, SMA(2:1).⁸⁶ Accordingly, solvent properties such as pH or the close vicinity of polymer and phospholipids in nanodiscs can cause an absorbance shift. Second, a common drawback of SEC is the unspecific binding of proteins or other sample constituents to the column matrix.⁸⁷ At acidic pH, SMA(2:1) might more strongly interact with the column material or partially precipitate and, thus, no longer contribute to the UV absorbance detected by SEC. Arginine might be an effective additive to reduce these

unspecific interactions.^{88,89} Nevertheless, it can be concluded that the decrease in total UV absorbance does not entirely compensate the pH-dependent effect on SMA(2:1) composition. Accordingly, the observed effect might be less pronounced or attenuated by column interactions, but still stays valid.

3. Lipid transfer behaviour and effective charge of SMA(2:1) nanodiscs

Summary (Manuscript 2)

Time-resolved Förster resonance energy transfer (TR-FRET) was used to quantify the lipid transfer kinetics of SMA(2:1)-bounded nanodiscs. To this end, fluorescently labelled and unlabelled SMA(2:1)/DMPC nanodiscs were mixed, leading to a random distribution of the FRET pair NBD-PE and Rh-PE among the total nanodisc concentration. As a result, NBD-PE emission was quenched and the donor fluorescence emission increased. It was shown that, similarly to SMA(3:1) nanodiscs, lipid molecules are predominantly transferred by nanodisc collisions. Interparticle diffusion through the aqueous phase only plays a significant role at low lipid concentrations. At similar conditions, collisional lipid transfer among SMA(2:1) nanodiscs was 40-fold slower than among SMA(3:1) nanodiscs. This is explained by the increased charge density of SMA(2:1) over SMA(3:1), leading to stronger Coulombic repulsions among polymer chains, and thus, less frequent collisions among SMA(2:1) nanodiscs.

Furthermore, the effect of ionic strength, I , on collisional lipid transfer of SMA(2:1) nanodiscs was studied. Accordingly, TR-FRET of SMA(2:1) nanodiscs was measured in the presence of 50, 100, 200, or 400 mM NaCl. With increasing NaCl concentrations, and thereby, ionic strength I , the NBD-PE quenching rate increased. This finding was expected, because decreasing Coulombic repulsions of the polymer's carboxylate groups leads to an increased nanodisc collision rate and thus accelerates their lipid transfer. To quantitatively describe this behaviour and yield effective nanodisc charge numbers, the collisional lipid-exchange rate constant, k_{col} , was fitted as a function of I using the Debye–Hückel limiting law and various extended versions. Best-fit curves showed that the Debye–Hückel limiting law describes the curve only reasonably well at low salt concentrations. An empirical extension, the Davies equation, is also valid at higher I and thus described the increase in k_{obs} better than the Debye–Hückel limiting law. From the Davies equation, the effective nanodisc charge number yielded $z = -3.6 \pm 0.4$. This result should however be interpreted with caution, because the equation is based on various assumptions that are invalid for polyanionic nanodiscs, such as the point charge description of the central ion. Therefore, another extension of the Debye–Hückel limiting law that takes into account the finite size of the nanodiscs was employed, yielding a reasonably good agreement between experimental and fitted data with an effective nanodisc charge of

$z = -33 \pm 11$. Although this approximated effective charge is still one order of magnitude lower than the expected nominal charge, it is more realistic than the nanodisc charge obtained by the Davies equation. This is because the effective nanodisc charge represents the local charge at the region of impact upon collision rather than the global nanodisc charge.

Finally, k_{obs} values of different membrane-mimetic systems were compared. Collisional lipid transfer was, as described earlier, two orders of magnitude slower among SMA(2:1) nanodiscs than among SMA(3:1), but still two to three orders of magnitude faster than among nanodiscs surrounded by a membrane scaffold protein (MSP) or large unilamellar vesicles (LUVs). This underlines that, in general, SMA nanodiscs are highly dynamic rather than kinetically trapped assemblies.

3.1. Manuscript 2

Role of Coulombic Repulsion in Collisional Lipid Transfer Among SMA(2:1)-Bounded Nanodiscs

Anne Grethen, David Glueck, and Sandro Keller

Journal of Membrane Biology, **2018**, 251, 443

Contribution

For this work, I designed, performed, analysed, and interpreted all TR-FRET experiments. I created all the figures and wrote the original draft of the manuscript.

Reprinted by permission from Springer Nature: Springer, JOURNAL OF MEMBRANE BIOLOGY, Role of Coulombic Repulsion in Collisional Lipid Transfer Among SMA(2:1)-Bounded Nanodiscs, Grethen A., Glueck D., Keller S. © (2018)



Role of Coulombic Repulsion in Collisional Lipid Transfer Among SMA(2:1)-Bounded Nanodiscs

Anne Grethen¹ · David Glueck¹ · Sandro Keller¹

Received: 26 October 2017 / Accepted: 24 February 2018
© Springer Science+Business Media, LLC, part of Springer Nature 2018

Abstract

Styrene/maleic acid (SMA) and related copolymers are attracting great interest because they solubilise membrane proteins and lipids to form polymer-encapsulated nanodiscs. These nanodiscs retain a lipid-bilayer core surrounded by a polymer rim and can harbour a membrane protein or a membrane-protein complex. SMA exists in different styrene/maleic acid molar ratios, which results in differences in hydrophobicity and solubilisation properties. We have recently demonstrated fast collisional lipid transfer among nanodiscs encapsulated by the relatively hydrophobic copolymer SMA(3:1). Here, we used time-resolved Förster resonance energy transfer to quantify the lipid-transfer kinetics among nanodiscs bounded by SMA(2:1), a less hydrophobic copolymer that is superior in terms of lipid and membrane-protein solubilisation. Moreover, we assessed the effects of ionic strength and, thereby, the role of Coulombic repulsion in the exchange of lipid molecules among these polyanionic nanodiscs. Collisional lipid transfer was slower among SMA(2:1) nanodiscs ($k_{\text{col}} = 5.9 \text{ M}^{-1} \text{ s}^{-1}$) than among SMA(3:1) nanodiscs ($k_{\text{col}} = 222 \text{ M}^{-1} \text{ s}^{-1}$) but still two to three orders of magnitude faster than diffusional lipid exchange among protein-encapsulated nanodiscs or vesicles. Increasing ionic strength accelerated lipid transfer in a manner predicted by the Davies equation, an empirical extension of the Debye–Hückel limiting law, or an extended equation taking into account the finite size of the nanodiscs. Using the latter approach, quantitative agreement between experiment and theory was achieved for an *effective* nanodisc charge number of $z \approx -33$, which is an order of magnitude less than their *nominal* overall charge.

Keywords Davies equation · Debye–Hückel theory · Lipid exchange · Polymer nanodiscs · SMALPs

Introduction

Various styrene/maleic acid (SMA) copolymers (Tonge and Tighe 2001) are able to solubilise membrane proteins from native or artificial membranes to form SMA-bounded nanodiscs consisting of proteins, lipids, and a copolymer belt (Knowles et al. 2009). These nanodiscs or SMA/lipid particles (SMALPs) retain a lipid bilayer core, and their formation is independent of conventional detergents (Orwick

et al. 2012; Dörr et al. 2016). Owing to these advantageous properties, SMALPs are increasingly recognised as a promising platform for rendering membrane proteins amenable to structural (Bersch et al. 2017; Broecker et al. 2017; Parmar et al. 2017), biophysical (Orwick-Rydmark et al. 2012; Dörr et al. 2014), and functional (Gulati et al. 2014; Logez et al. 2016) characterisation in a native-like environment. More recently, diisobutylene/maleic acid (DIBMA) has been shown to solubilise membrane proteins in a similar but milder fashion and to be compatible with UV spectroscopy and divalent cations (Grethen et al. 2017; Oluwole et al. 2017).

Rather than being static, kinetically trapped assemblies, SMALPs have turned out to be highly dynamic colloids that readily exchange membrane proteins and lipids. For instance, polymer-bounded nanodiscs can be used to transfer membrane proteins to a lipidic cubic phase for crystal growth and subsequent structure determination by X-ray crystallography (Broecker et al. 2017). Along the same lines, phospholipid

✉ Sandro Keller
mail@sandrokeller.com

Anne Grethen
grethen@rhrk.uni-kl.de

David Glueck
dglueck@rhrk.uni-kl.de

¹ Molecular Biophysics, Technische Universität Kaiserslautern (TUK), Erwin-Schrödinger-Str. 13, 67663 Kaiserslautern, Germany

molecules embedded in these nanodiscs can re-integrate into large unilamellar vesicles (LUVs) (Cuevas Arenas et al. 2016) or lipid monolayers at the air/water interface (Hazell et al. 2016). Recently, we have observed fast collisional lipid transfer among nanodiscs bounded by SMA(3:1), that is, a rather hydrophobic copolymer variant having a 3:1 molar ratio of styrene to maleic acid moieties (Cuevas Arenas et al. 2017). The exchange of lipids among SMA(3:1) nanodiscs is fast not only relative to other bilayer-forming colloids such as LUVs or protein-encapsulated nanodiscs but also on an absolute scale, considering that, owing to the many carboxylate groups in SMA, SMALPs are polyanionic particles that must experience substantial Coulombic repulsion.

To date, no lipid-exchange experiments have been reported for SMA(2:1), which is a more efficient solubiliser of both lipids (Grethen et al. 2017) and proteins (Morrison et al. 2016; Grethen et al. 2017) and, therefore, is emerging as the default copolymer for membrane-protein studies (Lee et al. 2016). Owing to its composition, SMA(2:1) is less hydrophobic and has an even higher charge density than SMA(3:1), which is expected to slow down the collisional exchange of phospholipids. To test this hypothesis and unravel the role of Coulombic repulsion, we explored the effect of ionic strength on the lipid-transfer kinetics among SMA(2:1) nanodiscs containing the zwitterionic phospholipid 1,2-dimyristoyl-*sn*-glycero-3-phosphocholine (DMPC). To this end, we used time-resolved Förster resonance energy transfer (TR-FRET) to quantify the lipid-exchange kinetics at different NaCl concentrations. Our results show that lipid exchange among SMA(2:1) nanodiscs is slower than among SMA(3:1) nanodiscs but still much faster than among other bilayer-based membrane mimics and that increasing ionic strength enables faster collisional lipid transfer as best described by the Davies equation and an extended Debye–Hückel equation accounting for the finite size of the nanodiscs.

Materials and Methods

Materials

DMPC was a kind gift from Lipoid (Ludwigshafen, Germany), *N*-(7-nitrobenz-2-oxa-1,3-diazol-4-yl)-1,2-dihexadecanoyl-*sn*-glycero-3-phosphoethanolamine (NBD-PE) was obtained from Fisher Scientific (Schwerte, Germany), and *N*-(lissamine rhodamine B sulphonyl)-1,2-dihexadecanoyl-*sn*-glycero-3-phosphoethanolamine (Rh-PE) from Biotium (Fremont, USA). SMA(2:1) copolymer solution (hydrolysed from styrene/maleic acid anhydride 2:1, tradename XIRAN SZ30010) was a kind gift from Polyscope (Geleen, Netherlands). Chloroform was from Fisher Scientific, NaCl from VWR (Darmstadt, Germany), and

tris(hydroxymethyl)aminomethane (Tris) from Carl Roth (Karlsruhe, Germany). All chemicals were obtained in the highest purity available.

Preparation of SMA(2:1) Stock Solution

SMA(2:1) is a random copolymer with a styrene/maleic acid molar ratio of 2:1, a mass-average molar mass of $M_w = 7 \text{ kg mol}^{-1}$, a number-average molar mass of $M_n = 2.7 \text{ kg mol}^{-1}$, and, thus, a dispersity of $M_w/M_n = 2.6$. Stock solutions of SMA(2:1) were prepared as described elsewhere (Vargas et al. 2015; Cuevas Arenas et al. 2016; Grethen et al. 2017). Briefly, 3 mL of SMA(2:1) copolymer solution was dialysed against buffer (50 mM Tris, pH 7.4) using a 5-mL QuixSep dialyser (Membrane Filtration Products, Seguin, USA) and a Spectra/Por 3 dialysis membrane (Spectrum Laboratories, Rancho Dominguez, USA) with a molar-mass cut-off of 3.5 kg mol^{-1} . Dialysis was performed for 24–36 h under gentle stirring with buffer exchange after 16 h. Dialysed SMA(2:1) was filtered through a 0.22- μm poly(vinylidene fluoride) (PVDF) filter (Carl Roth, Karlsruhe, Germany). Final SMA(2:1) concentrations were determined by refractometry on an Abbemat 500 (Anton Paar, Graz, Austria) using a molar refractive index increment of $dn/dc = 0.53 \text{ M}^{-1}$. Samples were stored at room temperature ($\sim 20^\circ \text{C}$).

Preparation of SMA(2:1) Nanodiscs

Fluorescently labelled SMALPs were produced by suspending dry lipid powders in chloroform and mixing these solutions in a dark glass vial at 98:1:1 mol% of DMPC, NBD-PE, and Rh-PE, respectively. At this mixing ratio, NBD-PE emission ($\lambda_{\text{ex}} = 475 \text{ nm}$, $\lambda_{\text{em}} = 530 \text{ nm}$) is efficiently quenched by FRET to Rh-PE ($\lambda_{\text{ex}} = 560 \text{ nm}$, $\lambda_{\text{em}} = 582 \text{ nm}$) (Nichols and Pagano 1982). The lipid mixture was dried in a rotary evaporator at 60°C and 20 kPa for 2 h and incubated in a desiccator at room temperature and 5 Pa for 16 h to remove traces of chloroform. The dry lipid film was suspended in 2.4 mL buffer (50 mM Tris, pH 7.4), and 10 freeze/thaw cycles were performed to produce multilamellar vesicles (MLVs). A stock suspension of labelled SMALPs was formed by incubating the MLVs with SMA(2:1) at 30°C for 16 h to yield final concentrations of 14.9 mM total lipid and 2.4 mM SMA(2:1). These concentrations correspond to an SMA(2:1)/lipid molar ratio of 0.16, which is above the minimal ratio required for complete solubilisation (Grethen et al. 2017). To produce a stock suspension of unlabelled SMALPs, DMPC powder was suspended in buffer (50 mM Tris, pH 7.4) and thoroughly mixed to produce DMPC MLVs without fluorescent lipids. These MLVs were solubilised at 30°C for 16 h to yield final concentrations of $\sim 45 \text{ mM}$ DMPC and $\sim 7 \text{ mM}$ SMA(2:1), which

corresponds to an SMA(2:1)/lipid molar ratio of ~ 0.16 . For each measurement series, labelled SMALPs were diluted to a final concentration of 0.5 mM total lipid and unlabelled SMALPs to final concentrations of 30, 20, 10, 5, 2.5, 1, and 0.5 mM DMPC. During this dilution step, NaCl was added from a buffered stock solution (2 M NaCl, 50 mM Tris, pH 7.4) to reach final NaCl concentrations of 50, 100, 200, or 400 mM. To confirm complete solubilisation, dynamic light scattering (DLS) experiments were performed on a Zetasizer Nano S90 (Malvern Instruments, Malvern, UK) coupled to a 633 nm He–Ne laser and a photodetector mounted at an angle of 90° . Measurements were carried out in a 45- μ L quartz glass cuvette with a 3 mm \times 3 mm cross-section (Hellma Analytics, Müllheim, Germany) at 30 °C. These measurements yielded z -average particle sizes and associated size-distribution widths of (24 ± 4) nm for both labelled and unlabelled SMALPs at all NaCl concentrations. We have previously shown that the hydrodynamic diameters of SMALPs are independent of ionic strength (Grethen et al. 2017).

TR-FRET

TR-FRET was performed on an SF.3 stopped-flow apparatus (Applied Photophysics, Leatherhead, UK) coupled to a right-angle photomultiplier. NBD-PE was excited by a (470 ± 20) nm light-emitting diode (LED) with the current set to 20 mA using a 2.0-OD attenuator to prevent fluorophore bleaching. Fluorescence emission was blocked below 513 nm and above 543 nm with a TECHSPEC OD 6 band-pass filter having a centre wavelength of 527 nm (Edmund Optics, Karlsruhe, Germany). The drive syringes, tubes, and quartz cuvette were thermostatted at 30 °C, and samples were equilibrated for at least 10 min prior to each measurement. 75- μ L aliquots of unlabelled SMALPs at DMPC concentrations of 30, 20, 10, 5, 2.5, 1, or 0.5 mM were mixed with equal volumes of labelled SMALPs harbouring 0.5 mM total lipid in a 20- μ L quartz glass cuvette with a 2 mm \times 2 mm cross-section. After each mixing step, 10,000 data points were acquired with an integration time of 0.2–6 ms. At each lipid concentration, 3–8 traces were recorded and averaged. Four measurement series at 50, 100, 200, and 400 mM NaCl were performed.

Theoretical Background

Kinetics of Phospholipid Exchange Among SMALPs

Lipid transfer among nanoparticles can take place through (i) desorption of lipid monomers and interparticle diffusion through the aqueous phase (Nichols and Pagano 1981, 1982; Nichols 1985) and (ii) lipid exchange through particle collisions (Nichols 1988; Fullington et al. 1990; Jones

and Thompson 1990; Fullington and Nichols 1993). If the particles that exchange lipid molecules are identical in size and shape, the observed diffusional rate constant can be written as (Nichols 1988; Fullington et al. 1990; Fullington and Nichols 1993)

$$k_{\text{obs,dif}}(c_L) = \frac{k_{\text{dif}}c_L}{c_L^0 + c_L} \quad (1)$$

where k_{dif} is the diffusional lipid-exchange rate constant and c_L^0 and c_L are the bulk solution concentrations of lipid in the donor and acceptor populations, respectively. For second-order (“bimolecular”) collision-dependent lipid transfer, the observed collisional rate constant is

$$k_{\text{obs,col}}(c_L) = k_{\text{col}}c_L \quad (2)$$

where k_{col} is the second-order collisional lipid-exchange rate constant. If both of the above-mentioned mechanisms contribute to the kinetics of lipid transfer, the overall observed lipid-exchange rate constant is given by the sum of Eqs. (1 and 2) (Nichols 1988; Fullington et al. 1990; Fullington and Nichols 1993)

$$k_{\text{obs}}(c_L) = \frac{k_{\text{dif}}c_L}{c_L^0 + c_L} + k_{\text{col}}c_L \quad (3)$$

For SMA(2:1) nanodiscs at different ionic strengths, inclusion of higher-order collisional events in the model did not further improve the fit, suggesting that simultaneous collisions of more than two SMALPs can be neglected. Furthermore, the collisional lipid-exchange rate constant based on lipid concentrations was converted to the corresponding rate constant referring to particle (i.e., SMALP) concentrations to allow for comparison with the diffusion limit (Cuevas Arenas et al. 2017).

Concentration-Dependent TR-FRET

When fluorescently labelled and unlabelled SMALPs are mixed, NBD-PE and Rh-PE molecules redistribute among all available SMALPs. This dilution of the fluorescent probes leads to a decrease in FRET efficiency and a dequenching of donor emission, which manifests in an exponential increase in the fluorescence emission intensity of NBD-PE at 530 nm according to

$$F(t) = F_\infty + e^{-k_{\text{obs}}t}(F_0 - F_\infty) + mt \quad (4)$$

Here, $F(t)$ is the intensity at time t ; F_0 and F_∞ are the baseline-corrected original and final intensities, respectively; and m is the slope of the final baseline, which accounts for linear signal drift at long times. For global data analysis, Eq. (3) was inserted into Eq. (4) to yield

$$F(t) = F_\infty + e^{-\left(\frac{k_{\text{dif}}c_L}{c_L^0 + c_L} + k_{\text{col}}c_L\right)t}(F_0 - F_\infty) + mt \quad (5)$$

In this fitting equation, k_{dif} and k_{col} are global fitting parameters, whereas F_0 , F_{∞} , and m are local (i.e., c_L -specific) fitting parameters. Best-fit parameter values and 95% confidence intervals were derived by nonlinear least-squares fitting in Excel spreadsheets (Kemmer and Keller 2010).

Dependence on Ionic Strength

The primary kinetic salt effect (Brønsted 1922; Brønsted and Teeter 1923; Bjerrum 1924) predicts k_{col} to depend on the ionic activity coefficient, γ , of the nanodiscs. Simple electrostatic theories of ionic solutions (see below) take $\log(\gamma)$ to be proportional to the square of the ionic charge number, z . Then, the primary kinetic salt effect is reflected in a simple expression of the form

$$\log\left(\frac{k_{\text{col}}}{\text{M}^{-1}\text{s}^{-1}}\right) = \log\left(\frac{k_{\text{col}}^0}{\text{M}^{-1}\text{s}^{-1}}\right) - 2\log(\gamma) \quad (6)$$

where k_{col}^0 is the hypothetical collisional lipid-exchange rate constant at $\gamma=1$.

Within the Debye–Hückel limit (Debye and Hückel 1923), γ depends on the ionic strength of the solution, I , and, thus, on the NaCl concentration according to

$$\log(\gamma) = -Az^2\sqrt{I} \quad (7)$$

with $A = 0.516 \text{ L}^{1/2} \text{ mol}^{-1/2}$ at 30 °C (Bergethon 2010). Inserting Eq. (7) into Eq. (6) yields the Brønsted–Bjerrum equation (Brønsted and Teeter 1923; Bjerrum 1924)

$$\log\left(\frac{k_{\text{col}}}{\text{M}^{-1}\text{s}^{-1}}\right) = \log\left(\frac{k_{\text{col}}^0}{\text{M}^{-1}\text{s}^{-1}}\right) + 2Az^2\sqrt{I}. \quad (8)$$

The Debye–Hückel limiting law as embodied in Eq. (8) typically provides reasonably good approximations only for $I \leq 10 \text{ mM}$, whereas the empirical extensions of Eq. (7) suggested by Guggenheim (1935) and Davies (1938) hold also at higher salt concentrations up to $I \approx 500 \text{ mM}$. Specifically, the Davies equation (Davies 1938) reads

$$\log(\gamma) = -Az^2\left(\frac{\sqrt{I}}{1 + \sqrt{I}} - 0.2I\right). \quad (9)$$

Using a factor of 0.3 instead of 0.2 in the last term of Eq. (9), as later suggested by Davies (1962), had no significant effect on the best-fit values of z and k_{col}^0 (data not shown). Inserting Eq. (9) into Eq. (6) thus leads to a modified expression of the form

$$\log\left(\frac{k_{\text{col}}}{\text{M}^{-1}\text{s}^{-1}}\right) = \log\left(\frac{k_{\text{col}}^0}{\text{M}^{-1}\text{s}^{-1}}\right) + 2Az^2\left(\frac{\sqrt{I}}{1 + \sqrt{I}} - 0.2I\right). \quad (10)$$

Both the original Debye–Hückel limiting law and the Davies equation rely on point-charge assumptions. By contrast, another extension of the Debye–Hückel equation accounts for the finite size of the nanodiscs, resulting in (Bergethon 2010)

$$\log(\gamma) = \frac{-Az^2\sqrt{I}}{1 + Br\sqrt{I}} \quad (11)$$

with $B = 3.30 \text{ nm}^{-1} \text{ L}^{1/2} \text{ mol}^{-1/2}$ at 30 °C and $r = 12 \text{ nm}$ being the SMALP radius. Inserting Eq. (11) into Eq. (6) leads to the following expression

$$\log\left(\frac{k_{\text{col}}}{\text{M}^{-1}\text{s}^{-1}}\right) = \log\left(\frac{k_{\text{col}}^0}{\text{M}^{-1}\text{s}^{-1}}\right) + 2\frac{Az^2\sqrt{I}}{1 + Br\sqrt{I}}. \quad (12)$$

This equation is valid only at low ionic strengths of $I \leq 100 \text{ mM}$. Therefore, we tried replacing the \sqrt{I} term in Eq. (12) by the Davies term in Eq. (9), which, however, had no significant effect on the quality of the fit and the best-fit values of z and k_{col}^0 (data not shown).

With the aid of either Eqs. (8, 10, or 12), best-fit parameter values and 95% confidence intervals of k_{col}^0 and z were derived by nonlinear least-squares fitting of k_{col} as a function of I in Excel spreadsheets (Kemmer and Keller 2010).

Diffusion-Limited Collisional Lipid Transfer

In order to estimate the lipid-exchange efficiency during SMALP/SMALP collisions, we calculated the diffusion-limited collisional rate constant that would be applicable to nonionic particles, which is described by the Stokes–Einstein–Smoluchowski equation (Kuriyan et al. 2012):

$$k_{\text{col,max}} = \frac{8RT}{3\eta}, \quad (13)$$

where R denotes the universal gas constant; T the absolute temperature; and η the dynamic viscosity of the buffer.

Results and Discussion

Since SMA(2:1) considerably differs from SMA(3:1) (Grethen et al. 2017) and has emerged as the most popular copolymer for membrane-protein solubilisation (Lee et al. 2016), we set out to quantify the kinetics of lipid exchange among SMA(2:1) nanodiscs for comparison with earlier results obtained on SMA(3:1) (Cuevas Arenas et al. 2017) and to elucidate the effect of ionic strength on the kinetics of collisional lipid transfer.

Lipid Transfer Among SMA(2:1) Nanodiscs

Lipid transfer among nanoparticles in general can occur through two major mechanisms, both of which significantly contribute to the observed rate constant, k_{obs} (Eq. 3). On the one hand, interparticle diffusion of lipid monomers through the aqueous phase plays a dominant role at low lipid concentrations (Eq. 1) (Nichols and Pagano 1981, 1982; Nichols 1985). On the other hand, lipid exchange through particle collisions manifests in a second-order kinetic contribution that becomes dominant at higher lipid concentrations (Eq. 2) (Nichols 1988; Fullington et al. 1990; Jones and Thompson 1990; Fullington and Nichols 1993).

We used TR-FRET to quantify the lipid-exchange kinetics among SMA(2:1) nanodiscs and to disentangle the contributions of the above-mentioned mechanisms. NBD-PE and Rh-PE form an efficient FRET pair when co-localised within the same nanodisc, but mixing with unlabelled nanodiscs leads to a redistribution of the fluorescent probes and dequenching of NBD-PE emission. Following this rationale, we observed a fast increase in the emission intensity of the NBD-PE donor when mixing labelled and unlabelled nanodiscs at various concentrations of unlabelled lipids at 30 °C in the presence of 200 mM NaCl (Fig. 1a). Local fits revealed k_{obs} values very similar to those retrieved from a global fit across all lipid concentrations used, showing a linear increase in k_{obs} except at the lowest lipid concentrations tested, where a downward curvature was discernible (Fig. 1b). Global data analysis returned a best-fit value and a 95% confidence interval of the collisional lipid-transfer rate constant of $k_{\text{col}} = (5.85 \pm 0.03) \text{ M}^{-1} \text{ s}^{-1}$, which is ~ 40 -fold lower than the corresponding value determined for SMA(3:1) nanodiscs ($k_{\text{col}} = 222 \text{ M}^{-1} \text{ s}^{-1}$) under identical conditions (Cuevas Arenas et al. 2017). The diffusional rate constant, k_{dif} , for SMA(2:1) nanodiscs amounted to $\sim 0.0039 \text{ s}^{-1}$, which is ~ 75 -fold smaller than the value for SMA(3:1) nanodiscs ($k_{\text{dif}} = 0.29 \text{ s}^{-1}$). We refrained from a more precise determination of k_{dif} and instead focussed on scrutinising the kinetics of collisional lipid transfer because the latter played a dominant role at all except the lowest lipid concentrations, that is, below 0.50 mM (Fig. 1c).

The difference in k_{col} between the two copolymer variants under otherwise identical conditions can be explained by the higher charge density on SMA(2:1) as compared with SMA(3:1), which leads to increased electrostatic repulsion and, thus, less frequent collisions among SMA(2:1) nanodiscs. The smaller value of k_{dif} in the case of SMA(2:1) can be explained by the observation that the lipid-bilayer architecture is better preserved by SMA(2:1) than by SMA(3:1). It has been shown (Grethen et al. 2017) that SMA(3:1) has a more drastic effect than SMA(2:1) on the thermotropic lipid phase transition in polymer-encapsulated nanodiscs, which suggests a stronger perturbation of acyl-chain packing

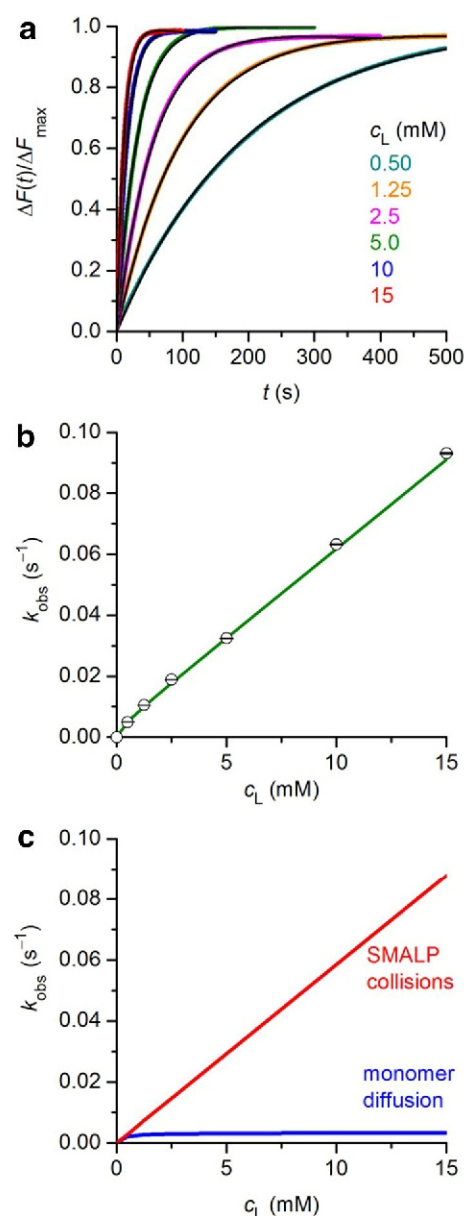


Fig. 1 Lipid exchange among fluorescently labelled and unlabelled SMA(2:1) nanodiscs at 200 mM NaCl as monitored by TR-FRET at 30 °C. **a** Normalised NBD-PE fluorescence emission, $\Delta F(t)/\Delta F_{\text{max}}$, as a function of time, t , after mixing labelled SMALPs at a total final lipid concentration of 0.25 mM with unlabelled SMALPs at various c_L . Shown are experimental data (coloured dots) and a global fit (black lines) based on Eq. (5). **b** Lipid-exchange rate constants, k_{obs} , derived from local fits to data in panel a according to Eq. (4) (circles) and derived from a global fit (green line) according to Eq. (5). Error bars are 95% confidence intervals of local fits. **c** Absolute contributions of diffusional and collisional lipid-exchange processes to k_{obs} . (Color figure online)

in the former case. Packing defects in the bilayer decrease the free-energy barrier for a lipid molecule to desorb from the bilayer, which is thought to be the rate-limiting step in the process of diffusional lipid exchange (Aniansson et al.

1976; Nichols 1985; Jones and Thompson 1990). Thus, the tighter and more “native-like” packing of lipids in nanodiscs surrounded by SMA(2:1) should impede the desorption of lipid monomers and, thereby, slow down the diffusional contribution to interparticle lipid exchange as compared with SMA(3:1), which has a more deleterious effect on bilayer architecture.

Role of Coulombic Repulsion in Collisional Lipid Transfer Among Polyanionic Nanodiscs

Raising the salt concentration is expected to enhance Coulombic shielding of the carboxylate groups of SMA(2:1), which should accelerate collisional lipid exchange among SMALPs. Following this rationale, we repeated TR-FRET

experiments such as those shown above (Fig. 1) at different ionic strengths, namely, in the presence of 50, 100, 200, or 400 mM NaCl. As expected, at a given lipid concentration, we observed a monotonous increase in the dequenching rate of NBD-PE with increasing NaCl concentration (Fig. 2a). This dependence was reflected in local and global fits, as k_{obs} increased with increasing NaCl concentration across the entire range of lipid concentrations tested (Fig. 2b). Table 1 summarises the k_{diff} and k_{col} values at the different NaCl concentrations tested.

To quantitatively capture the dependence of collisional lipid exchange on NaCl concentration and, thereby, on ionic strength, we fitted k_{col} as a function of I on the assumptions of either the Debye–Hückel limiting law for low values of I (Eq. (8); Fig. 2c, grey solid and dashed lines), the Davies

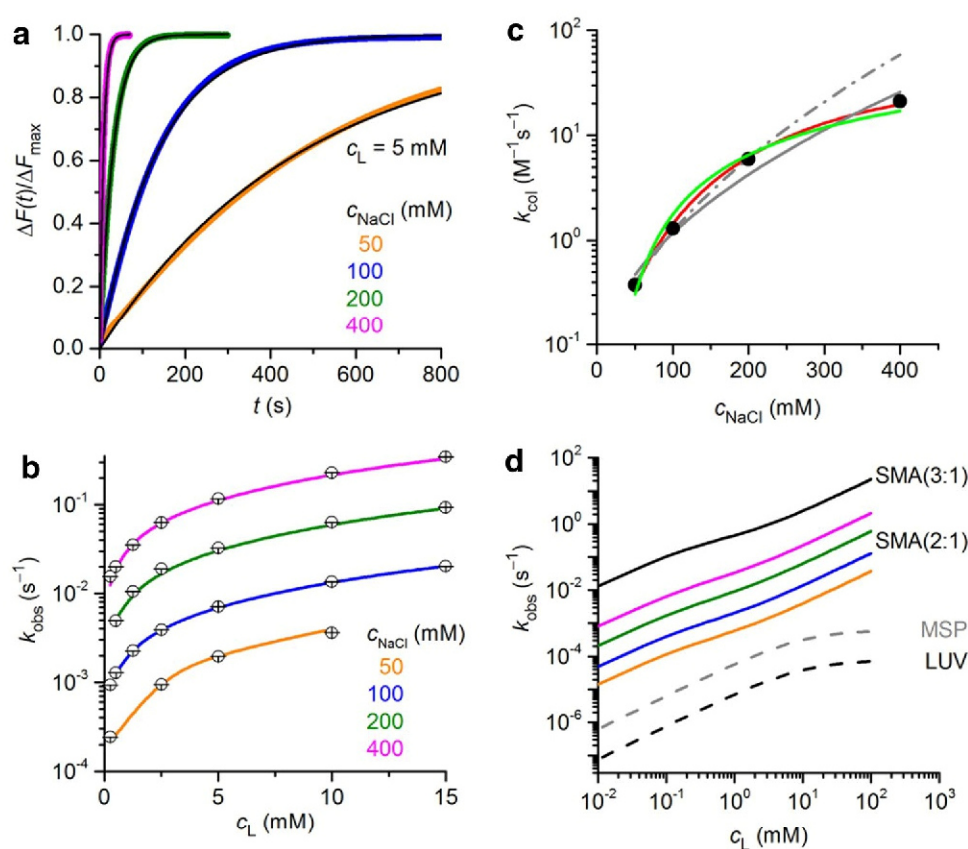


Fig. 2 Lipid exchange among fluorescently labelled and unlabelled SMA (2:1) nanodiscs at different ionic strengths as monitored by TR-FRET at 30 °C. **a** Normalised NBD-PE fluorescence emission, $\Delta F(t)/\Delta F_{\text{max}}$, as a function of time, t , after mixing labelled SMALPs with unlabelled SMALPs at a total lipid concentration of 5 mM in the presence of 50, 100, 200, or 400 mM NaCl. Shown are experimental data (coloured dots) and global fits across all lipid concentrations at a given NaCl concentration (black lines). **b** Observed lipid-exchange rate constants, k_{obs} , at different NaCl concentrations derived from local fits (circles) and global fits (solid lines). Error bars are 95% confidence intervals of local fits. **c** Collisional lipid-exchange rate constants, k_{col} , as functions of NaCl concentration, c_{NaCl} . Shown are

experimental data (circles) and fits based on Eq. (8) fitted to the entire dataset (grey solid line), Eq. (8) excluding the k_{col} value at $c_{\text{NaCl}} = 400$ mM (grey dotted line), Eq. (10) fitted to the entire dataset (red solid line), or Eq. (12) fitted to the entire dataset (green solid line). **d** Overall lipid-exchange rate constants, k_{obs} , as calculated from Eq. (5) using data from this work and previous publications (Cuevas Arenas et al. 2017). Membrane-mimetic systems include nanodiscs bounded by SMA(3:1) at 200 mM NaCl (Cuevas Arenas et al. 2017), SMA(2:1) (this work, colour code corresponds to the one in panels a and b), or MSP (Nakano et al. 2009), and LUVs (Nakano et al. 2007). (Color figure online)

Table 1 Diffusional rate constants, k_{dif} , and second-order collisional rate constants, k_{col} , characterising lipid transfer among SMA(2:1) nanodiscs at 50, 100, 200, and 400 mM NaCl and SMA(3:1) nanodiscs at 200 mM NaCl. Given are best-fit values and 95% confidence intervals

System	c_{NaCl} (mM)	k_{dif} (s^{-1})	k_{col} ($\text{M}^{-1} \text{s}^{-1}$)	Ref.
SMA(2:1)/DMPC nanodiscs	50	$2.4 \times 10^{-4} \pm 2 \times 10^{-5}$	0.37 ± 0.24	*
	100	$9.3 \times 10^{-4} \pm 7 \times 10^{-6}$	1.3 ± 0.004	*
	200	$3.9 \times 10^{-3} \pm 3 \times 10^{-5}$	5.9 ± 0.03	*
	400	$1.5 \times 10^{-2} \pm 1 \times 10^{-4}$	21 ± 0.1	*
SMA(3:1)/DMPC nanodiscs	200	$2.9 \times 10^{-1} \pm 5 \times 10^{-3}$	222 ± 1	Cuevas Arenas et al. (2017)

*This work

equation, which is an empirical extension applicable to higher I (Eq. (10); Fig. 2c, red solid line), or an extended equation taking into account the finite size of the nanodiscs (Eq. (12), Fig. 2c, green solid line). Best-fit curves underline that the Debye–Hückel limiting law described the observed increase in k_{obs} reasonably well only at low I values (i.e., excluding the data point at $c_{\text{NaCl}} = 400$ mM; grey dashed line). By contrast, the Davies model described the observed increase in k_{obs} across the entire range of I values better than the Debye–Hückel limiting law. The latter is based on a number of assumptions that are only poorly approximated or even clearly violated in the present case of polyanionic nanodiscs. These assumptions include the point charge and continuum representations of the central ion and its counterion cloud, respectively, the linearisation of the Poisson–Boltzmann equation, as well as the absence of ion pairing or counterion binding and of interactions other than Coulombic ion/ion interactions (Bergethon 2010).

Although the empirical extension embodied in the Davies equation does not account for any of these limitations in an explicit manner, it afforded a much closer agreement with experimental data than the Debye–Hückel limiting law (Fig. 2c). Therefore, we employed the Davies equation to fit k_{col} as a function of I , thus obtaining a SMALP charge number of $z = -3.6 \pm 0.4$. In the light of the above-mentioned assumptions, this value should be interpreted with caution. Most strikingly, the *effective* nanodisc charge retrieved from this analysis is two orders of magnitude smaller than the *nominal* charge of SMA(2:1) nanodiscs,

which can straightforwardly be estimated to amount to some hundred negative elementary charges. Importantly, the low absolute charge suggested by this simplistic analysis must not be interpreted as the “true” charge of a SMALP; rather, it should be regarded as a hypothetical point charge the activity of which would show the same dependence on salt concentration as found here for the collisional exchange of lipids among SMA(2:1) nanodiscs. Indeed, avoiding the poor point-charge approximation inherent to both of the above models by accounting for the finite size of SMALPs with the extended Debye–Hückel equation resulted in a reasonably good agreement between experimental data and fit and yielded $z = -33 \pm 11$. Although the effective charge number estimated by this approach is still an order of magnitude smaller than the nominal charge, it is within a range that, from simple structural considerations, appears more realistic than the above best-fit values of z . This is because, simply speaking, only the local charge density around the region of impact of one SMALP will be fully “felt” by the charges on the other SMALP during collisional lipid exchange. Moreover, in the above model, the colliding particles are considered to be spherical and to have uniform charge density, whereas SMALPs are discoidal structures with a highly anionic copolymer rim encircling a zwitterionic lipid-bilayer patch. Table 2 summarises the z and k_{col}^0 values obtained on the basis of the Debye–Hückel equation, the Davies equation, and the extended version of the Debye–Hückel equation taking into account the finite size of the nanodiscs.

Table 2 Effective SMA(2:1) nanodisc charge numbers, z , hypothetical collisional lipid-exchange rate constants at vanishing I , k_{col}^0 , and sums of squared residuals (SSRs) as quality indicators of fits based on the Debye–Hückel equation, the Davies equation, and an extended version of the Debye–Hückel equation that considers the finite size of

the nanodiscs. Given are best-fit values and 95% confidence intervals. Note that all k_{col}^0 values have broad and asymmetric confidence intervals and, therefore, are not further discussed in the text. The SSR for Eq. (8) excluding data at $c_{\text{NaCl}} = 400$ mM is not directly comparable to the other SSR values because fewer data points were fitted

Fitting equation	z	k_{col}^0 ($\text{M}^{-1} \text{s}^{-1}$)	SSR
Debye–Hückel, Eq. (8)	-2.0 ± 0.7	0.053 (0.003–0.95)	0.041
Debye–Hückel, Eq. (8), w/o data at $c_{\text{NaCl}} = 400$ mM	-2.3 ± 0.6	0.025 (0.003–0.27)	0.001
Davies, Eq. (10)	-3.6 ± 0.4	0.002 (0.0004–0.01)	0.005
Extended Debye–Hückel, Eq. (12)	-33 ± 11	4.6×10^{-26} (2.1×10^{-42} – 1.1×10^{-9})	0.036

A general limitation of the present approach is that the contributions from the SMA(2:1) copolymer itself and its counterions to the total ionic strength were not accounted for. However, adding various values reflecting different degrees of ionisation of SMA(2:1) to the ionic strength due to NaCl did not significantly affect the best-fit value of z , as this was largely absorbed by considerable changes in k_{col}^0 (data not shown). Finally, one would expect k_{col} to asymptotically approach a maximal rate constant at very high I , where neither the Debye–Hückel limiting law (Eq. 7) nor the Davies equation (Eq. 9) holds any longer. In the present case, we did not observe such behaviour, implying that the strong Coulombic repulsion among SMALPs was still far from being fully screened at 400 mM NaCl. Because SMA precipitates at even higher salt concentrations (Dörr et al. 2016; Lee et al. 2016; Oluwole et al. 2017), this asymptotic range is not accessible experimentally.

Comparison of Lipid-Exchange Rate Constants in Different Membrane Mimics

We extended our earlier compilation of k_{obs} values for various membrane-mimetic systems (Cuevas Arenas et al. 2017) and included those of SMA(2:1) nanodiscs at different ionic strengths (Fig. 2d). From this analysis, it becomes obvious that, even though lipid exchange among SMA(2:1) nanodiscs is two orders of magnitude slower than in the case of SMA(3:1) nanodiscs, it is still considerably faster than among nanodiscs surrounded by a membrane scaffold protein (MSP) or among LUVs and fast enough to allow lipid scrambling on typical experimental timescales of in vitro investigations employing SMALPs. This property allows identifying and studying strong protein/lipid interactions in SMALPs, as tightly bound lipids are excluded from the transfer among nanodiscs, whereas loosely bound lipid molecules will readily be released from the protein and exchange with protein-free nanodiscs.

Furthermore, it is informative to relate k_{col}^* , which denotes the second-order rate constant as referred to the concentration of nanodiscs (rather than lipid molecules), to the highest possible value for a diffusion-limited second-order reaction, $k_{\text{col,max}} = 8.2 \times 10^9 \text{ M}^{-1} \text{ s}^{-1}$ (Eq. 13). An SMA(2:1) nanodisc having a hydrodynamic diameter of 24 nm is estimated to contain ~ 1100 DMPC molecules, so that $k_{\text{col}}^* = 1100^2 \times k_{\text{col}} = 2.5 \times 10^7 \text{ M}^{-1} \text{ s}^{-1}$ at 400 mM NaCl, $7.0 \times 10^6 \text{ M}^{-1} \text{ s}^{-1}$ at 200 mM NaCl, $1.5 \times 10^6 \text{ M}^{-1} \text{ s}^{-1}$ at 100 mM NaCl, and $4.5 \times 10^5 \text{ M}^{-1} \text{ s}^{-1}$ at 50 mM NaCl. Accordingly, the apparent efficiency of lipid transfer among SMA(2:1) nanodiscs is 0.3% at 400 mM NaCl, 0.1% at 200 mM NaCl, 0.02% at 100 mM NaCl, and 0.01% at 50 mM NaCl. Thus, in the presence of 200 mM NaCl, the apparent lipid transfer efficiency of SMA(2:1) nanodiscs is substantially lower than that of SMA(3:1) nanodiscs

(4%) (Cuevas Arenas et al. 2017) but still higher than that of TX-100 micelles (0.02%) (Rharbi et al. 2000). Importantly, the pronounced salt dependence of the apparent lipid-exchange efficiency as referenced to the diffusion-limited maximum confirms that this quantity does not exclusively describe the efficiency of lipid exchange during a collision of two SMALPs, as Coulombic repulsion turns out to be an important determinant in reducing the frequency of collisional encounters as compared with nonionic particles. Conversely, this means that the actual lipid-exchange efficiency during a collision must be even higher than the apparent efficiency, which suggests an important role for the copolymer belt in enabling rapid lipid transfer.

Summary and Conclusions

Herein, we have demonstrated that lipid exchange among SMA(2:1) nanodiscs

- is dominated by collisional transfer at millimolar lipid concentrations, whereas diffusional transfer plays a significant role only at lower lipid concentrations;
- is slower than among nanodiscs encapsulated by SMA(3:1) but still considerably faster than among MSP nanodiscs or lipid vesicles;
- becomes substantially faster with increasing ionic strength, as described by the Davies equation or an extended Debye–Hückel equation that accounts for the finite size of the nanodiscs, provided that their effective charge number is taken to be lower than their nominal charge.

Acknowledgements Bartholomäus Danielczak (TUK) is gratefully thanked for helping with TR-FRET experiments. We thank Dr. Rodrigo Cuevas Arenas, Bartholomäus Danielczak, Erik Frotscher, Johannes Klingler, Florian Mahler, and Dr. Carolyn Vargas (all TUK) for fruitful discussions. This work was supported by the Carl Zeiss Foundation through the Centre for Lipidomics (CZSLip) and the Deutsche Forschungsgemeinschaft (DFG) through International Research Training Group (IRTG) 1830.

Compliance with Ethical Standards

Conflict of interest The authors declare no competing financial or non-financial interest.

References

- Aniansson EAG, Wall SN, Almgren M et al (1976) Theory of the kinetics of micellar equilibria and quantitative interpretation of chemical relaxation studies of micellar solutions of ionic surfactants. *J Phys Chem* 80:905–922

- Bergethon PR (2010) The physical basis of biochemistry: the foundations of molecular biophysics, 2nd edn. Springer, London
- Bersch B, Dörr JM, Hessel A et al (2017) Proton-detected solid-state NMR spectroscopy of a zinc diffusion facilitator protein in native nanodiscs. *Angew Chemie Int Ed* 56:2508–2512
- Bjerrum N (1924) Zur Theorie der chemischen Reaktionsgeschwindigkeit. *Z Phys Chem* 108:82–100
- Broecker J, Eger BT, Ernst OP (2017) Crystallography of membrane proteins mediated by polymer-bounded lipid nanodiscs. *Structure* 25:1–9
- Brønsted JN (1922) Zur Theorie der chemischen Reaktionsgeschwindigkeit. *Z Phys Chem* 102:169–207
- Brønsted JN, Teeter CEJ (1923) On kinetic salt effect. *J Phys Chem* 28:579–587
- Cuevas Arenas R, Danielczak B, Martel A et al (2017) Fast collisional lipid transfer among polymer-bounded nanodiscs. *Sci Rep* 7:45875
- Cuevas Arenas R, Klingler J, Vargas C, Keller S (2016) Influence of lipid bilayer properties on nanodisc formation mediated by styrene/maleic acid copolymers. *Nanoscale* 8(32):15016–15026
- Davies CW (1938) 397. The extent of dissociation of salts in water. Part VIII. An equation for the mean ionic activity coefficient of an electrolyte in water, and a revision of the dissociation constants of some sulphates. *J Chem Soc* 0:2093–2098.
- Davies CW (1962) Ion association. Butterworths, Washington
- Debye P, Hückel E (1923) Zur Theorie der Elektrolyte. I. Gefrierpunktniedrigung und verwandte Erscheinungen. *Phys Z* 24:185–206
- Dörr JM, Koorengevel MC, Schäfer M et al (2014) Detergent-free isolation, characterization, and functional reconstitution of a tetrameric K⁺ channel: the power of native nanodiscs. *Proc Natl Acad Sci USA* 111:18607–18612
- Dörr JM, Scheidelaar S, Koorengevel MC et al (2016) The styrene-maleic acid copolymer: a versatile tool in membrane research. *Eur Biophys J* 45:3–21
- Fullington DA, Nichols JW (1993) Kinetic analysis of phospholipid exchange between phosphatidylcholine/taurocholate mixed micelles: effect of the acyl chain moiety of the micellar phosphatidylcholine. *Biochemistry* 32:12678–12684
- Fullington DA, Shoemaker DG, Nichols JW (1990) Characterization of phospholipid transfer between mixed phospholipid-bile salt micelles. *Biochemistry* 29:879–886
- Grethen A, Oluwole AO, Danielczak B et al (2017) Thermodynamics of nanodisc formation mediated by styrene/maleic acid (2:1) copolymer. *Sci Rep* 7:11517
- Guggenheim EA (1935) L. The specific thermodynamic properties of aqueous solutions of strong electrolytes. *Phil Mag* 19:588–643
- Gulati S, Jamshad M, Knowles TJ et al (2014) Detergent-free purification of ABC (ATP-binding-cassette) transporters. *Biochem J* 461:269–278
- Hazell G, Arnold T, Barker RD et al (2016) Evidence of lipid exchange in styrene maleic acid lipid particle (SMALP) nanodisc systems. *Langmuir* 32:11845–11853
- Jones JD, Thompson TE (1990) Mechanism of spontaneous, concentration-dependent phospholipid transfer between bilayers. *Biochemistry* 29:1593–1600
- Kemmer G, Keller S (2010) Nonlinear least-squares data fitting in Excel spreadsheets. *Nat Protoc* 5:267–281
- Knowles TJ, Finka R, Smith C et al (2009) Membrane proteins solubilized intact in lipid containing nanoparticles bounded by styrene maleic acid copolymer. *J Am Chem Soc* 131:7484–7485
- Kuriyan J, Konforti B, Wemmer D (2012) The molecules of life. Physical and chemical principles. Garland Science, New York
- Lee SC, Knowles TJ, Postis VLG et al (2016) A method for detergent-free isolation of membrane proteins in their local lipid environment. *Nat Protoc* 11:1149–1162
- Logez C, Damian M, Legros C et al (2016) Detergent-free isolation of functional G protein-coupled receptors into nanometric lipid particles. *Biochemistry* 55:38–48
- Morrison KA, Akram A, Mathews A et al (2016) Membrane protein extraction and purification using styrene-maleic acid (SMA) copolymer: effect of variations in polymer structure. *Biochem J* 473:4349–4360
- Nakano M, Fukuda M, Kudo T et al (2009) Static and dynamic properties of phospholipid bilayer nanodiscs. *J Am Chem Soc* 131:8308–8312
- Nakano M, Fukuda M, Kudo T et al (2007) Determination of interbilayer and transbilayer lipid transfers by time-resolved small-angle neutron scattering. *Phys Rev Lett* 98:238101
- Nichols JW (1985) Thermodynamics and kinetics of phospholipid monomer-vesicle interaction. *Biochemistry* 24:6390–6398
- Nichols JW (1988) Phospholipid transfer between phosphatidylcholine-taurocholate mixed micelles. *Biochemistry* 27:3925–3931
- Nichols JW, Pagano RE (1982) Use of resonance energy transfer to study the kinetics of amphiphile transfer between vesicles. *Biochemistry* 21:1720–1726
- Nichols JW, Pagano RE (1981) Kinetics of soluble lipid monomer diffusion between vesicles. *Biochemistry* 20:2783–2789
- Oluwole AO, Danielczak B, Meister A et al (2017) Solubilization of membrane proteins into functional lipid-bilayer nanodiscs using a diisobutylene/maleic acid copolymer. *Angew Chemie Int Ed* 56:1919–1924
- Orwick-Rydmarm M, Lovett JE, Graziadei A et al (2012) Detergent-free incorporation of a seven-transmembrane receptor protein into nanosized bilayer Lipodisq particles for functional and biophysical studies. *Nano Lett* 12:4687–4692
- Orwick MC, Judge PJ, Procek J et al (2012) Detergent-free formation and physicochemical characterization of nanosized lipid-polymer complexes: Lipodisq. *Angew Chemie Int Ed* 51:4653–4657
- Parmar M, Rawson S, Scarff CA et al (2017) Using a SMALP platform to determine a sub-nm single particle cryo-EM membrane protein structure. *Biochim Biophys Acta* 1860:378–383
- Rharbi Y, Li M, Winnik MA, Hahn KG (2000) Temperature dependence of fusion and fragmentation kinetics of Triton X-100 micelles. *J Am Chem Soc* 122:6242–6251
- Tonge SR, Tighe BJ (2001) Responsive hydrophobically associating polymers: a review of structure and properties. *Adv Drug Deliv Rev* 53:109–122
- Vargas C, Cuevas Arenas R, Frotscher E, Keller S (2015) Nanoparticle self-assembly in mixtures of phospholipids with styrene/maleic acid copolymers or fluorinated surfactants. *Nanoscale* 7:20685–20696

3.2. Associated results:

Effective SMA(2:1) nanodisc charge numbers by ζ -potentials

In *Manuscript 2*, it was shown that Coulombic repulsions among SMA(2:1) nanodiscs decrease with elevated ionic strength. An extension of the Debye–Hückel limiting law yielded effective SMA(2:1) nanodisc charge numbers of $z = -33 \pm 11$. However, this method provides only an average effective nanodisc charge over a range of NaCl concentrations. Therefore, ζ -potential measurements were performed as a complementary method to validate the previous results and elucidate the effective nanodisc charge as functions of ionic strength I and SMA(2:1) nanodisc size.

3.2.1. Experimental section

SMA(2:1)-bounded nanodiscs containing 4 mM DMPC and 0.65–1.56 mM SMA(2:1) (corresponding to 0.18–0.42 % w/v SMA(2:1)) in 50 mM Tris, 0–100 mM NaCl, pH 7.4 were incubated for at least 16 h at 30°C. Measurements were performed on a Zetasizer Nano ZS (Malvern Panalytical, Malvern, UK) working with a 633-nm He–Ne laser and a backscatter detection angle of 173°. Samples were thermostatted for 2 min at 30°C before 3–8 measurements were performed at the same temperature in a high concentration zeta potential cell ZEN1010 (Malvern Panalytical) using the Smoluchowski model and the monomodal mode yielding average ζ -potentials. To avoid joule heating caused by high conductivity of the samples (because of elevated ionic strength), the voltage was manually reduced to 10 V. Measurements of nanodiscs at NaCl concentrations >100 mM were impeded because of the above-mentioned reasons. To validate the correct operation of the Zetasizer and to verify the cleanliness of the zeta cells, a polystyrene latex standard DTS1235 (Malvern Panalytical), having a zeta potential of $\zeta = -42 \pm 4.2$ mV, was measured at least after every three different samples. DLS measurements were performed as described in *Manuscript 2*.

3.2.2. Theoretical background

The following derivation follows the publication of Nitzsche and Simon (1997).⁹⁰

Charged particles in a dispersion are accelerated to the oppositely charged electrode in an electric field. Here, polyanionic nanodiscs are accelerated to the cathode. This force F_1 is described as

$$F_1 = E q \quad (1)$$

with E being the applied electric field and q the nanodisc surface charge. The main counteracting force is the Stoke frictional force F_2 :

$$F_2 = 6 \pi \nu r \eta \quad (2)$$

with ν being the nanodisc velocity, r being the radius of the nanodisc, and η being the solvent viscosity. An equilibrium of forces is reached, if

$$F_1 = F_2 \quad (3)$$

Inserting equation (1) and (2) in (3) gives an expression for the nominal surface charge of the nanodisc:⁹⁰

$$\frac{\nu}{E} = \frac{q}{6 \pi r \eta} \quad (4)$$

The negative nanodisc surface charge is compensated by protons or ions in the fluid phase, here mainly sodium ions. They form the electrical double layer which results from electrostatic attractions between the negative nanodisc charge and counterions screening the particle surface charge:

$$q = -4\pi \int_r^\infty a \rho da \quad (5)$$

and $a = r + \frac{1}{\kappa}$

with $\frac{1}{\kappa}$ being the effective thickness of the double layer and ρ being the charge density resulting from the nanodisc and its double layer. An approximation by Debye and Hückel⁹¹ of the Poisson equation, which describes the charge distribution in a physical space, results in

$$\rho \approx -\epsilon_0 \epsilon_r \kappa^2 \Phi \quad (6)$$

with ϵ_0 being the vacuum permittivity, ϵ_r being the dielectric constant, and Φ being the electrical potential. It has to be noted that the nanodisc shape is approximated to a sphere. Furthermore, the electrical potential decays exponentially from the surface potential Φ_0 :^{92–95}

$$\Phi = \Phi_0 \frac{r}{a} e^{-\kappa(a-r)} \quad (7)$$

Inserting equation (6) and (7) in (5) and integrating gives an expression for the nominal nanodisc surface charge:

$$q = 4\pi \varepsilon_0 \varepsilon_r r (1+\kappa r) \Phi_0 \quad (8)$$

Due to the particle movement in the electric field, the double layer is partially sheared off to the so-called “slipping plane”. The ζ -potential is the potential difference at this slipping plane, which is defined as the interface that separates the stationary layer of ions that is strongly associated with the suspended nanodisc and the mobile phase. Therefore, the absolute value of the surface potential is always larger than that of the ζ -potential, $|\Phi_0| > |\zeta|$, and, thus, a correction factor f needs to be introduced:

$$(1+\kappa r) \Phi_0 = \zeta f(\kappa r) \quad (9)$$

Inserting equation (8) and (9) in (4) leads to the general Henry equation that combines the electrophoretic mobility μ_e with ζ :

$$\frac{v}{E} = \mu_e = \frac{2 \varepsilon_0 \varepsilon_r \zeta f(\kappa r)}{3\eta} \quad (10)$$

Polymer-bounded nanodiscs have a large radius r compared with a small double layer, $\kappa r > 1$. Therefore, the following limiting case is valid here:

$$\lim_{a \rightarrow \infty} (f(\kappa r)) = \frac{3}{2} \quad (11)$$

Accordingly, the Henry equation is simplified to the Smoluchowski equation:

$$\mu_e = \frac{\varepsilon_0 \varepsilon_r \zeta}{\eta} \quad (12)$$

Insertion of equation (9) and (11) into (8) leads to an expression for the effective nanodisc charge q_1 :

$$q_1 = 6\pi \varepsilon_0 \varepsilon_r r \zeta \quad (13)$$

The effective nanodisc charge number z is defined by

$$z = \frac{q_1}{e} \quad (14)$$

with $e \approx 1.602 \cdot 10^{-19}$ being the elementary charge.

The surface charge density of the nanodiscs can be calculated using three alternatives. First, assuming the polymer is predominantly present at the nanodisc rim, only the circumference of the disc is taken into account to be negatively charged (as shown in Figure 3.1):

$$\rho(r)_{\text{lat}} = \frac{z}{2\pi r} \quad (15)$$

Second, the lateral surface of the disc is taken into account:

$$\rho(r)_{\text{lat}} = \frac{z}{2\pi r h} \quad (16)$$

with h being the nanodisc thickness averaged to 5 nm.⁴⁷

Third, the surface charge density is calculated for the whole nanodisc surface:

$$\rho(r)_{\text{disc}} = \frac{z}{2\pi r (r+h)} \quad (17)$$

3.2.3. Results

ζ -potentials of SMA(2:1)/DMPC nanodiscs were measured to elucidate the influence of ionic strength I (here: NaCl concentrations) and SMALP size on the effective nanodisc charge. To this end, SMA(2:1) nanodiscs having a diameter of 12, 16, or 24 nm at NaCl concentrations in the range of 0–100 mM were studied. Nanodisc hydrodynamic diameters, d , were validated by DLS, as shown by representative unimodal intensity-weighted size distributions, $f(d)$, at 50 mM NaCl (Figure 3.1.a). It has to be noted that the designation “0 mM NaCl” can be misleading. Herein, it means that no NaCl was added to the nanodiscs, although, various counterions of SMA(2:1) were potentially present, thus $I > 0$.

Overall, ζ -potentials of all SMA(2:1) nanodiscs were found to be in the range of –35 mV to –20 mV (Figure 3.1.b). Generally, the ζ -potential is an indicator of the colloidal stability of dispersed nanoparticles.⁹⁶ In particular, there is no strict definition found in literature, but nanoparticles with ζ at least below –20 mV and above +20 mV can be considered as stable in

solution.^{97,98} At small absolute values of ζ , however, they tend to aggregate or agglomerate due to dominant attractive forces such as van der Waals forces among the particles. Consequently, the herein measured ζ -potentials demonstrate the colloidal stability of SMALPs formed by SMA(2:1). This is in accordance with the previously reported ζ -potentials of SMA(3:1) nanodiscs⁹⁹ and the frequently described thermal and storage stability of protein-encapsulated nanodiscs.^{54,57,58,62,63} For bare SMA(2:1) copolymer (i.e., in the absence of lipid), the ζ -potential yielded -10 mV at 200 mM NaCl, which is somewhat smaller than the reported -37 mV of SMA(3:1).⁸² It has to be noted that, however, solvent conditions and polymer concentrations differ, and, thus, herein and previously reported ζ -potentials of SMA polymers are not directly comparable.

It was observed that ζ gradually became less negative with increasing NaCl concentrations (Figure 3.1.b). In particular, for nanodiscs of 24 nm, ζ increased from -30 mV at 0 mM NaCl to -20 mV at 100 mM NaCl. In accordance, the deduced effective nanodisc charge number (equation 13 and 14), $z(r)$, and the charge density at the nanodiscs' rim (equation 15), $\rho(r)_{\text{circ}}$, also became less negative. $z(r)$ increased from -30 at 0 mM NaCl to -21 at 100 mM NaCl (Figure 3.1.c), whereas $\rho(r)_{\text{circ}}$ increased from -0.4 to -0.3 effective charges per nm (Figure 3.1.d). As expected, elevated NaCl concentrations lead to Coulombic screening of the polymers' anionic carboxylate groups and, thus, to less negative ζ , $z(r)$, and $\rho(r)_{\text{circ}}$. Similar results were found for the smaller nanodiscs.

Furthermore, ζ also became less negative with reduced nanodisc size (Figure 3.1.b). More specifically, at 50 mM NaCl, ζ increased by 10 mV from 24-nm- to 12-nm-nanodiscs. Again, $z(r)$ and $\rho(r)_{\text{circ}}$ showed the same trend (Figure 3.1.c and d). In particular, at the same NaCl concentration, $z(r)$ increased from -25 for 24-nm-nanodiscs to -10 for 12-nm-nanodiscs. An explanation for this effect is the reduced circumference of small nanodiscs, leading to a superior nanodisc curvature, and, thus, to a reduced polymer charge density. Accordingly, less polymer is required for nanodisc formation.

Taken together, ζ -potentials demonstrated the high colloidal stability of SMA(2:1) nanodiscs. The deduced effective nanodisc charge numbers were in close agreement with $z = -33 \pm 11$ calculated by the extended Debye–Hückel equation in *Manuscript 2*. Furthermore, the results underlined that increasing ionic strength enhances Coulombic screening of SMA(2:1) and thus

leads to less negative $z(r)$. The reduced $z(r)$ of small nanodiscs can be ascribed to a decreased polymer concentration involved in nanodisc stabilisation.

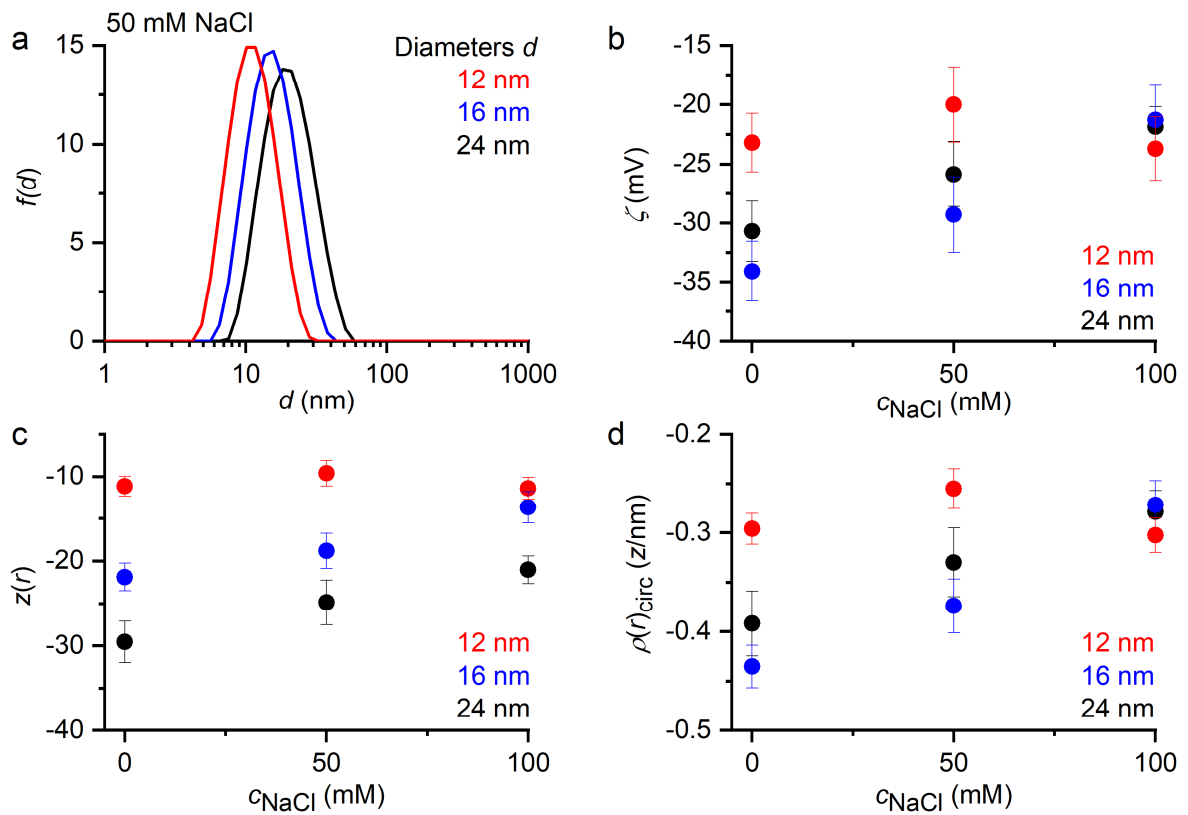


Figure 3.1: (a) Representative intensity-weighted particle size distributions, $f(d)$, for SMA(2:1)/DMPC nanodiscs with hydrodynamic diameters, d , of 12, 16, and 24 nm at 50 mM NaCl. (b) ζ -potentials of SMA(2:1)/DMPC nanodiscs as functions of 0, 50, and 100 mM NaCl. (c) Effective nanodisc charge numbers, $z(r)$, as functions of NaCl concentrations. (d) Effective nanodisc rim charge densities, $\rho(r)_{\text{circ}}$, as functions of NaCl concentrations.

4. Electroneutral polymers for membrane-protein research

Summary (Manuscript 3)

In *Manuscript 3*, two electroneutral copolymers forming lipid-bilayer nanodiscs from model and cellular membranes were introduced. A zwitterionic sulphobetaine (SB) side chain was attached to the polymer backbone of DIBMA and SMA(2:1), resulting in sulphobetaine maleimides termed as DIBMA-SB and SMA(2:1)-SB copolymers, respectively (Figure 1.4). In general, the reduction of polymer charge densities becomes increasingly important, because anionic copolymers such as SMA(2:1) and DIBMA can interfere with specific bioanalytical techniques and native protein/lipid interactions through Coulombic attractions/repulsions.

The equilibrium solubilisation efficiency of DIBMA-SB and SMA(2:1)-SB towards model membranes in the form of saturated DMPC was quantified by DLS and ^{31}P NMR spectroscopy. It was shown that DIBMA-SB was threefold more efficient than DIBMA, whereas SMA(2:1)-SB showed a similar high efficiency than SMA(2:1). Particularly interesting is the solubilisation power of the zwitterionic polymers towards anionic 1-palmitoyl-2-oleoyl-*sn*-glycero-3-phospho-(1'-*rac*-glycerol) (POPG) vesicles, underlining the polymers' compatibility with highly charged membranes through reduced Coulombic repulsions. The formation of nanodiscs was validated by transmission electron microscopy (TEM) and the electroneutrality of both polymers as well as corresponding nanodiscs was confirmed by ζ -potential measurements. Furthermore, it was found that, like DIBMA, DIBMA-SB and SMA(2:1)-SB have a mild effect on the lipid-bilayer integrity in the nanodisc core.

The performance of the new polymers was further addressed by solubilisation and extraction experiments of membrane proteins from complex human (HeLa) membranes. As gauged from SDS-PAGE and a colorimetric assay, the derivatised polymers were able to solubilise ~25% of the total membrane protein mass from HeLa membranes. In addition to the total protein extraction yields, the solubilisation of specific membrane proteins was elucidated by means of SEC and liquid chromatography coupled to tandem mass spectrometry (LC-MS/MS). Importantly, it was shown that DIBMA-SB preserves both homo- and heteromeric membrane-protein complexes. These protein assemblies were extracted from various cellular membranes and pertain to distinct structural classes. Furthermore, the new polymers are suitable for the cell-free membrane-protein synthesis, as shown by producing two functionally folded large

membrane proteins in the presence of these electroneutral polymer nanodiscs. Importantly, DIBMA-SB and SMA(2:1)-SB are also amenable to protein/lipid interaction studies because of their reduced Coulombic repulsions, as demonstrated using microfluidic diffusional sizing (MDS). Taken together, these findings underline the broad applicability of the herein presented electroneutral polymers in membrane-protein research.

4.1. Manuscript 3

Electroneutral amphiphilic copolymers forming lipid-bilayer nanodiscs for investigating membrane proteins

Anne Grethen,* David Glueck,* Manabendra Das,* Ogochukwu Patricia Mmeka, Eugenio Pérez Patallo, Annette Meister, Ritu Rajender, Jana Strate, Stefan Kins, Markus Räschle, Julian Victor, Manuel Etzkorn, Zoe Köck, Frank Bernhard, Jonathan Oyebamiji Babalola, Carolyn Vargas, and Sandro Keller

*shared first authorship

2021, in preparation

Contribution

For this work, I designed, performed and analysed multi-detection SEC experiments, created all figures and wrote the original draft of the manuscript. Furthermore, I assisted with ζ -potential measurements and their interpretation as well as with DLS experiments.

Electroneutral amphiphilic copolymers forming lipid-bilayer nanodiscs for investigating membrane proteins

Anne Grethen^{1,*}, David Glueck^{1-4,*}, Manabendra Das^{1,*}, Ogochukwu Patricia Mmeko^{1,5}, Eugenio Pérez Patallo¹, Annette Meister⁶, Ritu Rajender⁷, Jana Strate⁷, Stefan Kins⁷, Markus Räschle⁸, Julian Victor⁹, Manuel Etzkorn⁹, Zoe Köck¹⁰, Frank Bernhard¹⁰, Jonathan Oyebamiji Babalola⁵, Carolyn Vargas¹⁻⁴, and Sandro Keller¹⁻⁴

*shared first authorship

¹ *Molecular Biophysics, Technische Universität Kaiserslautern (TUK), Erwin-Schrödinger-Str. 13, 67663 Kaiserslautern, Germany*

² *Biophysics, Institute of Molecular Biosciences (IMB), NAWI Graz, University of Graz, Humboldtstr. 50/III, 8010 Graz, Austria*

³ *Field of Excellence BioHealth, University of Graz, Graz, Austria*

⁴ *BioTechMed-Graz, Graz, Austria*

⁵ *Department of Chemistry, University of Ibadan, 200284 Ibadan, Nigeria*

⁶ *HALOmem and Institute of Biochemistry and Biotechnology, Martin-Luther-University Halle-Wittenberg, Kurt-Mothes-Str. 3a, 06120 Halle (Saale), Germany*

⁷ *Human Biology, Technische Universität Kaiserslautern (TUK), Erwin-Schrödinger-Str. 13, 67663 Kaiserslautern, Germany*

⁸ *Molecular Genetics, Technische Universität Kaiserslautern (TUK), Paul-Ehrlich-Str. 24, 67663 Kaiserslautern, Germany*

⁹ *Institut für Physikalische Biologie, Heinrich-Heine-Universität Düsseldorf, Universitätsstr. 1, 40225 Düsseldorf, Germany*

¹⁰ *Centre for Biomolecular Magnetic Resonance, Institute for Biophysical Chemistry, Goethe University of Frankfurt/Main, Max-von-Laue-Str. 9, 60438 Frankfurt/Main, Germany*

Abstract

Polymer-encapsulated nanodiscs formed by amphiphilic copolymers are unique tools for structural and functional studies of membrane proteins. Unlike other membrane mimics, these nanodiscs self-assemble directly from cellular membranes and retain a native-like lipid-bilayer environment that is amenable to *in vitro* techniques otherwise restricted to soluble or detergent-solubilised proteins. However, existing polymers such as diisobutylene/maleic acid (DIBMA) and styrene/maleic acid (SMA) copolymers have high charge densities, which interfere with important biomolecular interactions and bioanalytical techniques through unspecific interactions. Designing electroneutral polymers that offer both high solubility and good protein-extraction efficiency has proven difficult. Herein, we describe neutral polymers

that are accessible through facile post-polymerisation modification of DIBMA and SMA backbones to furnish sulphobetaine maleimides. These copolymers quantitatively solubilise phospholipids, extract membrane proteins from bacterial and human cells, and preserve membrane-protein complexes. Unlike other polymeric membrane mimics, the new nanodiscs can be used in microfluidic protein/lipid interaction assays and cell-free protein translation.

Introduction

Amphiphilic copolymers such as diisobutylene/maleic acid (DIBMA)¹ and styrene/maleic acid (SMA)² copolymers are playing increasing roles in membrane-protein research. Unlike other membrane-mimetic systems, these polymers directly extract integral membrane proteins from cellular membranes to form protein/lipid nanodiscs that retain a native-like lipid-bilayer architecture surrounded by a copolymer belt.^{3,4} Therefore, these polymers have emerged as alternatives to conventional detergents for the solubilisation, extraction, and purification of integral membrane proteins in a more native-like environment than that afforded by a micellar assembly.⁵ By contrast, other bilayer-based membrane mimics such as membrane-scaffold protein (MSP) nanodiscs⁶ or liposomes require conventional detergents in time-consuming and potentially deleterious initial steps.⁷

SMA is a negatively charged random copolymer that exists in various styrene/maleic acid ratios and chain lengths, with SMA(2:1) being the most efficient lipid and protein solubiliser.^{8,9} In general, SMA nanodiscs render membrane proteins amenable to structural, dynamical, and functional analyses requiring nanoscopic particles.¹⁰⁻¹² DIBMA is an alternating copolymer that tends to solubilise membrane proteins in a milder but often less efficient manner than SMA(2:1). This nonaromatic polymer does not suffer from the strong far-UV absorbance typical of SMA and is compatible with fairly high concentrations of divalent cations.^{1,13,14} However, DIBMA is even more polyanionic than SMA(2:1). The high charge density of both polymers leads to unspecific Coulombic interactions with charged proteins and lipids, thus interfering, on the one hand, with labile protein/protein and protein/lipid interactions or enzymatic and ribosomal activities and, on the other hand, with many preparative and analytical techniques. The latter include cell-free protein translation, gel electrophoresis, and microfluidic diffusional sizing (MDS).

To overcome these bottlenecks, several attempts have been made at designing electrically neutral polymers. However, post-polymerisation modification of commercial SMA backbones thus far has produced polymers that are water-soluble only in pH ranges in which they carry a net charge.¹⁵ By contrast, zSMA^{16,17} is an electroneutral yet water-soluble copolymer bearing phosphocholine pendant groups that was successfully generated through *de novo* polymerisation and subsequent modification. Notwithstanding these favourable properties, the tedious synthetic route necessary to produce this polymer so far has prevented its

widespread use in membrane-protein applications. Here, we present the first examples of electroneutral polymers derived by straightforward post-polymerisation modification of DIBMA and SMA(2:1) backbones. Briefly, zwitterionic sulphobetaine (SB) side chains were attached to the maleic anhydride forms of DIBMA and SMA(2:1) to generate DIBMA-SB or SMA(2:1)-SB copolymers, respectively. We show that DIBMA-SB and SMA(2:1)-SB polymers efficiently but mildly solubilise phospholipid bilayers and extract membrane proteins from human cells. The new nanodiscs are amenable to gel electrophoresis without prior polymer removal, to studies of protein/lipid interactions by MDS, and to cell-free membrane-protein translation.

Results

Design and synthesis of electroneutral sulphobetaine copolymers

Description of the synthesis of both polymers (Figure 1). Size exclusion chromatography (SEC) coupled to a refractive index (RI) detection yielded mass-average molar masses of $M_w = 14$ kDa for DIBMA-SB and $M_w = 12.6$ kDa for SMA(2:1)-SB (Figure S5).

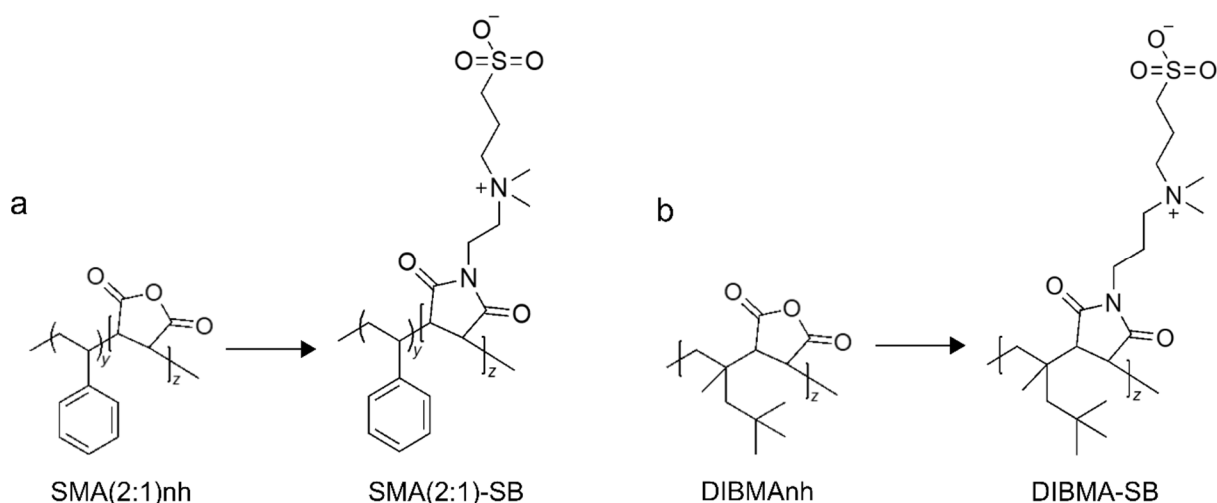


Figure 1. Structures and synthesis of (b) DIBMA-SB and (a) SMA(2:1)-SB.

Solubilisation of phospholipid membranes and nanodisc formation

We elucidated the ability of DIBMA-SB (Figure 2) and SMA(2:1)-SB (Figure S1) to solubilise lipid bilayers by subjecting unilamellar vesicles composed of the zwitterionic, saturated phospholipid 1,2-dimyristoyl-*sn*-glycero-3-phosphocholine (DMPC) to increasing polymer concentrations. The formation of polymer/DMPC nanoparticles was monitored by dynamic light scattering (DLS). Particle size distributions thus obtained (Figure 2a) showed that the hydrodynamic particle diameter (d) initially increased with increasing polymer/lipid mass ratio (m_p/m_l) but then steeply dropped to ~ 15 nm and further smoothly decreased to ~ 8 nm (Figure 2b). In comparison with commercially available, unmodified DIBMA, the neutral derivative DIBMA-SB formed 2–4-fold smaller and more narrowly distributed nanodiscs at a given m_p/m_l value, as deduced from particle diameters and peak distribution widths, respectively (Figure 2b). The solubilisation efficiency of SMA(2:1)-SB was similar to that of unmodified SMA(2:1) (Figure S1), which is intrinsically more efficient than unmodified DIBMA.⁹ Crucially, both derivatised polymers also proved effective in solubilising the anionic, unsaturated, long-chain phospholipid 1-palmitoyl-2-oleoyl-*sn*-glycero-3-phospho-(1'-*rac*-

glycerol) (POPG; Figure 2c and Figure S1). This finding underlines that, unlike polyanionic DIBMA and SMA(2:1), the new polymers are capable of efficiently solubilising negatively charged lipid bilayers exhibiting large lateral pressures among their acyl chains.

Nanoparticle formation was dissected in quantitative detail with the aid of ^{31}P NMR spectroscopy (Figure 2d and Figure S2). In the absence of polymer, the signal of large, slow-tumbling DMPC vesicles was broadened beyond detection; however, sharp, isotropic peaks gradually appeared upon titration with polymer, thereby evidencing the formation of small, fast-tumbling particles. In the language of the three-stage model commonly invoked for lipid-solubilisation equilibria,¹⁸ the first DIBMA-SB nanodiscs formed at a saturating (SAT) m_p/m_l ratio of $R_S^{b,SAT} = 0.038$, and solubilisation (SOL) was complete at $R_S^{m,SOL} = 0.26$ (Figure S2). As gauged by the latter value, the equilibrium solubilisation efficiency of DIBMA-SB was threefold higher than that of DIBMA ($R_S^{m,SOL} = 0.77$),¹ in support of the above DLS data (Figure 2b). In spite of the displayed elevated solubilisation power of SMA(2:1)-SB by DLS, the latter ($R_S^{m,SOL} = 0.60$) was found to have an equilibrium solubilisation efficiency similar to that of SMA(2:1) as determined by ^{31}P NMR ($R_S^{m,SOL} = 0.52$) (Figure S1).

Negative-stain transmission electron microscopy (TEM; Figure 2e and Figure S1) of polymer/DMPC nanoparticles demonstrated the presence of homogeneously sized nanodiscs with an average diameter of (11.5 ± 2.0) nm and a lipid-bilayer thickness of (4.9 ± 0.8) nm, as shown by face-on and edge-on views, respectively. ζ -potential measurements confirmed the absence of a significant negative charge, both on the bare DIBMA-SB polymers and on nanodiscs formed in mixtures with zwitterionic DMPC (Figure 2f). In stark contrast with this, polyanionic DIBMA and its nanodiscs displayed substantially negative ζ -potentials of $-(15-20)$ mV. Similar results were obtained for the SMA(2:1) polymers and the corresponding nanodiscs (Figure S1).

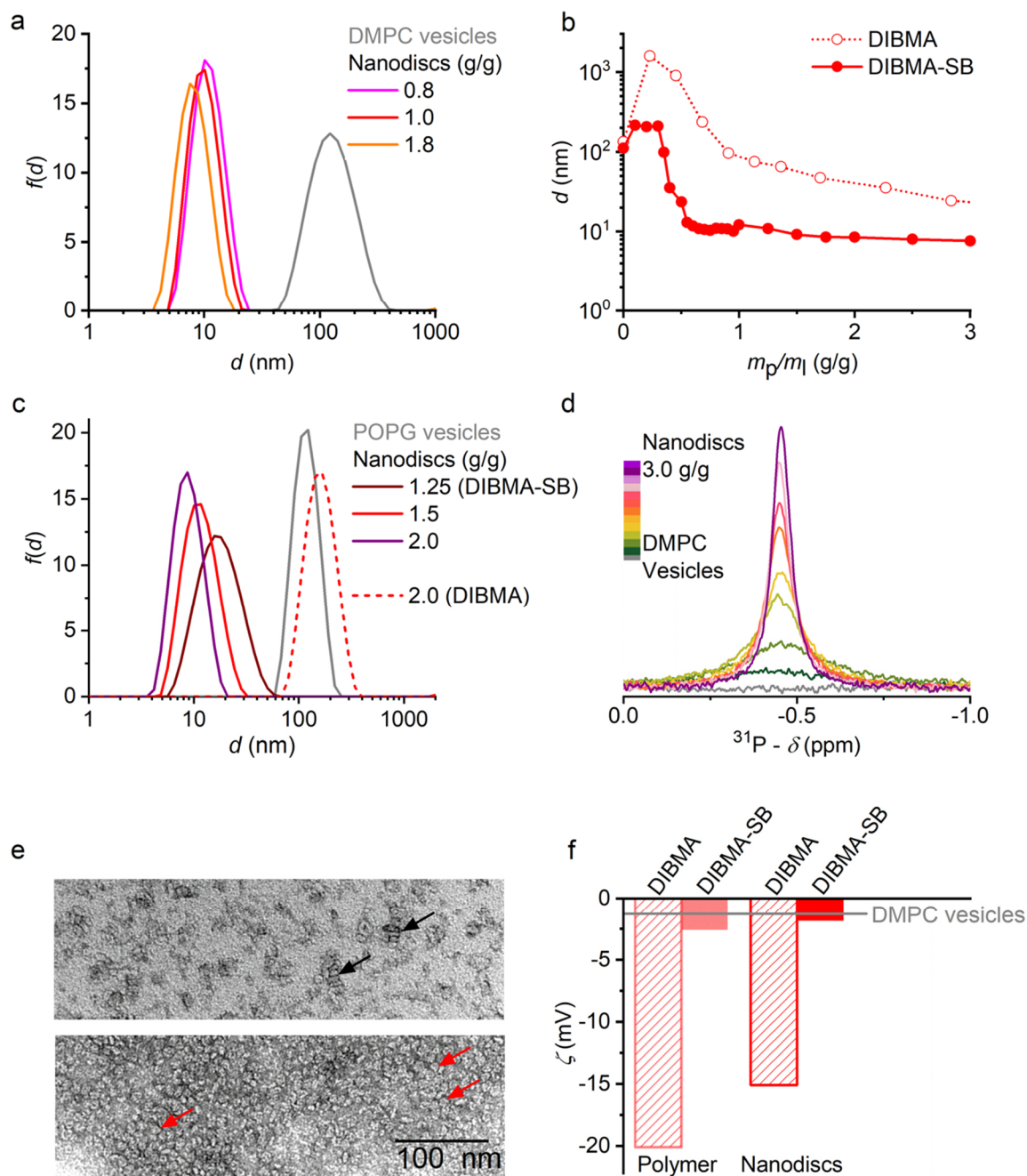


Figure 2. Solubilisation of lipid vesicles and nanodisc formation by DIBMA-SB. (a) Intensity-weighted particle size distributions, $f(d)$, of aqueous mixtures of DIBMA-SB and the zwitterionic, saturated phospholipid DMPC at various polymer/lipid mass ratios, m_p/m_l , as obtained from DLS. (b) z-Average particle diameters, d , as functions of m_p/m_l derived from particle size distributions such as shown in panel a. “Error” bars denote peak widths of particle size distributions as given by $\sigma = \sqrt{\text{PDI}}$ z , with PDI being the polydispersity index. (c) Intensity-weighted particle size distributions, $f(d)$, of aqueous mixtures of DIBMA-SB or DIBMA and the anionic, unsaturated phospholipid POPG at various m_p/m_l as obtained from DLS. (d) ^{31}P NMR spectra of 4 mg/mL DMPC in the presence of increasing concentrations of DIBMA-SB. (e) Negative-stain EM images of DIBMA-SB/DMPC nanodiscs at $m_p/m_l = 1$ prepared on a carbon-coated copper grid (top) or on a Formvar-coated copper grid (bottom). Representative face-on and edge-on nanodisc views are highlighted by red and black arrows, respectively.

(f) ζ -potentials of polymers and polymer-encapsulated DMPC nanodiscs in the presence of 100 mM NaCl. All other experiments were carried out at 50 mM Tris, 200 mM NaCl, pH 7.4.

Enhanced tolerance towards changes in pH and divalent cations

Across the pH range of 6.5–8.3, DIBMA-SB nanodiscs formed at similar m_p/m_l ratios (Figure 3a), attesting to a robust, pH-independent solubilisation efficiency. In stark contrast with this, polyanionic DIBMA suffers from decreasing solubilisation power with increasing pH.¹³ Moreover, DIBMA-SB nanodiscs exhibited excellent colloidal stability in the presence of Mg^{2+} or Ca^{2+} concentrations as high as 80 mM, which manifested both in a clear visual appearance (Figure 3b) and in particle size distributions that remained unaffected by these divalent cations (Figure S4). A similarly high colloidal stability was observed for SMA(2:1)-SB (Figure S4), whereas DIBMA and SMA(2:1) precipitate in the presence of considerably lower concentrations of divalent cations.¹³ Thus, in contrast with their polyanionic counterparts, the electroneutral polymers do not strongly interact with Mg^{2+} and Ca^{2+} and, consequently, are less susceptible to conformational transitions and precipitation induced therefrom.

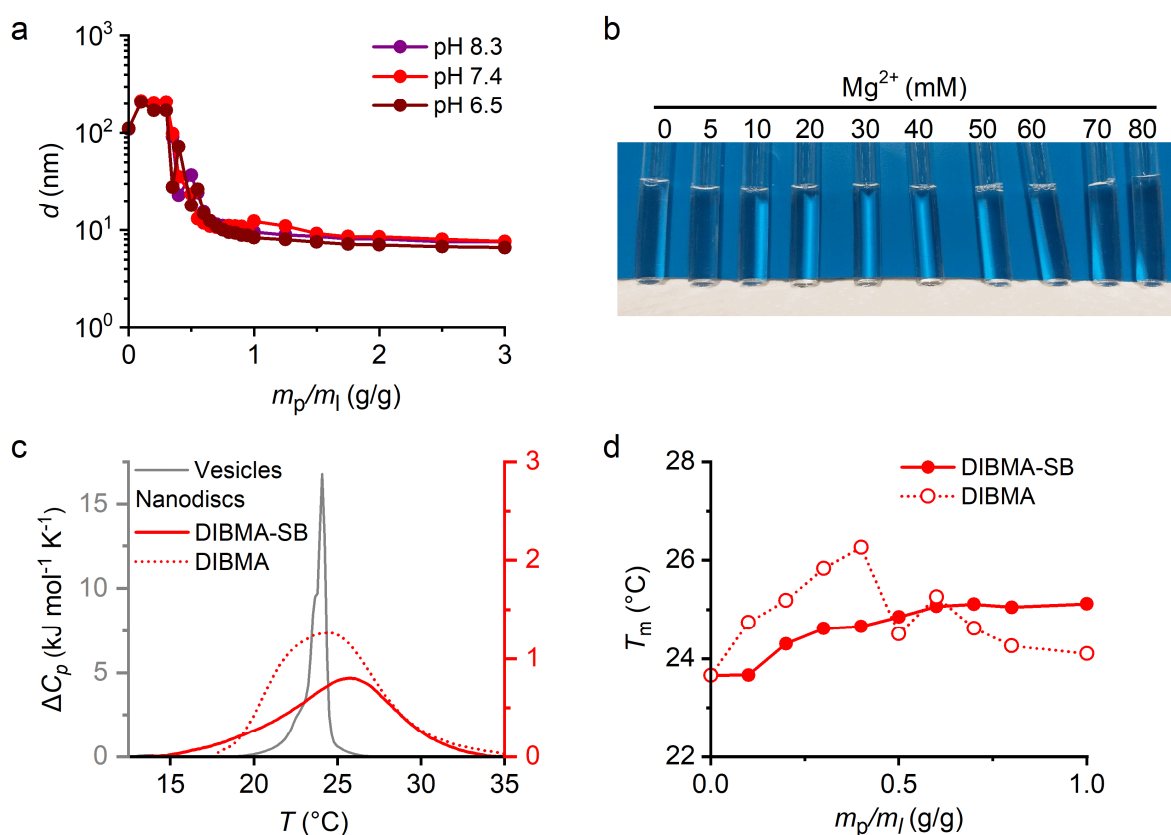


Figure 3. Tolerance towards pH and divalent cations as well as thermotropic phase transitions in DIBMA-SB nanodiscs formed from DMPC. (a) z-Average diameters, d , as functions of m_p/m_l at different pH values. (b) Visual appearance of nanodiscs in the presence of increasing Mg^{2+} concentrations. (c) DSC thermograms showing excess molar isobaric heat capacities, ΔC_p , of

4 mg/mL DMPC LUVs and DIBMA-SB or DIBMA nanodiscs at $m_p/m_l = 1.0$. (d) Gel-to-fluid phase transition temperatures, T_m , of 4 mg/mL DMPC at various m_p/m_l . Experiments were carried out at 50 mM Tris, 200 mM NaCl, pH 7.4 unless noted otherwise.

Gentle effects on lipid-bilayer phase transitions

We exploited differential scanning calorimetry (DSC) to elucidate the temperature-dependent behaviour of DMPC upon encapsulation by DIBMA-SB (Figure 3c,d) or SMA(2:1)-SB (Figure S7). With increasing temperature, DMPC vesicles exhibit a gel-to-fluid transition at $\sim 24^\circ\text{C}$, which is reflected in a sharp peak in the isobaric heat capacity (C_p ; Figure 3c). The expected and observed broadening of this peak upon addition of DIBMA-SB (Figure 3c) confirmed the formation of nanoscale bilayer patches with a much smaller cooperative unit than in vesicular bilayers.^{19,20} In spite of this alteration in peak shape, the phase transition temperature (T_m) of DMPC increased only slightly and monotonically with increasing concentrations of DIBMA-SB, whereas titration with DIBMA resulted in an initial increase followed by a sudden drop of T_m (Figure 3d). For SMA(2:1)-SB nanodiscs, T_m also slightly increased, whereas SMA(2:1) caused a significant decrease in the main phase transition temperature (Figure S7). In conclusion, the observation that the T_m of DMPC was not lowered by DIBMA-SB or SMA(2:1)-SB indicates that these polymers have only mild effects on the acyl chain packing of the phospholipids that they encapsulate.²¹ The modest rise in T_m most likely reflects partial dehydration of lipid headgroups.⁹

Extraction of human membrane proteins

The polymers' performance in fragmenting complex cellular membranes and, thus, their usefulness for membrane-protein research was studied using HeLa cells (Figure 4 and Figure S8). Across the human membrane proteome, we found DIBMA-SB to extract 25% of the entire protein mass at polymer concentrations as low as 4 mg/mL (corresponding to 24% of the membrane concentration (w/w); Figure 4a). For comparison, the "gold-standard" detergent *n*-dodecyl- β -D-maltopyranoside (DDM) was about twice as efficient in terms of total membrane-protein mass extracted. Importantly, SDS-PAGE revealed that DIBMA-SB extracted membrane proteins of largely different sizes (Figure 4b), as was also found for SMA(2:1)-SB (Figure S8).

To dissect the protein-extraction behaviour of DIBMA-SB in greater detail, we turned to fractionation of whole-cell HeLa extracts by means of size exclusion chromatography (SEC)

followed by in-depth analysis using liquid chromatography coupled to tandem mass spectrometry (LC-MS/MS). In total, we identified 2424 proteins that were extracted by DIBMA-SB, corresponding to 24% of the entire HeLa proteome.²² In spite of these large numbers of distinct membrane proteins, DIBMA-SB nanodiscs revealed a narrower, more well-defined size distribution (Figure 4c) than conventional DIBMA nanodiscs (Figure 4d). While the latter spanned an apparent molecular weight range of 200–2000 kDa, DIBMA-SB nanodiscs were more homogeneous in size, covering a range of 100–500 kDa. This observation in complex samples derived by fragmentation of cellular membranes correlates well with the above finding that chemically defined, single-lipid nanodiscs made with the aid of DIBMA-SB are both smaller and more narrowly distributed in size than their DIBMA counterparts (Figure 2b).

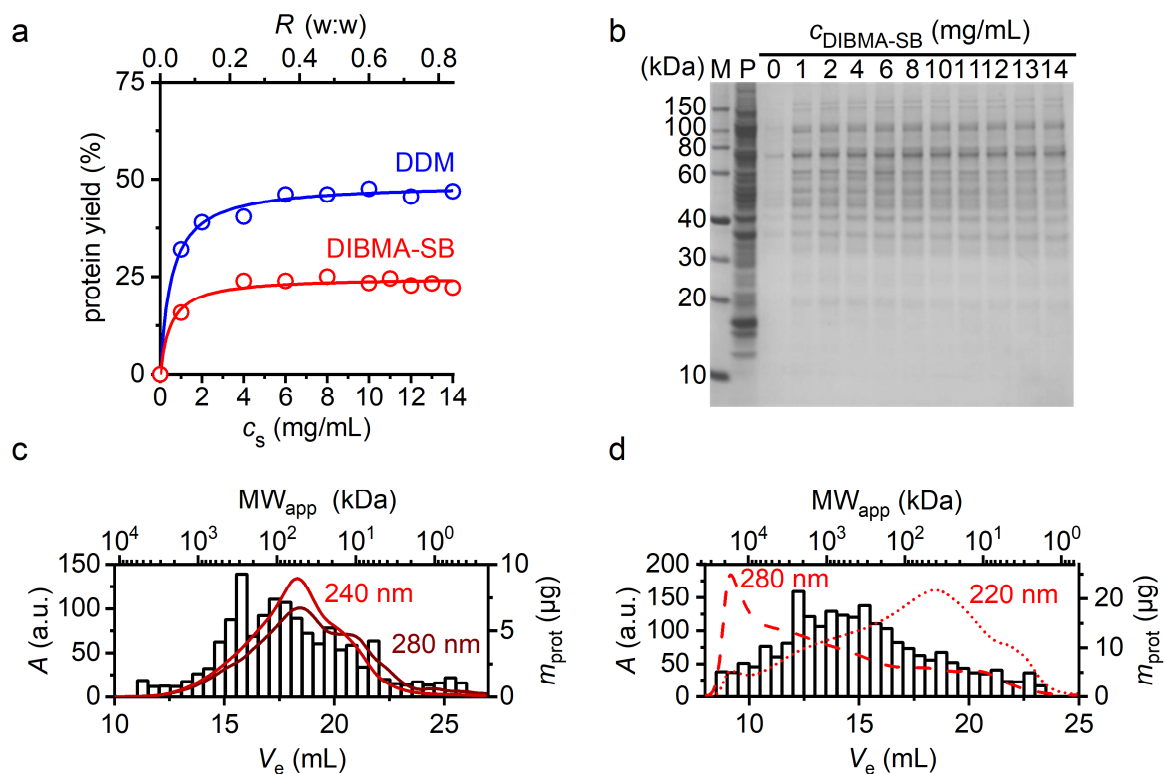


Figure 4. Extraction of membrane proteins from human cells using DIBMA-SB. (a) Overall yields of extracted membrane proteins as functions of polymer or detergent concentration as determined by a colorimetric protein assay. *Lower abscissa*: surfactant concentration (c_s); *upper abscissa*: surfactant/membrane mass ratio (R); *ordinate*: solubilised protein yield. (b) SDS-PAGE showing membrane proteins extracted from HeLa cells by increasing DIBMA-SB concentrations. (c) SEC elution profiles of whole-cell extracts obtained by subjecting HeLa cells to 12 mg/mL DIBMA-SB. *Lower abscissa*: elution volume (V_e); *upper abscissa*: apparent molecular weight (MW_{app}) of protein-containing nanodiscs; *left ordinate/solid lines*: UV absorbance (A) at 280 nm and 240 nm; *right ordinate/bars*: total membrane-protein mass (m_{prot}) found in each elution fraction. (d) SEC elution profiles of HeLa whole-cell extracts using

DIBMA; axes as in panel c. Protein extraction and SEC experiments were carried out at 50 mM Tris, 150 mM NaCl, pH 7.4.

Preservation of membrane-protein complexes

After addressing the whole-proteome extraction capability of the new polymers, we focused on a set of structurally and functionally diverse examples of membrane proteins pertaining to various cellular membranes. To this end, we analysed the SEC elution profiles of select proteins as obtained from LC-MS/MS after extraction by DIBMA-SB: (i) Noncovalent membrane-protein complex: The Na⁺/K⁺ ATPase (ATP1) is a heterotrimeric membrane-protein complex crucial for maintaining an electrochemical potential difference across the plasma membrane.²³ Importantly, the α - and β -subunits of this complex, which have largely different molecular weights of 113 kDa and 35 kDa, respectively, were found to co-elute in a single peak exhibiting a maximum at ~700 kDa (Figure 5a). The excellent correlation between the elution profiles of these two subunits strongly indicates that DIBMA-SB extracted the intact complex from HeLa cells. In contrast with the α - and β -subunits, the γ -subunit consists of a single transmembrane helix. Such small and hydrophobic peptides oftentimes cannot be detected by mass spectrometry, which was also the case here. (ii) Covalent membrane-protein complex: The insulin receptor (INSR) and the insulin-like growth factor receptor (IGF1R) are receptor tyrosine kinases that exist in the plasma membrane as covalently bound homo- or heterodimers having very similar molecular weights of ~310 kDa.²⁴ As thus expected, both proteins were found to co-elute with high correlation, exhibiting maxima at ~1500 kDa (Figure 5a). (iii) Multipass β -sheet membrane protein: The voltage-dependent anion channel 1 (VDAC1) is an abundant β -barrel protein localised predominantly to the mitochondrial outer membrane. This protein, which has been implicated in Alzheimer's and Parkinson's disease,²⁵ occurs in monomeric, homodimeric, and homotrimeric forms.²⁶ Indeed, we observed a broad elution profile peaking at ~110 kDa but with a pronounced shoulder on the left-hand side indicative of oligomeric species (Figure 5b). (iv) Single-pass α -helical membrane protein: Cytochrome C450 reductase (POR) is found in the membrane of the smooth endoplasmic reticulum, to which it is anchored through a single transmembrane helix.²⁷ Previous investigations on a POR fragment in MSP nanodiscs after solubilisation with the harsh detergent Triton showed that the presence of a native-like lipid bilayer is crucial for protein function.²⁸ Here, we found that the full-length protein can readily be extracted without the

use of conventional detergents to form well-defined lipid-bilayer nanodiscs, as demonstrated by the observation that the protein eluted in a fairly narrow peak at ~ 205 kDa.

In general, for all membrane proteins and membrane-protein complexes studied, the elution profile peaked at an apparent molecular weight, MW_{app} , that amounted to 3–5 times the nominal molecular weight of the bare protein constituents. This finding suggests that the contribution of the lipid-bilayer patch and the polymer belt to the overall size of the protein/lipid/polymer assembly scales in a roughly linear fashion with the size of the encapsulated protein component(s). Taken together, we conclude that DIBMA-SB nanodiscs are compatible with broad-band fractionation of inherently complex samples by SEC and, crucially, preserve both homo- and heteromeric membrane-protein complexes extracted from various cellular membranes.

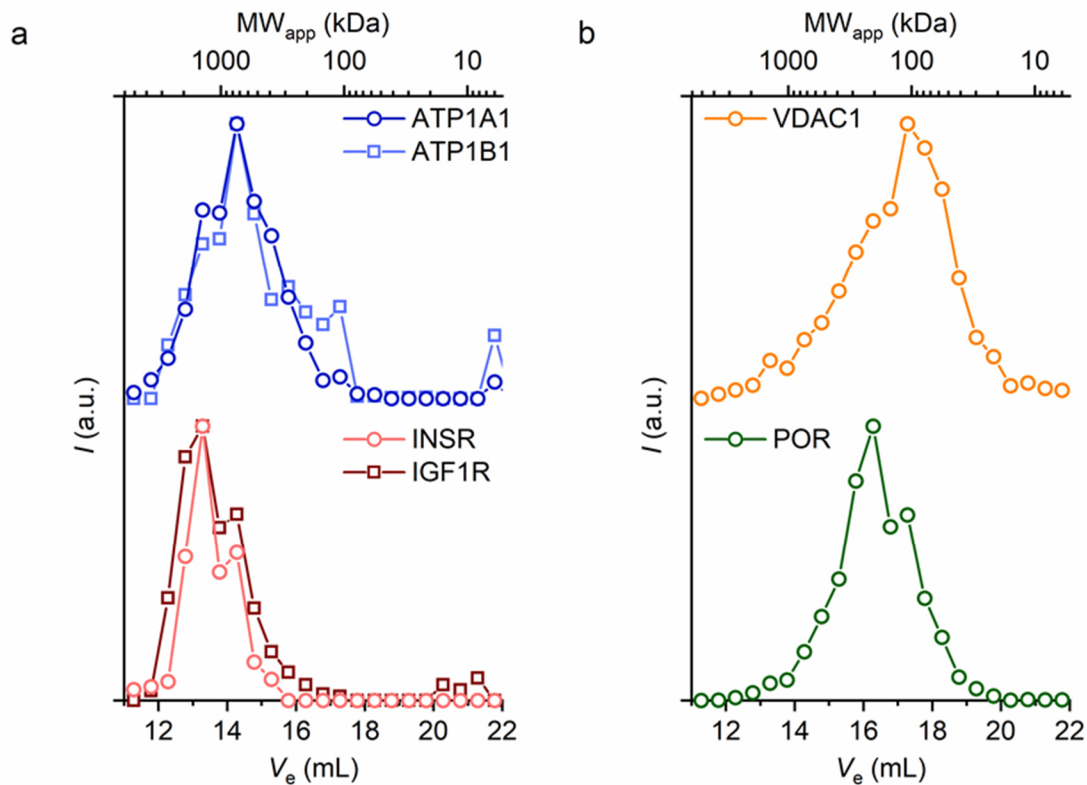


Figure 5. SEC elution profiles of (a) membrane-protein complexes and (b) monomeric membrane proteins extracted from HeLa cells as determined by LC-MS/MS. ATP1A1/B1: α/β subunits, respectively, of Na^+/K^+ ATPase; INSR: insulin receptor; IGF1R: insulin-like growth factor 1 receptor; VDAC1: voltage-dependent anion channel 1; POR: NADPH/cytochrome P450 reductase. *Lower abscissa*: elution volume (V_e); *upper abscissa*: apparent molecular weight (MW_{app}) of protein-containing nanodiscs; ordinate: normalised raw peptide intensity (I).

Reliable protein/lipid interaction studies without unspecific interactions

We assessed the usefulness of DIBMA-SB and SMA(2:1)-SB polymers for protein/lipid interaction studies by means of MDS, a recent powerful method capable of detecting small changes in hydrodynamic particle size.^{29–31} First, we titrated the soluble but membrane-interacting protein α -synuclein in its monomeric form either with mixed DMPG/DMPC nanodiscs carrying an anionic surface charge or with zwitterionic DMPC nanodiscs, both formed from SMA(2:1)-SB (Figure 6a). Crucially, the apparent hydrodynamic radius of α -synuclein remained unaffected in the presence of DMPC nanodiscs but increased to a value of $r_H = 8$ nm in the presence of DMPG/DMPC nanodiscs, thereby reflecting the charge-dependent lipid specificity of α -synuclein.³² Second, we used guanine nucleotide-binding protein subunit $\beta 1$ (GB1) as a negative control, which indeed showed no interactions with lipid-bilayer nanodiscs formed from SMA(2:1)-SB (Figure 6b). Third, we found the peptidic adrenocorticotrophic hormone (ACTH) to bind to anionic DMPG in a lipid-concentration-dependent manner but not to zwitterionic DMPC encapsulated by either SMA(2:1)-SB or DIBMA-SB (Figure 6c,d). In sharp contrast with this expected observation,³³ lipid specificity was lost when the same membrane-interaction assay was performed using nanodiscs encapsulated by conventional SMA(2:1). In the latter case, ACTH indiscriminately bound to both DMPC and DMPG nanodiscs, suggesting unspecific interactions of the peptide hormone with the polyanionic polymer (Figure 6c). Taken together, these three examples demonstrate that the new, electroneutral polymers do not interfere with native-like protein/lipid interactions and, thereby, enable sensitive membrane-interaction assays that are inhibited by existing polymer-based nanodiscs.

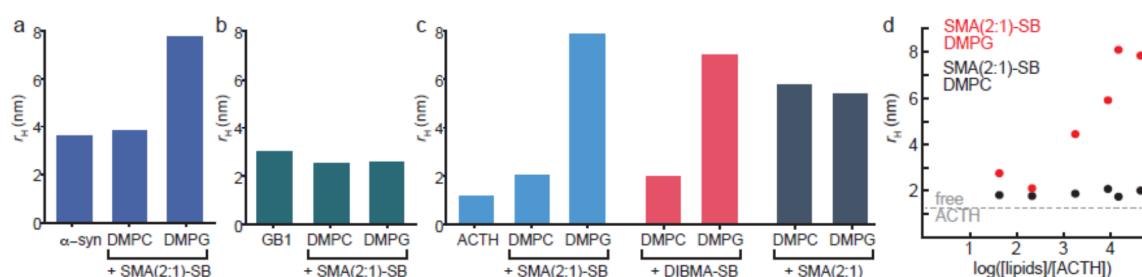


Figure 6. Hydrodynamic radii, r_H , of indicated nanodiscs and proteins as derived from microfluidic diffusional sizing measurements.

Suitability for cell-free membrane-protein synthesis

The co-translational insertion of membrane proteins synthesised in a cell-free manner into preformed nanoscopic membranes is a new and straightforward strategy for generating membrane-protein samples in native-like lipid environments without the use of conventional detergents.³⁴ Although the implementation of polymer nanodiscs would offer substantial benefits, previous approaches have almost exclusively relied on MSP nanodiscs. This is because the addition of existing, polyanionic copolymers such as DIBMA and SMA(2:1) adversely affects the concentration of free Mg^{2+} , which needs to be tightly controlled during cell-free protein synthesis (Figure S9a). By contrast, we observed that the electroneutral polymers DIBMA-SB and SMA(2:1)-SB were readily tolerated by the cell-free system, as exemplified by the efficient synthesis of green fluorescent protein (GFP). A variety of nanodiscs formed by different polymer/DOPG ratios were screened for their suitability in supporting cell-free membrane-protein production. DOPG was used for nanodisc formation because it has previously been found to perform best on the selected membrane proteins with MSP nanodiscs.³⁵ For both DIBMA-SB and SMA(2:1)-SB, SEC indicated the most homogenous nanodiscs at a polymer/DOPG molar ratio of 1:10, which was thus used for the following experiments (Figure S9b and c).

The light-gated proton pump proteorhodopsin (PR) was used as a first model protein for cell-free synthesis in the presence of increasing nanodisc concentrations (Figure 7a).³⁶ PR expression was quantified by measuring its specific UV absorbance at 530 nm directly in the cell-free reaction. With SMA(2:1)-SB, we obtained a PR concentration of 65 μ M at a nanodisc concentration of 80 μ M, meaning that, on average, >80% of all nanodiscs harboured a PR monomer. With DIBMA-SB, the nanodisc concentration had to be doubled to obtain a similar PR concentration (Figure 7a). PR-containing nanodiscs were then affinity-purified by taking advantage of the C-terminal Strep-tag attached to the protein. Subsequent SEC profiles revealed that PR/DIBMA-SB nanodiscs eluted as a single peak comparable to that observed for PR embedded in nanodiscs encircled by the MSP variant MSP1E3D1 (Figure 7b). By contrast, PR/SMA(2:1)-SB nanodiscs eluted predominantly in the void peak, indicating the presence of relatively large aggregates.

As a second model system, the turkey β 1-adrenergic receptor (T β 1AR) was investigated as a representative of G-protein coupled receptors (GPCRs). To this end, we synthesised a thermostabilised, GFP-coupled variant of T β 1AR in the presence of increasing concentrations

of polymer-bounded lipid-bilayer nanodiscs (Figure 7c).³⁵ The T β 1AR construct was modified by fusion of GFP to its C-terminal end.³⁵ The cell-free synthesized and solubilized T β 1AR-GFP fusion could thus be quantified by measuring the GFP fluorescence. Finally, we assessed the functional folding of the T β 1AR-GFP fusion construct directly in the cell-free reaction mixture by radioligand binding of the specific antagonist [³H]-alprenolol, which binds T β 1AR in a 1:1 stoichiometry.³⁵ As gauged by the fraction of ligand binding, the yield of active (i.e., binding-competent) T β 1AR in the presence of 240 μ M DIBMA-SB nanodiscs amounted to \sim 13%, in comparison with \sim 18% in the presence of MSP1E3D1 nanodiscs (Figure 7c). With SMA-SB nanodiscs, the yield of active receptor amounted to only \sim 4.7%, even at the highest nanodisc concentration of 240 μ M (Figure 7c).

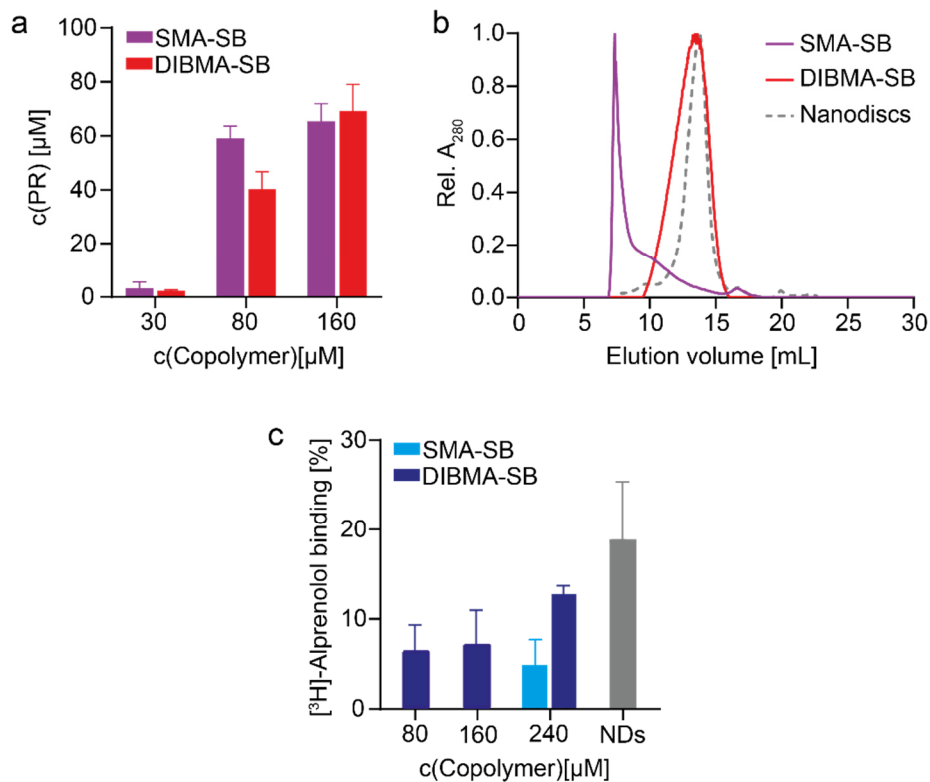


Figure 7. Cell-free synthesis of membrane proteins into preformed electroneutral polymer nanodiscs. (a) Synthesis yields of PR in the presence of increasing concentrations of DIBMA-SB or SMA(2:1)-SB nanodiscs. (b) SEC elution profiles of PR synthesised in the presence of 160 μ M nanodiscs and of a PR reference synthesised in the presence of MSP1E3D1 nanodiscs. (c) Binding of [³H]-alprenolol to T β 1AR-GFP as quantified by a filter binding assay. Shown is the percentage of T β 1AR-GFP that can bind the ligand. Error bars indicate standard deviations of experimental triplicates.

Discussion

We have developed electroneutral DIBMA-SB and SMA(2:1)-SB polymers that can be synthesised by simple modification of commercially available polymer backbones of DIBMA and SMA(2:1), respectively. This allows a low-cost and straightforward production of these polymers in non-specialised laboratories. Previously reported zwitterionic polymers have found limited application because they are produced by laborious and expensive *de novo* polymer synthesis¹⁶ or because they have low aqueous solubility within the rather narrow pH range typically used for *in vitro* studies of membrane proteins.¹⁵ Here, we demonstrate that, starting from polyanionic, commercial precursors, electroneutral polymers can be obtained that are sufficiently water-soluble, possess a high tolerance towards changes in solvent conditions such as pH and ionic strength, and—most importantly—extract individual membrane proteins, entire membrane-protein complexes, as well as surrounding lipids directly from cellular membranes to form lipid-bilayer nanodiscs in an efficient yet gentle fashion. Our observation that the electroneutral polymers, in contrast with their precursors DIBMA and SMA(2:1), efficiently solubilise anionic lipids such as POPG and DOPG is readily explained by the fact that Coulombic repulsion between polymer and lipid molecules is abolished upon derivatisation of the polymer's carboxylate moieties.

In addition, the electroneutral polymers introduced herein offer considerable advantages for membrane-protein research. On the one hand, they significantly extend the range of bioanalytical and preparative techniques compatible with lipid-bilayer nanodiscs to include methods such as MDS and cell-free protein production, which otherwise would suffer from unspecific Coulombic interactions. Herein, we show by MDS that electroneutral polymers do not interfere with native-like protein/lipid interactions and, thus, enable sensitive membrane-interaction assays. Furthermore, functionally folded forms of large integral membrane proteins can be synthesised in a cell-free manner at levels and in qualities similar to those previously reported for MSP nanodiscs.^{35,39} Even for a method as simple and common as SDS-PAGE, DIBMA-SB and SMA(2:1)-SB provide substantial benefits, as they do not need to be removed prior to gel electrophoresis in order to avoid smearing on the gel. In addition to the favourable properties and new applications demonstrated above, the absence of a net charge on the new sulphobetaine polymers bodes well for other applications. These may include, for example, protein purification by affinity chromatography, where unspecific Coulombic interactions with the column matrix can cause inefficient separation or loss of protein,³⁷

and surface plasmon resonance (SPR) spectroscopy, which tends to suffer from repulsive interactions between highly charged nanodiscs and fixation chips.³⁸

Supporting Information

Materials and Methods

Materials. DMPC was a kind gift from Lipoid (Ludwigshafen, Germany), POPG and DOPG were purchased from Avanti Polar Lipids (Alabaster, USA). SMA(2:1) hydrolysed from styrene/maleic anhydride (2:1) (tradename Xiran SZ30010) was kindly provided by Polyscope (Geleen, Netherlands). DIBMA (Sokalan CP 9) was a kind gift from BASF (Ludwigshafen, Germany). D₂O was purchased from Deutero (Kastellaun, Germany), C0mplete (EDTA-free), adenosine triphosphate (ATP), tRNA from *E. coli* MRE 600, and pyruvate kinase (PK) from Roche Diagnostics (Rotkreuz, Switzerland), and formic acid from Honeywell (Morristown, USA). Acetonitrile (ACN), chloroacetamide, MS-grade H₂O, and NaCl were purchased from VWR (Darmstadt, Germany). 85% (w/v) H₃PO₄ in D₂O, Na₂HPO₄, acetyl phosphate (AcP), Mg(OAc)₂, KOAc, cytidine triphosphate (CTP), guanosine triphosphate (GTP), uridine triphosphate (UTP) and polyethyleneglycol (PEG) 8000 were from Sigma–Aldrich (Steinheim, Germany), and ammonium bicarbonate (ABC), CaCl₂, Coomassie Brilliant Blue G250, dithiothreitol (DTT), ethylenediamine tetraacetic acid (EDTA), MgCl₂, NaH₂PO₄, sodium dodecyl sulphate (SDS), sucrose, tris(hydroxyl-methyl)amino-methane (Tris), Tris–HCl, all aminoacids, bovine serum albumin (BSA) folic acid, 2-(4-(2-Hydroxyethyl)-1-piperazinyl)-ethansulfonic acid (HEPES), CaCl₂ and NaN₃ were from Carl Roth (Karlsruhe, Germany), and KH₂PO₄ and phosphoenolpyruvic acid (PEP) were from AppliChem (Darmstadt, Germany). DDM was from Glycon (Luckenwalde, Germany), urea was from Grüssing (Filsum, Germany), standard polymers (poly(ethylene oxide) (PEO) 24k, Dextran 65k, Dextran 73k, Pullulan 105k) were from Malvern Panalytical (Malvern, UK) and RiboLock RNase Inhibitor was from Thermo Scientific (Langenselbold, Germany). All chemicals were purchased in the highest purity available.

Polymer synthesis.

Preparation of polymer stock solutions. Polymer powders were lyophilised using a Martin Christ Alpha 2–4 LSCplus (Osterode am Harz, Germany) and suspended in either Tris buffer (50 mM Tris, 150 or 200 mM NaCl, pH 7.4 or 8.3) or phosphate buffer (50 mM Na₂HPO₄/NaH₂PO₄, 200 mM NaCl, pH 6.5). Samples were then transferred to a preheated ultrasonic bath (Bandelin Sonorex RK 52 H, Berlin, Germany) at 50–70°C for 15–60 min with vortexing steps in between until the solutions cleared up. Polymer stock solutions were sterile-

filtered using 0.45- μm poly(vinylidene fluoride) syringe filters (Carl Roth, Karlsruhe, Germany).

Vesicle preparation. DMPC or POPG powders were suspended in either Tris buffer (pH 7.4 and 8.3) or phosphate buffer (pH 6.5) to a final lipid concentration of 50–100 mg/mL. Suspensions were vortexed for 10 min prior to at least 31-fold extrusion through two stacked polycarbonate membranes with a nominal pore diameter of 100 nm. Lipid suspensions were then extruded at 30°C using a block-heated Mini-Extruder (Avanti, Alabama, USA) to form large unilamellar vesicles (LUVs). Particle size distributions were obtained by DLS (see below), yielding hydrodynamic LUV diameters of ~ 140 nm.

Dynamic light scattering. Samples containing 4 mg/mL DMPC or POPG—which was added in the form of LUVs—and 0–12 mg/mL DIBMA-SB or SMA(2:1)-SB in either Tris buffer (pH 7.4 or 8.3) or phosphate buffer (pH 6.5) were incubated for at least 16 h at 30–35°C (DMPC) or 25°C (POPG). DLS measurements were carried out on a Zetasizer Nano S90 (Malvern Panalytical, Malvern, UK) equipped with a 633-nm He–Ne laser and a detection angle of 90°. Samples were thermostatted for 2 min at 30–35°C (DMPC) or 25°C (POPG) before measurements were performed in a 45- μL quartz glass cuvette with a cross-section of 3 mm \times 3 mm (Hellma Analytics, Müllheim, Germany). Each sample was measured twice: first, with the attenuator position automatically optimised for determination of particle size distributions and, second, with the attenuator set to the maximum to guarantee comparability of total light scattering intensities. Effects of buffer components and concentrations on the viscosity and RI of the solvent were accounted for during data analysis. Autocorrelation functions were fitted using a non-negatively constrained least-squares function⁴⁰ to yield intensity-weighted particle size distributions and by cumulant analysis⁴¹ to obtain z-average particle diameters and associated polydispersity indices (PDIs). Distribution widths of z-average diameters, σ , were calculated as $\sigma = \sqrt{\text{PDI}}$ z. In the case of multimodal distributions, the hydrodynamic particle diameter was taken as the location of the first peak corresponding to the smallest size, which is justified by the steep dependence of light scattering intensity on particle size.

³¹P NMR spectroscopy. Samples containing 2, 4, 6, or 8 mg/mL DMPC LUVs and 0–24 mg/mL DIBMA-SB or SMA(2:1)-SB were prepared from stock solutions in Tris buffer at pH 7.4. 10% D₂O (v/v) was added to the sample buffer to provide a lock signal. DMPC/polymer mixtures were incubated at 30°C for at least 16 h. NMR measurements were performed at 30°C on an Avance 600 spectrometer (Bruker Biospin, Rheinstetten, Germany) operating at a ³¹P

resonance frequency of 243 MHz using a 5-mm broadband inverse probe. 128 scans were acquired with an inverse-gated decoupling sequence using an acquisition time of 2.2 s, a sweep width of 7310 Hz, and a relaxation delay of 10 μ s. Data were multiplied by an exponential function with a line-broadening factor of 1.0 Hz before Fourier transformation. Chemical shifts were referenced to 85% (w/v) H₃PO₄ in D₂O as external standard at 0 ppm. Signal peaks were integrated using the software Bruker Topspin 4.0.5.

Negative-stain transmission electron microscopy. TEM samples were prepared by loading 5 μ L polymer-bounded nanodiscs at $m_p/m_l = 1$ onto Quantifoil Cu grids (300 mesh) coated with carbon film (Quantifoil Micro Tools GmbH, Großlöbichau, Germany) or on Cu grids coated with Formvar film (Plano, Wetzlar, Germany). Excess liquid was blotted off with a strip of filter paper after 30 s followed by staining with 5 μ L 1% (w/v) aqueous uranyl acetate solution. Specimens were dried and examined in an EM 900 transmission electron microscope (Carl Zeiss Microscopy GmbH, Oberkochen, Germany), and micrographs were recorded with an SM-1k-120 slow-scan charge coupled device (SSCCD) camera (TRS, Moorenweis, Germany).

ζ -potential measurements. Samples containing 4 mg/mL polymer, 4 mg/mL DMPC in the form of LUVs, or polymer-bounded nanodiscs made from 4 mg/mL DMPC and 4 mg/mL polymer in Tris buffer (50 mM Tris, 100 mM NaCl, pH 7.4) were incubated at 35°C for at least 16 h. Measurements were performed on a Zetasizer Nano ZS (Malvern Panalytical) equipped with a 633-nm He–Ne laser and a backscatter detection angle of 173°. Polymers, nanodiscs, or DMPC LUVs were thermostatted at 35°C for 2 min before measurements were performed at the same temperature in a folded capillary cell DTS1070 (Malvern Panalytical). A monomodal measurement protocol was used, which applies a rapidly alternating electric field, from which the mean ζ -potential was derived. To avoid Joule heating caused by high conductivity, the voltage was manually reduced to 10 V. To ensure correct operation and verify the cleanliness of the cells, a polystyrene latex standard DTS1235 (Malvern Panalytical) having a ζ -potential of $-(42 \pm 4)$ mV was measured after at least every third new sample.

Differential scanning calorimetry. Samples containing 4 mg/mL DMPC LUVs and 0–4 mg/mL polymer in Tris buffer (pH 7.4) were incubated at 35°C for 16 h. Sample and reference cells were filled with buffer and were repeatedly heated and cooled at a rate of 30°C h⁻¹. With usual exception of the first upscan, successive heating and cooling scans overlaid very closely. Data were averaged, blank-subtracted, and normalised against the molar amount of DMPC in the

sample using the software MicroCal Origin 5.0 (OriginLab, Northampton, USA). The melting temperature, T_m , was determined as the temperature at which the excess molar isobaric heat capacity, ΔC_p , reached a maximum.

Solubilisation of HeLa membranes. Confluent HeLa cells were harvested at 4°C by aspiration of the cell medium, followed by two washing steps with 5 mL phosphate-buffered saline (140 mM NaCl, 2,7 mM KCl, 10 mM Na₂HPO₄, 1.8 mM KH₂PO₄) and 5 mL Tris buffer (150 mM NaCl, pH 7.4) and scraping using a sterile cell scraper. Cells were collected, pelleted at 800 *g* for 10 min, resuspended in 3 mL Tris buffer supplemented with 250 mM sucrose and homogenised in a precooled Potter–Elvehjem tissue grinder (Corning, New York, USA). The cellular crude extract containing the membranes was ultracentrifuged at 265'000 *g* for 30 min. The pellet was washed in 3 mL Tris buffer, and the centrifugation step was repeated once. To maintain a uniform membrane protein concentration across all experiments, the pellet was weighed and resuspended in an appropriate volume of Tris buffer to a membrane concentration of 60 mg/mL (wet weight), which was further diluted to 16.7 mg/mL upon addition of polymer or detergent. After overnight incubation of the solubilisation mixture at room temperature on a rotary wheel, samples were ultracentrifuged at 100'000 *g* and 20°C for 80 min. Pellets containing unsolubilised material were resuspended in Tris buffer containing 2% (*w/v*) SDS in equal volumes as supernatant samples containing nanodiscs. Both supernatant and pellet samples were subjected to SDS-PAGE and a BCA protein assay (see below).

SDS-PAGE. Protein-extraction yields were determined by SDS-PAGE using a NUPAGE Bis–Tris precast gel with a polyacrylamide gradient of 4–12% (Thermo Fisher Scientific, Schwerte, Germany). Pellet and supernatant samples were diluted with SDS buffer (25 mM DTT, 106 mM Tris-HCl, 141 mM Tris, 2% (*w/v*) SDS, 10% (*w/v*) glycerol, 0.51 mM EDTA, 0.22 mM Coomassie Brilliant Blue G250, and 0.175 mM Phenol Red, pH 8.5), denatured at 95°C for 10 min and centrifuged at 10'000 *g* for 2 min. A voltage of 200 V was applied for 45 min at 50 W. Gels were stained for 60 min in 3.2 mM Coomassie Brilliant Blue R250 in 40% methanol and 10% (*v/v*) ethanoic acid, destained for 48 h in water with a paper towel to remove excess Coomassie dye, and photographed.

Multiple-detection size exclusion chromatography. Mass-average molar masses of DIBMA-SB, SMA(2:1)-SB, and the corresponding polymer nanodiscs were determined by SEC

on an OmniSEC system (Malvern Panalytical) equipped with a Superose 6 Increase 10/300 GL column (GE Healthcare, Freiburg, Germany) and coupled to UV, static light scattering, and refractive index detectors. The column was equilibrated at 30°C with 3 column volumes (CVs) Tris buffer (pH 7.4) under a steady flow rate of 0.5 mL/min. 50- μ L aliquots of 2.5, 5, 7.5, or 10 mg/mL polymer and polymer/DMPC nanodiscs with m_p/m_l ranging from 0.5 to 2.0 were injected. Polymer standards (PEO 24k, Dextran 65k, Dextran 73k, and Pullulan 105k, all Malvern Panalytical) were used to generate a calibration curve to estimate mass-average molar masses of lipid-free polymers. Chromatograms of polymer nanodiscs were analysed with the software OmniSEC 11.0.

Size exclusion chromatography of solubilised Hela proteins. SEC was carried out on an Äkta Purifier 10 system equipped with a Superose 6 Increase 10/300 GL column and a UV detector (both GE Healthcare) at 8°C. For DIBMA-SB and SMA(2:1)-SB, supernatant samples containing nanodiscs were concentrated using Amicon tubes (Merck, Darmstadt, Germany) with a 10-kDa cut-off. The column was equilibrated with 2 CVs precooled Tris buffer (150 mM NaCl, pH 7.4) before 500- μ L aliquots of polymer-extracted membrane proteins were injected. 500- μ L fractions were collected at a flow rate of 0.3 mL/min. UV absorbance was recorded at 280 nm for protein detection, 220 nm for DIBMA detection, and 240 nm for DIBMA-SB detection. Collected fractions were lyophilised and stored at -80°C.

Protein assay and precipitation. Lyophilised SEC fractions were resuspended in 110 μ L water. To determine the total amount of protein in each fraction, 10 μ L of each sample was subjected to a BCA protein assay⁴² (Thermo Fisher Scientific) performed on a FLUOstar Omega plate reader (BMG Labtech, Ortenberg, Germany). Proteins in the remaining 100 μ L were precipitated using a modified variant of a published chloroform/methanol precipitation procedure.⁴³ Briefly, 400 μ L methanol was added to 100 μ L ice-cold sample, and the mixture was vortexed for 3 s. 200 μ L chloroform was added, the mixture was vortexed again for 3 s, and 300 μ L water was added. The sample was vortexed thoroughly for 10 s and centrifuged at 14'000 g for 3 min in a precooled centrifuge at 4°C. The upper aqueous phase was removed before addition of another 4 volumes of methanol, vortexing for 15 s, and centrifugation at 5000 g and 20'000 g for 1 min and 4 min, respectively. The supernatant was discarded, and the protein pellet was dried either in a vacuum desiccator (DWK Life Sciences, Wertheim, Germany) at room temperature over night or in a Jouan RC1010 vacuum concentrator (Thermo Fisher Scientific) at 40°C for 45 min.

In-solution digest and sample clean-up. Precipitated SEC fractions were resuspended in 25 μ L urea ABC buffer (8M urea, 25 mM ammonium bicarbonate). DTT and chloroacetamide were added separately to final concentrations of 12.5 mM and 25 mM, respectively, and the sample was incubated for 30 min. Samples were diluted to 4 M urea with ABC buffer, Lys-C was added to reach a final Lys-C/protein mass ratio of 1:100, and the mixture was incubated at 37°C for at least 3 h. After the initial digest, the urea concentration was further diluted to 1 M, ACN and trypsin were added to a final concentration of 5% (v/v) and a trypsin/protein mass ratio of 1:100, respectively, and the mixture was incubated at 37°C for at least 12 h. An additional digest was performed by addition of trypsin to a final trypsin/protein mass ratio of 1:50 followed by another incubation at 37°C for 3 h. Samples were acidified by addition of formic acid to a final concentration of 2% (v/v). Sample clean-up and desalting were performed following a modified version of the STAGE tipping protocol.⁴⁴ To this end, STAGE tips were prepared with 2 layers of Empore C18 filter extraction discs and equilibrated with 25 mM ABC and 0.1% (v/v) formic acid, which was also used for column washing after sample loading. Peptides were then eluted by pushing 25 mM ABC, 80% (v/v) ACN, 0.1% (v/v) formic acid through the tips. The eluate was dried in a RVC 2-25 CD plus vacuum concentrator (Martin Christ, Osterode am Harz, Germany) at 30 mbar and 40°C for 60 min and submitted to mass spectrometry.

Mass spectrometry. Protein identification and quantification were performed on an Easy-nLC 1200 HPLC coupled to a Q Exactive HF Mass Spectrometer (Thermo Fisher Scientific). Peptides were separated on reversed-phase columns with a 75- μ m inner diameter (New Objective, Woburn, Massachusetts, USA) packed with ReproSil-Pur 120 C18-AQ (Dr. Maisch, Ammerbruch-Entrigen, Germany) and injected directly into the mass spectrometer. After resuspension in 5 μ L 2% (v/v) ACN and 0.1% (v/v) formic acid in MS-grade H₂O, 4 μ L of each fraction was loaded onto 30-cm columns and eluted with a 1.5-h gradient. For all MS runs, data were acquired in a data-dependent fashion using a top 15 method for peptide sequencing.

MS data were analysed with MaxQuant (version 1.6.3.3) using a label-free algorithm.⁴⁵ A false-discovery rate (FDR) of 0.01 for peptides and a minimum peptide length of 7 amino acid residues were required. For Andromeda search, trypsin allowing for cleavage N-terminal of proline was chosen as enzyme specificity. Cysteine carbamidomethylation was selected as a fixed modification, and protein N-terminal acetylation and methionine oxidation were

selected as variable modifications. A maximum of two missed cleavages was allowed. Initial mass deviation of precursor ion was limited to 7 ppm and mass deviation for fragment ions to 0.5 Da. Protein identification required at least one unique in each protein group. “Match between run” was used to transfer identities within all replicate samples of the unfractionated samples and between adjacent SEC fractions. For data analysis, an Excel spreadsheet and the Solver were used for non-linear least-squares fitting⁴⁶. MS data matrices were processed with the MaxQuant companion software Perseus.⁴⁷

Microfluidic diffusional sizing. MDS measurements with post-separation labelling⁴⁸ using injection-moulded disposable plastic chips were performed on a Fluidity One instrument (Fluidic Analytics, Cambridge, UK). Triplicate measurements for each sample were carried out and averaged hydrodynamic radii with standard deviations were plotted. Nanodisc and protein concentrations were in the range of X μ M.⁴⁹

Assembly of DOPG nanodiscs for cell-free protein expression assays. DOPG LUVs extruded to a size of 200 nm and polymer stock solutions (50 mM Tris, 150 mM NaCl, pH 7.4) were mixed in various molar copolymer:lipid ratios (1:2.5, 1:5, 1:10 and 1:20) and incubated at RT for 24 h. Nanodisc formation was monitored by clearance of the turbid solution. Subsequently, the mixtures were centrifuged at 20,000 *g* to remove larger aggregates. Supernatants were concentrated using Amicon tubes (Merck, Darmstadt, Germany) with a 10-kDa cut-off.

To monitor the size of formed polymer nanodiscs, SEC was carried out at 12 °C using a Superdex 200 Increase 3.2/300 GL column connected to an Äkta purifier system (both GE Healthcare, Freiburg, Germany). Prior injection of X mL nanodisc samples, the column was equilibrated in pre-cooled buffer (50 mM Tris, 150 mM NaCl, pH 7.4). The chromatography was conducted at a flow rate of 0.05 mL/min and UV absorbance was recorded at 240 nm.

Cell-free protein expression. Cell-free expression was carried out as described in detail previously.^{34,35} Briefly, S30 lysates were prepared from *E. coli* A19 strain. Analytical scale reactions were performed in 55 μ L reaction mixtures (RM) separated from a feeding mixtures (FM) with dialysis membranes with a MWCO of 12–14 kDa (Carl Roth, Karlsruhe, Germany). The volume ratio of RM to FM was 1:15. For membrane protein expression, preformed copolymer nanodiscs were added into the RM in final concentrations of 30–240 μ M. Reactions were incubated at 30°C for 16–20 h with shaking. After expression, RMs were collected and centrifuged at 18,000 *g* and 4°C for 10 min to remove precipitates.

Size exclusion chromatography of cell-free expressed PR. After expression, PR was purified via a C-terminal Strep-tag. The PR solution was diluted 1:3 in buffer X (100 mM Tris, 100 mM NaCl, pH 8.0), loaded and reloaded twice on a Strep column pre-equilibrated with the same buffer. The column was washed with 10 CV buffer and PR was eluted using buffer supplemented with 25 mM d-Desthiobiotin (Sigma-Aldrich, Steinheim, Germany). The purified protein was concentrated in Amicon tubes (Merck, Darmstadt, Germany) with a 10-kDa cut-off and centrifuged at 20,000 *g* and 4°C for 10 min before injecting onto the SEC column.

SEC was carried out at 12°C using a Superose 6 10/300 GL column connected to an Äkta purifier system (GE Healthcare, Freiburg, Germany). The column was equilibrated in pre-cooled buffer X before injecting the PR sample. The run was conducted at a flow rate of 0.3 mL/min and UV absorbance was recorded at 280 nm.

Radioligand filter binding assay. Final concentrations of 10 nM T β 1AR and 50 nM [3 H]dihydroalprenolol (Biotrend, Köln, Germany) were incubated in 30 μ L volumes of binding buffer (50 mM HEPES, pH 7.5, 1 mM CaCl $_2$, 5 mM MgCl $_2$, 0.2% (w/v) BSA) for 1 h at RT with gentle shaking. Unspecific binding was determined by pre-incubating the samples with 40 μ M non-labelled alprenolol (Torcis, Bristol, UK) for 1 h before adding [3 H]dihydroalprenolol. GF/B glass fibre filters (Merck, Darmstadt, Germany) were pre-treated with 0.3% (w/v) polyethyleneimine for 30 min and washed 5 times with 150 μ L filter wash buffer (50 mM HEPES, pH 7.5, 0.5% (w/v) BSA). Samples were transferred to glass fibre filters and subsequently washed 7 times with 150 μ L 50 mM HEPES, pH 7.5, 500 mM NaCl, 0.1% (w/v) BSA). Filters were solubilised in 2 mL Rotiszint eco plus (Carl Roth, Karlsruhe, Germany) and radioactivity was measured on a Hidex 300 SL liquid scintillation counter (Hidex, Turku, Finland).

Supplementary Figures

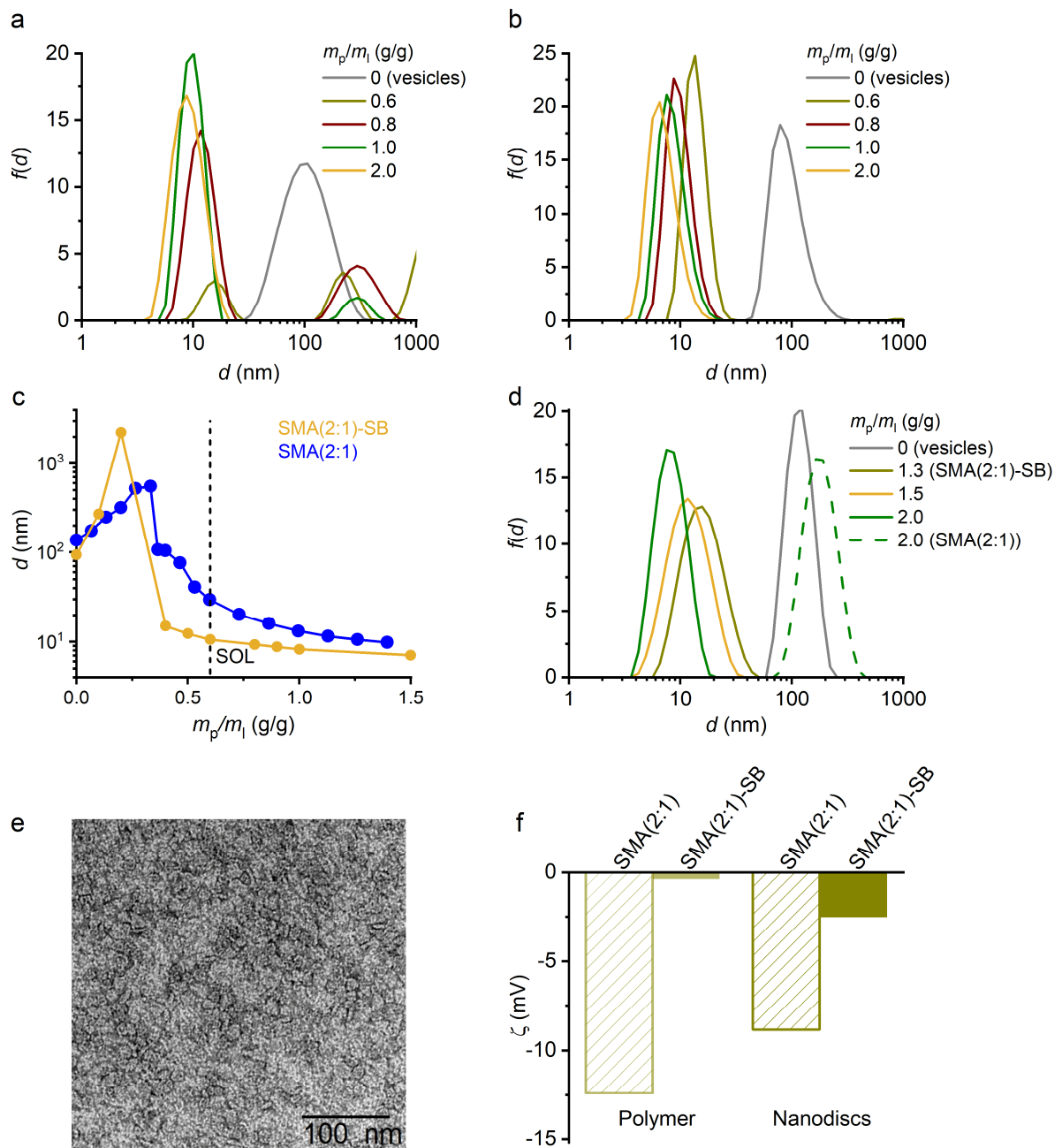


Figure S1. Solubilisation of lipid vesicles and nanodisc formation by SMA(2:1)-SB. (a) Intensity-weighted particle size distributions, $f(d)$, of aqueous mixtures of SMA-SB and DMPC at various polymer/lipid mass ratios, m_p/m_l . (b) Corresponding volume-weighted particle size distributions, $f(d)$, at various m_p/m_l . (c) Hydrodynamic particle diameters, d , as functions of m_p/m_l derived from particle size distributions such as shown in panel (a). (d) Intensity-weighted particle size distributions, $f(d)$, of aqueous mixtures of SMA(2:1)-SB or SMA(2:1) and POPG at various m_p/m_l as obtained from DLS. (e) Negative-stain EM images of SMA(2:1)-SB/DMPC nanodiscs at $m_p/m_l=1$ prepared on Formvar-coated Cu grids. (f) ζ -potentials of SMA(2:1), SMA(2:1)-SB, and the respective polymer-encapsulated DMPC nanodiscs in the presence of 100 mM NaCl. Experiments were carried out at 50 mM Tris, 200 mM NaCl, pH 7.4 unless noted otherwise.

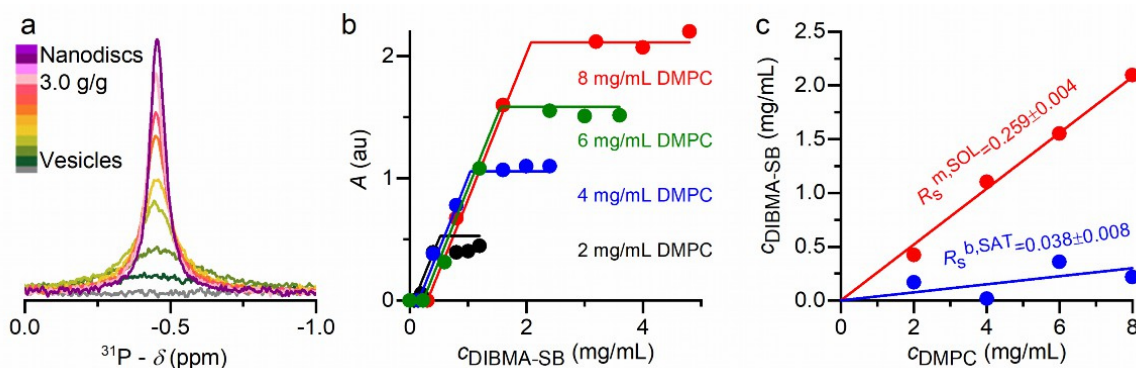


Figure S2. Solubilisation of DMPC vesicles by DIBMA-SB at 30°C as monitored by ^{31}P NMR. (a) NMR spectra of 4 mg/mL DMPC vesicles upon exposure to increasing DIBMA-SB concentrations. (b) Peak areas, A , at four different DMPC concentrations as functions of DIBMA-SB concentrations, showing experimental data (*circles*) and global fits (*solid lines*). (c) Phase diagram of DIBMA-SB/DMPC at 30°C showing the saturation (SAT) and solubilisation (SOL) boundaries defining the onset and completion of nanodisc formation, respectively. Experiments were carried out at 50 mM Tris, 200 mM NaCl, pH 7.4.

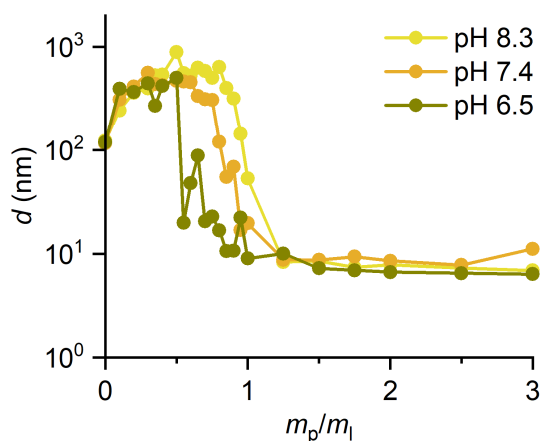


Figure S3. pH tolerance of SMA(2:1)-SB nanodiscs at 50 mM Tris and 200 mM NaCl. Shown are z-average diameters, d , of SMA(2:1)-SB/DMPC nanodiscs as functions of m_p/m_l at different pH values as derived from DLS. Experiments were carried out at 50 mM Tris, 200 mM NaCl, pH 7.4 unless noted otherwise.

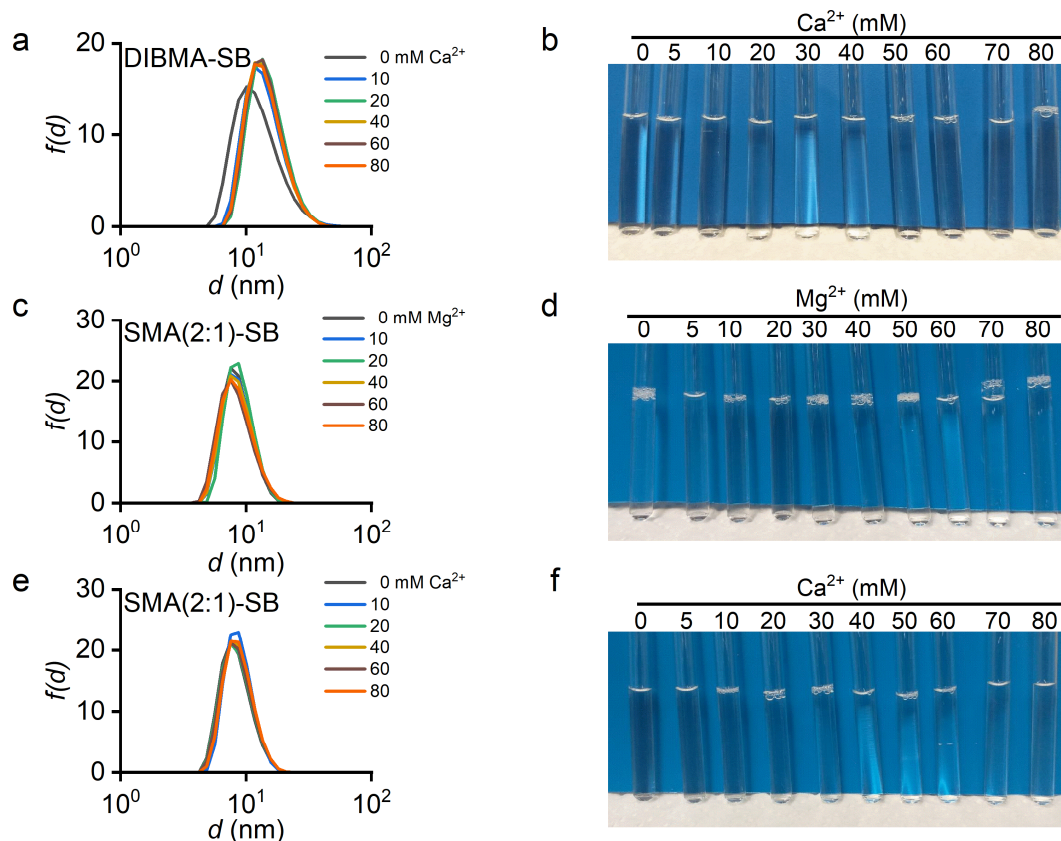


Figure S4. Tolerance towards divalent cations of DIBMA-SB and SMA(2:1)-SB. (a) Volume-weighted particle size distributions, $f(d)$, of DIBMA-SB/DMPC nanodiscs at increasing Ca^{2+} concentrations. (b) Visual appearance of nanodiscs in the presence of increasing Ca^{2+} concentrations. (c) Volume-weighted particle size distributions, $f(d)$, of SMA(2:1)-SB/DMPC nanodiscs at increasing Mg^{2+} concentrations. (d) Visual appearance of nanodiscs in the presence of increasing Mg^{2+} concentrations. (e) Volume-weighted particle size distributions, $f(d)$, of SMA(2:1)-SB/DMPC nanodiscs at increasing Ca^{2+} concentrations. (f) Visual appearance of nanodiscs in the presence of increasing Ca^{2+} concentrations. Experiments were carried out at 50 mM Tris, 200 mM NaCl, pH 7.4.

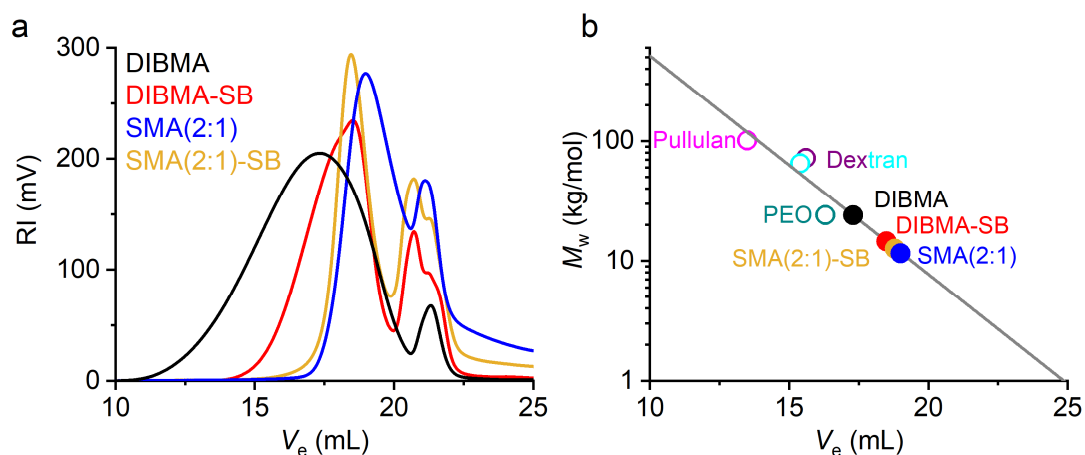


Figure S5. (a) SEC elution profiles of DIBMA, DIBMA-SB, SMA(2:1), and SMA(2:1)-SB as monitored by refractive index (RI). (b) Calibration curve determined using polymer standards PEO, Dextran, and Pullulan, yielding mass-average molar masses of $M_w = 14$ kg/mol for DIBMA-SB and $M_w = 12.6$ kg/mol for SMA(2:1)-SB. Experiments were carried out at 50 mM Tris, 200 mM NaCl, pH 7.4.

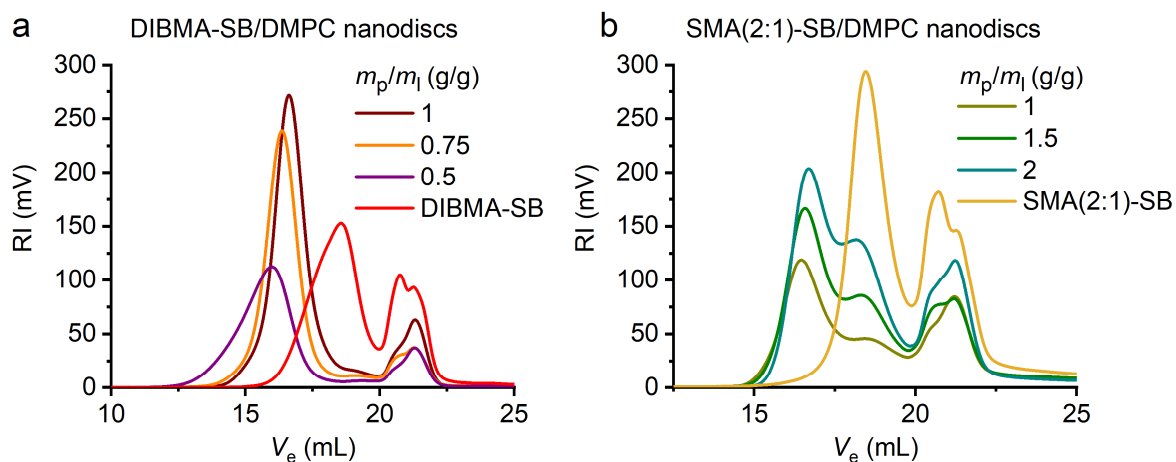


Figure S6. (a) SEC elution profiles of DIBMA-SB/DMPC nanodiscs at various m_p/m_l , confirming the absence of excess (“free”) polymer as well as a decrease in nanodisc size with increasing m_p/m_l . (b) SEC profiles of SMA(2:1)-SB/DMPC nanodiscs at various m_p/m_l . Experiments were carried out at 50 mM Tris, 200 mM NaCl, pH 7.4.

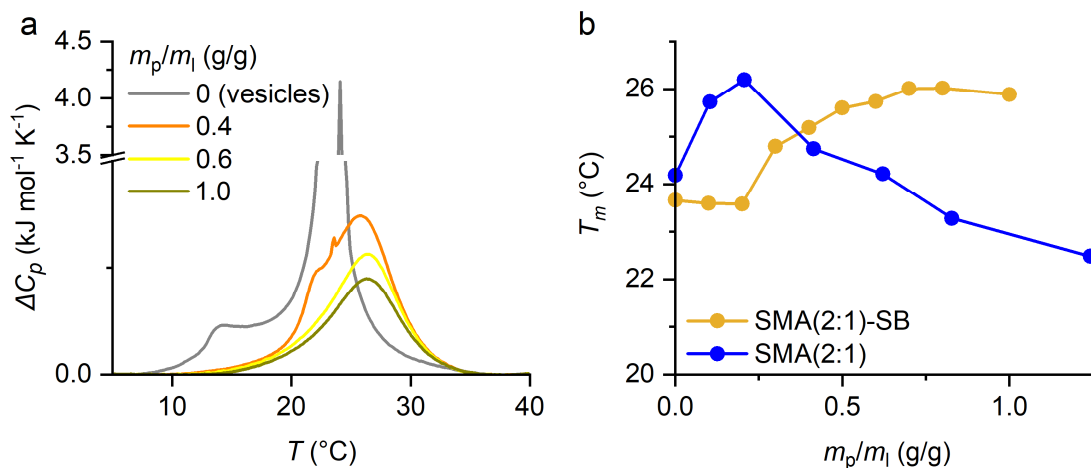


Figure S7. Thermotropic phase transitions in SMA(2:1)-SB nanodiscs. (a) DSC thermograms showing excess molar isobaric heat capacities, ΔC_p , of 4 mg/mL DMPC in the presence of increasing concentrations of SMA(2:1)-SB. (b) Gel-to-fluid phase transition temperatures, T_m , of 4 mg/mL DMPC at various m_p/m_l . Experiments were carried out at 50 mM Tris, 200 mM NaCl, pH 7.4.

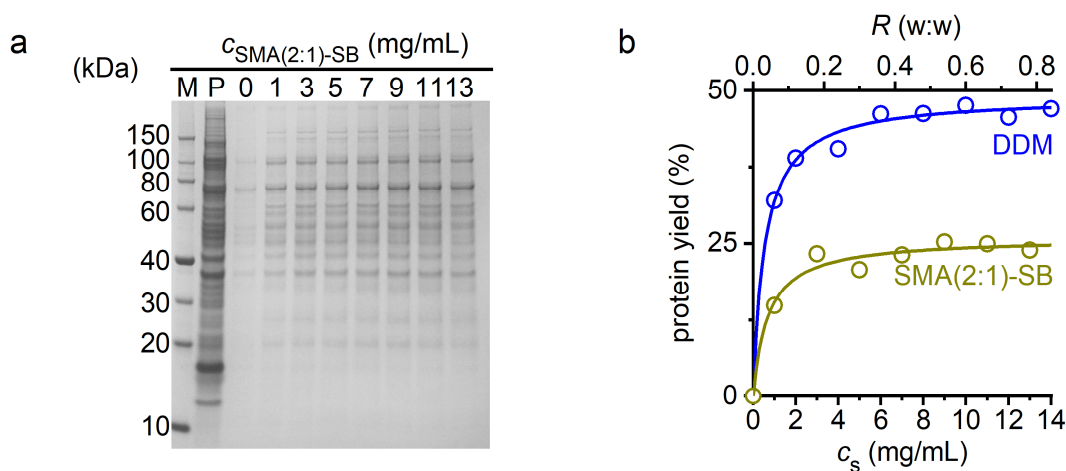


Figure S8. Extraction of membrane proteins from human cells using SMA(2:1)-SB. (a) SDS-PAGE showing membrane proteins extracted from HeLa cells by increasing concentrations of SMA(2:1)-SB. (b) Overall yields of extracted membrane proteins as functions of polymer or detergent concentration as determined by a colorimetric protein assay. *Lower abscissa*: surfactant concentration (c_s); *upper abscissa*: surfactant/membrane mass ratio (R); *ordinate*: solubilised protein yield.

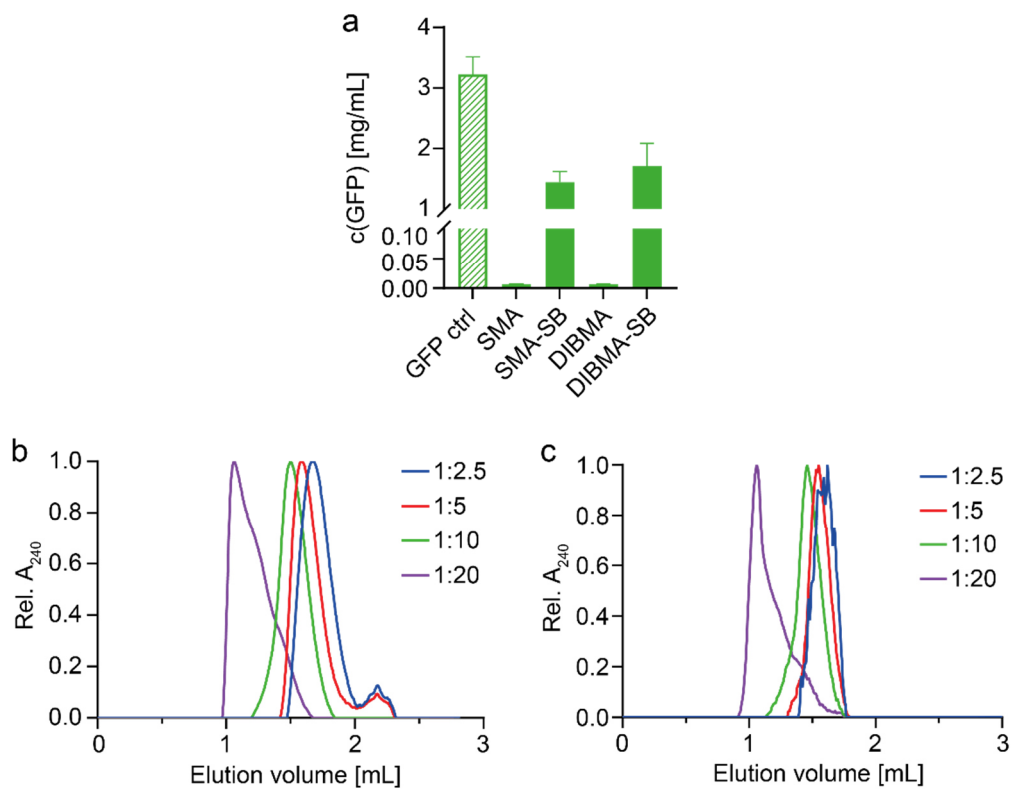


Figure S9. (a) Cell-free GFP expression in the presence of, DIBMA, DIBMA-SB, SMA(2:1), and SMA(2:1)-SB. DIBMA and SMA(2:1) disrupt the expression completely, while SMA(2:1)-SB and DIBMA-SB are tolerated by the system. All experiments have been performed in independent triplicates. (b) and (c) SEC elution profiles of preformed DIBMA-SB and SMA(2:1)-SB nanodiscs, respectively. Particles have been formed with various polymer:lipid molar ratios (1:2.5, 1:5, 1:10 and 1:20). At a ratio of 1:10, both nanodisc types show the most homogenous distribution.

References

1. Oluwole, A. O. *et al.* Solubilization of membrane proteins into functional lipid-bilayer nanodiscs using a diisobutylene/maleic acid copolymer. *Angew. Chemie Int. Ed.* **56**, 1919–1924 (2017).
2. Tonge, S. R. & Tighe, B. J. Responsive hydrophobically associating polymers: a review of structure and properties. *Adv. Drug Deliv. Rev.* **53**, 109–122 (2001).
3. Knowles, T. J. *et al.* Membrane proteins solubilized intact in lipid containing nanoparticles bounded by styrene maleic acid copolymer. *J. Am. Chem. Soc.* **131**, 7484–7485 (2009).
4. Dörr, J. M. *et al.* The styrene-maleic acid copolymer: a versatile tool in membrane research. *Eur. Biophys. J.* **45**, 3–21 (2016).
5. Seddon, A. M., Curnow, P. & Booth, P. J. Membrane proteins, lipids and detergents: not just a soap opera. *Biochim. Biophys. Acta, Biomembr.* **1666**, 105–117 (2004).
6. Bayburt, T. H., Grinkova, Y. V. & Sligar, S. G. Self-assembly of discoidal phospholipid bilayer nanoparticles with membrane scaffold proteins. *Nano Lett.* **2**, 853–856 (2002).
7. Lee, S. C. *et al.* A method for detergent-free isolation of membrane proteins in their local lipid environment. *Nat. Protoc.* **11**, 1149–1162 (2016).
8. Morrison, K. A. *et al.* Membrane protein extraction and purification using styrene-maleic acid (SMA) co-polymer: effect of variations in polymer structure. *Biochem. J.* **473**, 4349–4360 (2016).
9. Grethen, A., Oluwole, A. O., Danielczak, B., Vargas, C. & Keller, S. Thermodynamics of nanodisc formation mediated by styrene/maleic acid (2:1) copolymer. *Sci. Rep.* **7**, 11517 (2017).
10. Bersch, B., Dörr, J. M., Hessel, A., Killian, J. A. & Schanda, P. Proton-detected solid-state NMR spectroscopy of a zinc diffusion facilitator protein in native nanodiscs. *Angew. Chemie Int. Ed.* **56**, 1–6 (2017).
11. Sahu, I. D. *et al.* Characterization of the human KCNQ1 voltage sensing domain (VSD) in lipodisc nanoparticles for electron paramagnetic resonance (EPR) spectroscopic studies of membrane proteins. *J. Phys. Chem. B* **124**, 2331–2342 (2020).
12. Grime, R. L. *et al.* Single molecule binding of a ligand to a G-protein-coupled receptor in real time using fluorescence correlation spectroscopy, rendered possible by nano-encapsulation in styrene maleic acid lipid particles. *Nanoscale* **12**, 11518–11525 (2020).
13. Oluwole, A. O. *et al.* Formation of lipid-bilayer nanodiscs by diisobutylene/maleic acid (DIBMA) copolymer. *Langmuir* **33**, 14378–14388 (2017).
14. Gulamhussein, A. A., Uddin, R., Tighe, B. J., Poyner, D. R. & Rothnie, A. R. A comparison of SMA (styrene maleic acid) and DIBMA (diisobutylene maleic acid) for membrane protein purification. *Biochim. Biophys. Acta, Biomembr.* **1862**, 183281 (2020).
15. Ravula, T., Hardin, N. Z., Ramadugu, S. K. & Ramamoorthy, A. pH tunable and divalent metal ion tolerant polymer lipid nanodiscs. *Langmuir* **33**, 10655–10662 (2017).

16. Fiori, M. C., Jiang, Y., Altenberg, G. A. & Liang, H. Polymer-encased nanodiscs with improved buffer compatibility. *Sci. Rep.* **7**, 7432 (2017).
17. Fiori, M. C. *et al.* Extraction and reconstitution of membrane proteins into lipid nanodiscs encased by zwitterionic styrene-maleic amide copolymers. *Sci. Rep.* **10**, 9940 (2020).
18. Vargas, C., Cuevas Arenas, R., Frotscher, E. & Keller, S. Nanoparticle self-assembly in mixtures of phospholipids with styrene/maleic acid copolymers or fluorinated surfactants. *Nanoscale* **7**, 20685–20696 (2015).
19. Shaw, A. W., McLean, M. A. & Sligar, S. G. Phospholipid phase transitions in homogeneous nanometer scale bilayer discs. *FEBS Lett.* **556**, 260–264 (2004).
20. Jamshad, M. *et al.* Structural analysis of a nanoparticle containing a lipid bilayer used for detergent-free extraction of membrane proteins. *Nano Res.* **8**, 774–789 (2015).
21. Scheidelaar, S. *et al.* Molecular model for the solubilization of membranes into nanodisks by styrene maleic acid copolymers. *Biophys. J.* **108**, 279–290 (2015).
22. Nagaraj, N. *et al.* Deep proteome and transcriptome mapping of a human cancer cell line. *Mol. Syst. Biol.* **7**, 548 (2011).
23. Bublitz, M., Morth, J. P. & Nissen, P. P-type ATPases at a glance. *J. Cell Sci.* **124**, 2515–2519 (2011).
24. Slaaby, R. *et al.* Hybrid receptors formed by insulin receptor (IR) and insulin-like growth factor I receptor (IGF-IR) have low insulin and high IGF-1 affinity irrespective of the IR splice variant. *J. Biol. Chem.* **281**, 25869–25874 (2006).
25. Rostovtseva, T. K. *et al.* α -synuclein shows high affinity interaction with voltage-dependent anion channel, suggesting mechanisms of mitochondrial regulation and toxicity in Parkinson disease. *J. Biol. Chem.* **290**, 18467–18477 (2015).
26. Boulbrima, A., Temple, D. & Psakis, G. The multiple assemblies of VDAC: from conformational heterogeneity to β -aggregation and amyloid formation. *Biochem Soc Trans* **44**, 1531–1540 (2016).
27. Wang, M. *et al.* Three-dimensional structure of NADPH – cytochrome P450 reductase : Prototype for FMN- and FAD-containing enzymes. *PNAS* **94**, 8411–8416 (1997).
28. Prade, E. *et al.* A minimal functional complex of cytochrome P450 and FBD of cytochrome P450 reductase in nanodiscs. *Angew. Chemie Int. Ed.* **57**, 8458–8462 (2018).
29. Gang, H. *et al.* Microfluidic diffusion platform for characterizing the sizes of lipid vesicles and the thermodynamics of protein-lipid interactions. *Anal. Chem.* **90**, 3284–3290 (2018).
30. Macikova, L. *et al.* Putative interaction site for membrane phospholipids controls activation of TRPA1 channel at physiological membrane potentials. *FEBS J.* **286**, 3664–3683 (2019).
31. Azouz, M. *et al.* Microfluidic diffusional sizing probes lipid nanodiscs formation. *Biochim. Biophys. Acta, Biomembr.* **1862**, 183215 (2020).
32. Viennet, T. *et al.* Structural insights from lipid-bilayer nanodiscs link α -Synuclein

- membrane-binding modes to amyloid fibril formation. *Commun. Biol.* **1**, 44 (2018).
33. Verhallen, P. F. J., Demel, R. A., Zwiers, H. & Gispen, W. H. Adrenocorticotrophic hormone (ACTH)-lipid interactions. Implication for involvement of amphipathic helix formation. *Biochim. Biophys. Acta, Biomembr.* **775**, 246–254 (1984).
 34. Rues, R.-B., Gräwe, A., Henrich, E. & Bernhard, F. Membrane Protein Production in *E. coli* Lysates in Presence of Preassembled Nanodiscs. *Meth. Mol. Biol.* **1586**, 291–312 (2017).
 35. Rues, R. B., Dötsch, V. & Bernhard, F. Co-translational formation and pharmacological characterization of beta1-adrenergic receptor/nanodisc complexes with different lipid environments. *Biochim. Biophys. Acta - Biomembr.* **1858**, 1306–1316 (2016).
 36. Henrich, E. *et al.* Analyzing native membrane protein assembly in nanodiscs by combined non-covalent mass spectrometry and synthetic biology. *Elife* **6**, e20954 (2017).
 37. Ejima, D., Yumioka, R., Arakawa, T. & Tsumoto, K. Arginine as an effective additive in gel permeation chromatography. *J. Chromatogr. A* **1094**, 49–55 (2005).
 38. Luna, V. M. *et al.* Generation of membrane proteins in polymer-based lipoparticles as flow cytometry antigens. *Eur. Polym. J.* **109**, 483–488 (2018).
 39. Shelby, M. L., He, W., Dang, A. T., Kuhl, T. L. & Coleman, M. A. Cell-Free Co-Translational Approaches for Producing Mammalian Receptors: Expanding the Cell-Free Expression Toolbox Using Nanolipoproteins. *Front. Pharmacol.* **10**, 744 (2019).
 40. Hassan, P. A., Rana, S. & Verma, G. Making sense of Brownian motion: Colloid characterization by dynamic light scattering. *Langmuir* **31**, 3–12 (2015).
 41. Koppel, D. E. Analysis of macromolecular polydispersity in intensity correlation spectroscopy: the method of cumulants. *J. Chem. Phys.* **57**, 4814–4820 (1972).
 42. Smith, P. K. *et al.* Measurement of protein using bicinchoninic acid. *Anal. Biochem.* **150**, 76–85 (1985).
 43. Wessel, D. & Flügge, U. I. A method for the quantitative recovery of protein in dilute solution in the presence of detergents and lipids. *Anal. Biochem.* **138**, 141–143 (1984).
 44. Rappsilber, J., Mann, M. & Ishihama, Y. Protocol for micro-purification, enrichment, pre-fractionation and storage of peptides for proteomics using StageTips. *Nat. Protoc.* **2**, 1896–1906 (2007).
 45. Cox, J. & Mann, M. MaxQuant enables high peptide identification rates, individualized p.p.b.-range mass accuracies and proteome-wide protein quantification. *Nat. Biotechnol.* **26**, 1367–1372 (2008).
 46. Kemmer, G. & Keller, S. Nonlinear least-squares data fitting in Excel spreadsheets. *Nat. Protoc.* **5**, 267–281 (2010).
 47. Tyanova, S. *et al.* The Perseus computational platform for comprehensive analysis of (prote)omics data. *Nat. Methods* **13**, 731–740 (2016).
 48. Yates, E. V. *et al.* Latent analysis of unmodified biomolecules and their complexes in solution with attomole detection sensitivity. *Nat. Chem.* **7**, 802–809 (2015).

49. Falke, M. *et al.* α -Synuclein-derived lipoparticles in the study of α -Synuclein amyloid fibril formation. *Chem. Phys. Lipids* **220**, 57–65 (2019).

5. Discussion

5.1. Paving the way of polymer nanodiscs for membrane-protein applications

The majority of this work focused on the biophysical characterisation of the most popular and commonly used anionic SMA(2:1) copolymer, two electroneutral sulphobetaine maleimide copolymers SMA(2:1)-SB and DIBMA-SB, and the corresponding nanodiscs. To this end, the solubilisation efficiency of these polymers towards model and cellular membranes was elucidated as functions of pH, ionic strength, lipid unsaturation, lipid acyl-chain length, and lipid charge. The presented data also include detailed studies on the integrity of the encapsulated lipid-bilayers and the nanodisc charge. In addition, the lipid-transfer kinetics among SMA(2:1) nanodiscs were quantified.

Taken together, the polymer- and membrane-dependent nanodisc properties thus deduced provide indispensable information for the key application of polymer nanodiscs in membrane-protein research. This is because these properties can, to a certain extent, be extrapolated to nanodiscs formed from complex cellular membranes. In the end, they result in two key criteria that govern the successful use of amphiphilic copolymers in membrane-protein studies. They are, on the one hand, the **protein extraction efficiency** in terms of protein yield from cellular membranes and, on the other hand, the **protein stabilisation** within nanodiscs over time and under varying environmental conditions.

In a more global context, the polymer toolbox with various properties such as charge densities, chain length, or monomer units progressively grows.^{37,100} As different polymer properties lead to a vast variety of nanodisc features, it is of utmost importance to provide an **in-depth characterisation of the specific polymers and their corresponding nanodiscs**. As a consequence, this allows for adjusting the nanodisc properties to specifically suit target membrane proteins or experimental requirements.

5.2. Polymer concentration determination by refractometry and UV absorption

In order to use amphiphilic polymers for solubilisation studies, they need to be suspended in an aqueous buffer. Here, however, the commercially available polymers SMA(2:1), SMA(3:1), and DIBMA were present in a concentrated NaOH solution. Hence, they were dialysed against the aqueous buffer of choice, which subsequently necessitates the determination of polymer

stock concentrations. Refractometry and UV spectroscopy are **complementary techniques suited for quantitative measurements**, because they both linearly depend on the concentration. UV spectroscopy, however, is only valuable to molecules that have a chromophoric activity such as phenyl rings in SMA(2:1), and, is thus less suited for aliphatic DIBMA (*Manuscript 1*). Furthermore, UV absorption depends not only on the polymers' chemical structure, but also on its chemical environment and thus can lead to intensity differences or absorbance spectra shifts depending on solvent properties.⁸⁶ By contrast, the refractive index, at a specific wavelength and temperature, only depends on the elemental composition of the structure of interest.¹⁰¹ Due to these reasons, refractometry was the straightforward tool of choice to determine polymer concentrations¹⁰² and is also widely used in SEC for polymer characterisation (*Manuscript 3*).¹⁰³

5.3. The equilibrium solubilisation efficiency of amphiphilic copolymers

In the following chapter, the equilibrium solubilisation efficiency of studied copolymers is discussed and compared on a mass concentration scale. At first, the solubilisation capacity at similar conditions among SMA, DIBMA, and their neutral derivatives is reviewed. Subsequently, the effects of membrane and solvent properties are highlighted. It should be emphasised that herein, the solubilisation efficiency is discussed from a thermodynamic rather than a kinetic viewpoint.

A comparison of solubilisation efficiencies at similar conditions

At near-physiological conditions, **SMA(2:1)** (with an average S/MA molar ratio of 2:1) was found to be the **most efficient solubiliser** followed by the less hydrophobic DIBMA (DIB/MA ratio: 1:1) and the more hydrophobic SMA(3:1) (S/MA ratio: 3:1) towards saturated DMPC model membranes (*Manuscript 1*). This was derived from ³¹P NMR and DLS studies showing that a reduced polymer/lipid mass ratio was required for the onset and completion of SMA(2:1) nanodisc formation. Here, the intrinsic polymer hydrophobicity, which arises predominantly from the average hydrophilic (MA) to hydrophobic (S or DIB) group ratio, seems to be the dominant factor governing the polymers' solubilisation efficiency. The results thus suggest that, among the compared polymers, SMA(2:1) possesses a near-optimal hydrophobicity required for efficient lipid bilayer disruption and nanodisc formation. DIBMA, on the one hand, presents a lower affinity to the membrane hydrophobic core due to the fairly

high content of hydrophilic MA moieties (~50%). SMA(3:1), on the other hand, contains less MA (~25%) than SMA(2:1) (~33%), thus reducing the initial polymer interactions with hydrophilic lipid head groups required for subsequent membrane insertion.

The electroneutral **SMA(2:1)-SB and DIBMA-SB** polymers showed **similarly high solubilisation capacities as SMA(2:1)** (*Manuscript 3*). These polymers were generated through attachment of a zwitterionic sulphobetaine (SB) side chain to the maleic anhydride groups of SMA(2:1) and DIBMA, respectively. In general, this renders the derivatised polymers more hydrophobic than their anionic counterparts. This is because SB groups feature fairly long hydrocarbon chains between the charged groups and are connected to the polymer backbone through hydrophobic maleimide rings (Figure 1.4). Furthermore, as DIBMA has a higher maleic anhydride content than SMA(2:1), DIBMA experiences a superior modification over SMA(2:1). Accordingly, the resulting increase in hydrophobicity is more pronounced for DIBMA-SB, thus shifting the hydrophobicity of the latter close towards the near-optimum of SMA(2:1). Hence, the solubilisation power of DIBMA-SB noticeably increases, whereas for SMA(2:1)-SB, the effect is less pronounced.

Effects of solvent properties on solubilisation efficiency

First, the influence of **pH** on the studied polymers is elucidated in more detail. SMA(2:1) showed a superior equilibrium solubilisation efficiency towards phospholipids at pH 8.3 than at pH 6.4 (*Manuscript 1*). This is because the pH value, among other solvent properties, influences the previously discussed intrinsic polymer hydrophobicity, thus adjusting the polymer solubilisation efficiency. More specifically, at neutral pH, SMA(2:1) is partially protonated (~50%), because the pK_a values of the carboxylate groups correspond to ~5.5 and ~8.6, respectively.³⁹ Accordingly, at elevated or alkaline pH, the polymers' maleic acid moieties are largely deprotonated, thus reducing the effective hydrophobicity of SMA(2:1). This results in stronger Coulombic repulsion among these moieties, provoking an extended polymer conformation so that polymer chains more efficiently wrap around the lipid bilayer. As a consequence, less polymer is required for complete encapsulation, which manifests in a superior solubilisation capacity. By contrast, at moderately acidic pH, the largely protonated carboxylate groups cause an elevated polymer hydrophobicity and a collapsed conformation, which results in a reduced solubilisation efficiency. A strongly acidic pH < 5 leads to the total collapse of polymer chains, resulting in polymer precipitation and loss of solubilisation

capacity.^{33,74} The results from *Manuscript 1* are strongly supported by SEC data showing that, at similar polymer/lipid molar ratios, 30–40 % more SMA(2:1) is required at pH 6.4 than at pH 8.3 to form nanodiscs (Figure 2.3).

For DIBMA, the opposite effect was observed; at slightly acidic pH, the equilibrium solubilisation efficiency was elevated over moderately alkaline pH.⁷⁴ For the same reasons as elucidated for SMA(2:1), the effective hydrophobicity of DIBMA increases at acidic pH and thus, renders the polymer more hydrophobic than at near-physiological conditions. Accordingly, the effective hydrophobicity approaches the one of SMA(2:1), thus leading to an improved solubilisation efficiency. At alkaline conditions, DIBMA turns even less hydrophobic than at pH 7.4, thus further reducing its solubilisation capacity towards lipid membranes. This underlines once more the postulation of an optimal polymer hydrophobicity required for a high membrane solubilisation efficiency.

The solubilisation efficiency of SMA(2:1)-SB and DIBMA-SB was little to not affected by varying pH values (*Manuscript 3*). This is because the SB side chain features a sulphonate group with a pK_a value corresponding to -1.9 ^{104,105} and a trimethyl-ammonium group having a pK_a value close to ~ 10 .¹⁰⁶ Accordingly, in the studied pH range of 6–8.5, the derivatised polymers are predominantly zwitterionic, i.e. carry a net neutral charge.^{107,108} As a result, their hydrophobicity and conformation is not considerably affected, rendering the solubilisation efficiency of these polymers largely pH-independent.

Secondly, the effect of **ionic strength** on the equilibrium solubilisation efficiency is highlighted. For SMA(2:1), varying NaCl concentrations had little effect on the solubilisation power towards zwitterionic model membranes (*Manuscript 1*). It was however shown that the solubilisation of KcsA from anionic *E. coli* membranes was more efficient at elevated ionic strength.⁴⁸ In general, elevated ionic strength leads to Coulombic screening of negatively charged carboxylate groups by sodium ions, thus promoting the polymers' effective hydrophobicity. Accordingly, this results in an elevated membrane affinity, and, hence, solubilisation efficiency. Although the solubilisation capacity of SMA(2:1) seems to be more affected by protonation than by Coulombic screening, the latter enhances the solubilisation of highly anionic *E. coli* membranes.¹⁰⁹ DIBMA also showed a superior solubilising efficiency at elevated ionic strength, even towards zwitterionic phospholipids.⁷⁴ In accordance with the pH-

independence on the solubilisation efficiency of the electroneutral polymers, it is expected that ionic strength also has little effect.

Finally, the influence of divalent cations such as Ca^{2+} and Mg^{2+} on DIBMA solubilisation efficiency is briefly discussed. Elevated concentrations of **divalent cations** showed a pronounced increase in equilibrium solubilisation efficiency towards model and cellular membranes.¹¹⁰ This effect cannot be explained by Coulombic screening only and is caused by association of divalent cations to the maleic acid groups, thus leading to their partial neutralisation. These experiments were not conducted for SMA polymers, as they are less tolerant towards divalent cations and precipitate already at low millimolar concentrations.³² It is again expected that divalent cations have little effect on the solubilisation efficiency of derivatised polymers.

Taken together, it was shown that the intrinsic polymer hydrophobicity can be altered by solvent properties such as pH, ionic strength, or divalent cations, thus adjusting the polymer solubilisation efficiency towards membranes. The electroneutral polymers, however, are generally less susceptible to changes of solvent properties.

Effects of membrane properties on solubilisation efficiency

The solubilisation efficiency of SMA(2:1), SMA(3:1), and DIBMA towards unsaturated POPC was reduced compared with saturated DMPC (*Manuscript 1*). Moreover, electroneutral SMA(2:1)-SB and DIBMA-SB also showed a decreased solubilisation efficiency towards unsaturated lipid bilayers (data not shown). An explanation is that **lipid unsaturation** increases the lateral pressure in the acyl-chain region of the bilayer, thus impeding the insertion of the polymers' hydrophobic moieties. For DIBMA, the effect is even more drastic than for SMA, because the intercalation of bulky diisobutylene moieties is more drastically impeded than of planar aromatic groups.⁷⁴

Along these lines, it should be noted that the herein used unsaturated POPC carries longer acyl chains than saturated DMPC. It can thus be deduced that the resulting superior **membrane thickness** of POPC further enhances the observed reduced solubilisation efficiency. In fact, the dependency of lipid acyl-chain length on DIBMA solubilisation efficiency was confirmed in a systematic study.⁷⁴ For SMA, a similar trend was observed from a kinetic viewpoint.⁴⁰ The reduced polymer efficiency is caused by stronger van der Waals forces and

hydrogen bonds within thick bilayers.¹¹¹ From a thermodynamic viewpoint, this results in more unfavourable Gibbs free energies for the transfer of phospholipids from vesicular bilayers to polymer nanodiscs, thus decreasing the polymers' insertion power.⁷⁴ Accordingly, more polymer is required for the complete solubilisation of target membranes.

Importantly, the electroneutral polymers proved effective in solubilising negatively charged lipid-bilayers formed by POPG, whereas SMA(2:1) and DIBMA were not able to form nanodiscs from anionic model membranes (*Manuscript 3*). This demonstrates that the latter impede polymer insertion into the membrane acyl-chain region due to Coulombic repulsions among negatively charged polymers and charged lipid head groups. Electroneutral polymers are thus able to solubilise the long-chained and unsaturated POPG, but show a reduced solubilising efficiency towards its neutral counterpart POPC. This underlines that the **membrane charge** might have a more drastic effect on membrane solubilisation than lipid unsaturation or membrane thickness. Accordingly, electroneutral polymers potentially provide a considerable advantage over anionic SMA and DIBMA in terms of membrane protein extraction from highly anionic cellular membranes such as those of *E. coli*.^{40,109,112}

Altogether, it became clear that, in addition to solvent properties, membrane characteristics such as membrane thickness, lateral pressure, or charge influence the polymers' solubilisation behaviour.

5.4. The nanodisc size

Previously, it has been shown that the **size** of SMA(3:1)-bounded nanodiscs **decreases with increasing polymer/lipid ratios**.^{43,46} This is also valid for the polymer nanodiscs formed by SMA(2:1), DIBMA, and their neutral derivatives (*Manuscripts 1 and 3*).⁷⁴ In other words, at similar lipid concentrations, elevated polymer concentrations lead to the fragmentation into smaller nanodiscs. This can be readily explained by the fact that, as more polymer is available, more polymer is involved in nanodisc formation, reducing the lipid number per nanodisc, and, thus, the lipid-bilayer core. Accordingly, this results in a reduced nanodisc size and goes along with a larger number of nanodiscs. This rationale is however only valid up to a specific polymer/lipid ratio; increasing the polymer concentration above this limit, the nanoparticle size remains constant at ~8 nm for SMA(2:1), SMA(2:1)-SB, and DIBMA-SB and at ~15 nm for DIBMA. This indicates, at first glimpse, that a minimal nanodisc diameter is preserved. However, a more nuanced picture is required, especially in the case of SMA(2:1) nanodiscs. In

combination with data on the lipid-bilayer integrity showing that the latter is strongly perturbed within SMALPs at high polymer concentrations, the question arises whether these particles still can be defined as nanodiscs. It is likely that, at fairly high SMA(2:1) concentrations, the polymer chains partition into the lipid bilayer, thus forming **polymer/lipid mixed micelles** rather than nanodiscs with a well-defined, native-like lipid bilayer, in accordance with conventional surfactant/lipid mixtures (see also Section 5.7).¹¹³

Generally, the nanodisc size is closely linked to the equilibrium solubilisation efficiency; a superior solubilisation efficiency goes along with a reduced polymer concentration required for nanodisc formation. As already mentioned, the pH value affects the solubilisation capacity of SMA(2:1) and DIBMA and hence, also the nanodisc size. More specifically, at similar polymer/lipid ratios, larger SMA(2:1) nanodiscs are formed at acidic (i.e., at a reduced solubilisation efficiency) than at alkaline pH (i.e., at a superior solubilisation efficiency). By means of SEC, it was observed that at pH 6.4, an excess SMA(2:1) fraction of only 5–30% was present compared with >50% at pH 8.3 (Figure 2.3). As discussed earlier in great detail, the increased effective hydrophobicity of SMA(2:1) at acidic pH leads to the adoption of a more compact polymer conformation. Hence, a larger number of polymer chains is required to wrap around the nanodisc, leading to an increase in nanodisc size. In general, this implies that, on an absolute scale, the SMA(2:1) concentration effectively involved in nanodisc formation is higher at acidic than at alkaline pH.

At a molecular level, a similar hypothesis holds for pH-, NaCl-, and divalent-cation-dependent DIBMALP size that goes along with the polymers' solubilisation efficiency.^{74,110} Slightly acidic pH, NaCl concentrations above ≥ 300 mM, or low millimolar divalent cation concentrations reduce Coulombic repulsions among carboxylate groups. This renders the conformation of DIBMA less extended yet not too compact, thus improving its membrane affinity. The resulting reduction in required polymer leads to the formation of smaller nanodiscs.

5.5. The nanodisc charge

In the course of this thesis, the effective SMA(2:1) nanodisc charge was elucidated in great detail by means of two independent methods, namely by an extended Debye-Hückel equation (*Manuscript 2*) and by ζ -potential measurements (Figure 3.1).

At near-physiological conditions, the carboxylate groups of SMA(2:1) are partially protonated, as mentioned earlier.³⁹ This means that theoretically, an SMA(2:1) polymer chain having a number-average molecular weight of $M_n = 2.7$ kg/mol contains on average eight carboxylate repeating units and thus, eight negative charges. Assuming that the polymer makes up 40–50% of the size-dependent nanodisc weight of 200–800 kDa, a nanodisc contains > 250 negative elementary charges.⁴⁷ In the following discussion, this theoretical charge is referred to as the *nominal* nanodisc charge.

An extended version of the Debye-Hückel equation describing the experimentally determined collisional lipid-exchange rate constants, k_{col} , as functions of ionic strength, I , provided an *effective* nanodisc charge number of $z = -33$. This is, however, an order of magnitude lower than the *nominal* charge number (*Manuscript 2*), because the reported *effective* charge number describes the local charge at the nanodisc region of impact upon collision. At similar hydrodynamic sizes, the effective DIBMALP charge number amounted to $z = -47$.¹¹⁴ This reflects the increased maleic acid content of DIBMA over SMA(2:1), and, thus, the higher charge density.

Complementary, the SMA(2:1) nanodisc charge was addressed by ζ -potential measurements. At 0–100 mM NaCl, similar nanodisc sizes yielded *effective* charge numbers of $z \approx -25$, which is in line with results obtained in *Manuscript 2* (Figure 3.1). In this case, by contrast, the *effective* nanodisc charge number arises from the partially sheared-off electrostatic double layer, due to nanodisc movement in an electric field. Simply speaking, an absorbed stationary phase of ions as inferred by Coulombic attractions screens the *nominal* nanodisc surface charge, thus leading to a decreased *effective* nanodisc charge.⁹⁰ Accordingly, it has to be highlighted that the *effective* nanodisc charge is differently defined for both methods used; while it results from local charges for best-fit values of the extended Debye-Hückel equation, it issues from the partial Coulombic screening in ζ -potential measurements. Notwithstanding this caveat, the results obtained from these two complementary methods were in close agreement.

Furthermore, the influence of nanodisc size on its effective charge and charge density was studied by ζ -potentials. It was shown that large nanodiscs have a superior charge number $z(r)$ than their smaller counterparts (Figure 3.1.c). This can be readily explained by a reduced amount of polymer required for small nanodisc encapsulation. Due to the smaller

circumference, the curvature of small nanodiscs increases. Accordingly, this also leads to an elevated polymer curvature to closely interact with lipid-acyl chains, reducing the required polymer concentration and, thus, the *effective* nanodisc charge. This finding is however not reflected in deduced charge densities at the nanodisc rim, $\rho(r)_{\text{circ}}$, which were found to be fairly constant over different nanodisc sizes (Figure 3.1.d). In fact, despite the decrease in polymer concentration, it is plausible that $\rho(r)_{\text{circ}}$ does not significantly change due to the reduced nanodisc area that can harbor negative charges. As discussed for DIBMALPs, it is even probable that a higher charge density is found in small nanodiscs, even though on an absolute scale, they carry less charges.¹¹⁴ Taken together, the effective charge number and the charge density of nanodiscs have to be considered independently.

In addition, the nanodisc charge is not only affected by its size, but also by the solvent properties discussed previously. Here, the effect of ionic strength on the nanodisc charge was studied. With increasing NaCl concentrations, the effective SMA(2:1) nanodisc charge number decreased (Figure 3.1.c). This was expected, because Coulombic screening of the carboxylate groups increases with elevated ionic strength. It is also illustrated by the nanodisc Debye length that increases from $\lambda_D = 0.5$ nm at 400 mM NaCl to 1.35 nm at 50 mM NaCl, underlining an electric potential decay over a shorter distance at elevated ionic strength.^{115,116}

Taken together, the nanodiscs formed by polyanionic SMA(2:1) and DIBMA were elucidated in great detail regarding their effective charge numbers and charge densities. Finally, the net neutral charge of zwitterionic SMA(2:1)-SB and DIBMA-SB polymers and corresponding nanodiscs was validated by ζ -potentials (*Manuscript 3*). Indeed, negligible ζ -potentials, going along with insignificant charge numbers and densities, were found for both polymers and nanodiscs at near-physiological conditions.

5.6. The colloidal stability of polymer nanodiscs

In general, the colloidal stability of particles is defined as the equilibrium stabilisation of particles suspended in a medium. The so-called DLVO theory describes the combined effect of attractive and repulsive forces on the colloidal stability of particles. In case the short-range, attractive van der Waals forces outweigh repulsive forces, particles tend to aggregate or agglomerate in order to reduce their surface energy.¹¹⁷ The following section sheds light on the predominant stabilising repulsive forces among nanodiscs formed by SMA, DIBMA, and the derivatised zwitterionic polymers.

SMALPs and DIBMALPs can be stored, in the absence of protein, for long periods of time (weeks or even months) by preserving their hydrodynamic size. Furthermore, they show a high thermal stability, and, are fairly stable towards pH, ionic strength, and divalent cations (*Manuscript 1*).^{32,39,74} Taken together, these observations, combined with the fairly negative ζ -potentials of SMA(2:1) nanodiscs^{97,98} (Figure 3.1), underline a **high colloidal stability** that can be readily explained by the nanodiscs' polyanionic nature. As discussed in the previous section, these nanodiscs have a highly negative charge number. Accordingly, it is straightforward that SMALPs and DIBMALPs are largely stabilised through **Coulombic repulsions** in an aqueous environment.

The electroneutrality of SMA(2:1)-SB and DIBMA-SB underline that Coulombic forces are drastically reduced among nanodiscs formed by these polymers. It has to be noted that, in addition to Coulombic repulsions, the **free solvation energy** (or free Born energy; specifically here: free hydration energy) of nanodiscs also has a strong stabilising effect.¹¹⁷ In more detail, nanodiscs are enclosed by a hydration shell, as water molecules strongly interact with the hydrophilic polymer groups, either anionic (SMA and DIBMA) or zwitterionic (SMA-SB and DIBMA-SB), on the nanodisc surface. In fact, nanodiscs formed by the zwitterionic polymers represent an accumulation of dipoles that display similar free solvation energies as polyanionic SMALPs or DIBMALPs.¹¹⁸ Thus, it is energetically highly unfavorable to break their hydration shells in order to bring nanodiscs together.¹¹⁹ Accordingly, even though Coulombic forces are reduced among zwitterionic nanodiscs, they are stabilised in solution through **repulsive hydration forces**.

A minor stabilising effect might be generated by the "free" or **excess polymer** in solution, found for all nanodisc species except those formed by DIBMA-SB (Figure 2.1 and *Manuscript 3*). It was previously reported that the addition of non-adsorbing polymer leads to superior nanoparticle stabilisation against aggregation and sedimentation through **steric hindrance**. This effect is referred to as the gel network stabilisation, because the polymer chains generate a stabilising "network" around the particles.^{120,121} However, in this case, this seems to make, if any, only a small contribution to the colloidal stability of nanodiscs, because SMALPs were shown to be stable in size after the removal of "free" SMA(2:1) (Figure 2.2 and Section 5.9).

5.7. The lipid transfer among polymer nanodiscs

In *Manuscript 2*, the lipid transfer behaviour of SMA(2:1) nanodiscs was elucidated in great detail. In accordance with SMA(3:1) nanodiscs and DIBMALPs, it was shown that SMALPs formed by SMA(2:1) exchange lipid molecules among each other predominantly through collisions.^{71,114} At similar conditions, the collisional lipid transfer among SMA(2:1) nanodiscs is more efficient than among DIBMALPs, but less efficient than among the more hydrophobic SMA(3:1) nanodiscs. This is simply because SMA(3:1) nanodiscs are most hydrophobic, followed by SMA(2:1) and DIBMA nanodiscs, as reflected by the effective SMALP and DIBMALP charge numbers. Hence, SMALPs experience less **Coulombic repulsions** among each other than DIBMALPs, resulting in more frequent collisions, and thus, increased lipid transfer kinetics. Along this rationale, it is expected that nanodiscs formed by electroneutral polymers are even more efficient in lipid exchange.

As discussed previously, solvent properties such as elevated ionic strength or acidic pH reduce the effective nanodisc charge density through Coulombic screening. As expected, elevated I accelerated the lipid transfer among nanodiscs, because increasing NaCl concentrations enhance Coulombic screening of the polymers' carboxylate groups. As a corollary, the collision rate is elevated, and thus, the lipid transfer kinetics among nanodiscs, as shown for SMA(2:1) and DIBMA (*Manuscript 2*).¹¹⁴

From a molecular viewpoint, it is a credible hypothesis that, upon collision, nanodiscs transiently fuse at the region of impact to exchange lipid molecules. More specifically, the polymer rim of each nanodisc has to "open" to enable the formation of a common nanodisc core and thus, the direct contact of lipids from colliding nanodiscs.¹²² If a collision takes place, this transient fusion is possibly enabled because the polymer chains are shorter than the total nanodisc circumference. Therefore, a notable yet minor effect that potentially plays a role in lipid transfer kinetics, in addition to Coulombic screening, is the **polymer chain length**. As SMA(2:1) ($M_w = 2.7$ kg/mol) is significantly smaller than DIBMA ($M_w = 8.4$ kg/mol), it is plausible that the shorter polymer chains of SMA(2:1) facilitate the local disruption of the polymer barrier. In fact, it was previously shown that short SMA(2:1) chains enable faster lipid transfer kinetics than their long counterparts.¹²³ Accordingly, in addition to the favourable SMA(2:1) hydrophobicity over DIBMA, the smaller SMA(2:1) chains possibly have an additional enhancing effect on the nanodisc lipid exchange. Along this rationale, this explanation also

holds for the effect observed at superior ionic strength. As already known, the effective polymer chain length, or, in other words, the polymer conformation, is influenced by solvent properties. Accordingly, enhanced Coulombic screening at elevated I not only reduces the Coulombic repulsion among nanodiscs, but additionally reduces the effective polymer chain length, thus further facilitating the nanodisc lipid exchange.

A completely different consideration that potentially influences the lipid exchange kinetics is that SMA(2:1) perturbs the lipid-bilayer nanodisc core to a larger extent than DIBMA (*Manuscript 1*), as discussed in more detail further below. Accordingly, this leads to a looser **lipid packing** in SMALPs, thus increasing the lipid mobility. During a transient fusion of two SMA(2:1) nanodiscs, this could also have an accelerating effect on the lipid transfer.

In a more general context, these results underline that, in spite of Coulombic repulsion among nanodiscs in combination with their free hydration energy, anionic polymer nanodiscs are highly dynamic rather than kinetically trapped nanoparticles. In comparison with MSP nanodiscs and vesicles, they exchange lipids considerably faster (*Manuscript 2*). Therefore, polymer nanodiscs and, especially, nanodiscs formed by electroneutral polymers, are promising tools to study native or specific protein/lipid interactions.⁷² This is because lipids that strongly interact with harboured membrane proteins are impeded from the fast lipid exchange, thus leading to a local enrichment in interacting lipid species.^{54,55}

5.8. The nanodisc lipid-bilayer architecture

The lipid-bilayer properties of polymer nanodiscs were investigated by differential scanning calorimetry (DSC) (*Manuscripts 1 and 3*). For DMPC vesicles, the main gel-to-fluid phase transition temperature, T_m , is close to 24 °C. DIBMA had the smallest effect on T_m , followed by SMA(2:1) and SMA(3:1). More specifically, for SMA(3:1), T_m decreased drastically with increasing polymer/lipid ratios and, strikingly, already at sub-solubilising polymer concentrations. For SMA(2:1), however, a substantial drop in T_m was only observed at fairly high polymer concentrations, that is, at small nanodisc sizes. DIBMA, by contrast, only provoked a slight reduction in T_m (*Manuscript 1*). The electroneutral derivatives SMA(2:1)-SB and DIBMA-SB behaved similarly to DIBMA and only insignificantly changed T_m (*Manuscript 3*). These findings show that **DIBMA and the derivatised polymers have a relatively mild effect on the lipid acyl-chain packing** in the nanodisc core, thus, predominantly preserving a vesicle-like lipid-bilayer integrity.

Regarding the commercially available polymers from *Manuscript 1*, the intercalation of styrene moieties was suggested to be the cause of the superior lipid acyl-chain perturbation in SMA nanodiscs. More specifically, SMA(3:1) has the highest styrene content, which hydrophobically interacts with lipid acyl chains and, thus, perturbs the bilayer architecture to the largest extent. DIBMA, by contrast, does not contain styrene at all and the interactions with aliphatic DIB seem to be reduced due to its high flexibility and comparably small surface area. Hence, DIBMA largely preserves the lipid-acyl chain integrity. In addition, this rationale goes along with the polymers' hydrophobicity, as SMA(3:1) is also the most hydrophobic polymer, followed by SMA(2:1) and DIBMA. A more nuanced picture is however required since SMA(2:1)-SB, which carries the same amount of styrene moieties than SMA(2:1), showed the above-mentioned gentle effect on lipid-acyl chains. The hydrophilic sulphobetaine (SB) side chains are likely to protrude from the nanodisc to interact with water molecules. In contrast with the rather short maleic acid moieties that also orient away from the lipid acyl-chains, the **SB group** is simply longer, thus **reducing the polymer/lipid interactions at their interface**. Accordingly, for SMA(2:1)-SB and DIBMA-SB nanodiscs, on an absolute scale, a lower polymer fraction is interacting with the lipid bilayer core, thus largely preserving its integrity.

5.9. "Free" or excess polymer after nanodisc formation

In general, a certain concentration of amphiphilic copolymer is **excluded from the formation of nanodiscs** and thus termed as **"free" or excess polymer**.^{34,79} This phenomenon was observed for all nanodisc species, except for DIBMA-SB (*Manuscript 3*).¹¹⁰ For SMA(2:1), the "free" polymer fraction was studied in detail by means of SEC (Figure 2.1 and 2.2). At near-physiological conditions, 30–50% of the total SMA(2:1) concentration was present in the form of "free" polymer, depending on the polymer/lipid ratio (Figure 2.3). Interestingly, this fraction was found to be already present at and slightly above the SOL boundary, thus underlining that excess polymer cannot be explained by the nanodisc saturation with polymer only. Instead, a more likely scenario is the **existence of a polymer fraction that does not or less efficiently interacts with formed nanodiscs** at any polymer/lipid ratio. An indication for this hypothesis is that the "free" polymer fraction can be removed without having an effect on the SMALP size. Furthermore, the comparison of the elution behaviour of the bare SMA(2:1) polymer and the "free" SMA(2:1) fraction suggests that the excess polymer is composed of shorter chains, as reflected by the peak shift towards higher elution volumes

(Figure 2.1). As shorter SMA(2:1) chains are more hydrophobic than long ones due to their elevated styrene content, it seems plausible that long polymer chains solubilise phospholipids more efficiently.³⁴ Accordingly, the **short polymer chains are potentially less reactive towards phospholipid membranes** and, thus, remain to a large extent free in solution. This explanation, however, is in stark contrast with a report showing that short polymer chains more efficiently solubilise lipids than longer ones, at least from a kinetic viewpoint.¹²³ Taken together, the properties of the “free” polymer fraction that is not involved in nanodisc formation is not yet finally clarified.

5.10. Membrane protein solubilisation and stabilisation in polymer nanodiscs

This section focuses on the polymer-mediated membrane-protein solubilisation behaviour deduced from the previously discussed polymer and nanodisc features.

The solubilisation of *E. coli* membrane proteins using SMA(3:1), SMA(2:1), and DIBMA showed that SMA(2:1) is the most efficient polymer in terms of total **protein extraction yields** (*Manuscript 1*). These results validate the findings on the polymers' equilibrium solubilisation efficiency using model membranes, as addressed above. Furthermore, the pH-dependent solubilisation efficiency of SMA(2:1) follows the same trend for both model and *E. coli* membranes. Specifically, lipid solubilisation and protein extraction was most efficient at moderately alkaline pH for both model and cellular membranes. Complementary to the findings from *Manuscript 1*, the superior SMA(2:1) performance with respect to yield, purity, and stability towards specific membrane proteins was previously reported.⁸⁴ It is straightforward that high protein extraction yields and stabilities are of utmost importance for downstream bioanalytical or structural analysis.^{69,124} As a consequence, it can be concluded that SMA(2:1) is, among anionic polymers and despite its high far-UV absorbance or low divalent cation tolerance, particularly suitable for membrane-protein research. However, a general drawback in using SMA and DIBMA is that native or specific protein/lipid interactions are often difficult to study, because anionic copolymers might interfere through unspecific interactions. Accordingly, in spite their reduced protein extraction yield, electroneutral SMA(2:1)-SB and DIBMA-SB display promising tools to tackle these questions, as gauged from interaction studies of α -synuclein using microfluidic diffusional sizing (*Manuscript 3*). The sulphobetaine side chains were demonstrated to be exceptionally resistant to nonspecific

protein interactions, possibly due to the tightly bound water molecules to both zwitterionic groups.^{108,125}

In addition to the protein extraction yield and stability, the **protein size** that can be solubilised in a nanodisc is an additional important criterion. Whereas SMA(2:1) extracts a greater amount of proteins, DIBMA is able to solubilise larger membrane proteins and membrane-protein complexes (*Manuscript 1*). The electroneutral polymers, especially DIBMA-SB, also proved effective in solubilising large membrane-protein assemblies of varying types (*Manuscript 3*). As discussed above, this is possibly due to the preservation of a native-like lipid-bilayer integrity, especially at elevated polymer concentrations. Furthermore, an additional benefit of DIBMA is the formation of slightly larger nanodiscs than SMA and the derivatised polymers, thus granting more space for large membrane proteins.

Along this rationale, used polymer concentrations are crucial for providing a native-like nanodisc core, and, thus, high membrane **protein stability**. This seems to be especially important for SMA(2:1), because it is the most popular and efficient polymer thus far, yet has a potentially perturbing effect on the lipid-bilayer integrity. Accordingly, increasing the polymer concentration on target membranes does not necessarily lead to elevated protein yields or stability in nanodiscs (*Manuscript 3*).⁴⁸ Reduced protein stabilities were even reported when using high SMA concentrations for membrane solubilisation.⁶¹ In other words, the **“less is more” approach** should be considered when solubilising membrane proteins using amphiphilic polymers. This is because, as already discussed, reduced yet solubilising polymer concentrations result in an elevated lipid-bilayer integrity within nanodiscs and an increased particle size. They hence offer a large and more native-like nanodisc core, accordingly enhancing membrane protein stability. In addition, unspecific polymer/protein or polymer/lipid interactions can be reduced to a certain extent.

Importantly, the “free” or excess polymer fraction was found to interfere with enzyme activity assays or other bioanalytical studies, possibly through unspecific Coulombic interactions.⁵⁹ Accordingly, the removal of excess polymer is recommended and feasible through SEC, dialysis, or filtration.^{123,126} For the mentioned applications, the absence of “free” polymer in DIBMA-SB nanodiscs possibly displays an advantage over other polymers, because intermediate removal steps can be omitted (*Manuscript 3*).

In a global context, the present findings imply that the polymers studied in this thesis all have advantages and drawbacks with respect to specific scientific questions or target membrane proteins. Accordingly, the polymer choice for extracting and stabilising a target protein should be taken after careful consideration and depending on the respective research goals.

5.11. Future directions

Currently, the variety of amphiphilic copolymers that form polymer-bounded nanodiscs for the use in membrane-protein research is rapidly growing.³⁶ The scientific community is striving to improve polymer properties with respect to protein extraction, purification, and stabilisation. To this end, one major goal is to **decrease the polymer charge density**. On the one hand, charged nanodiscs can have masking or perturbing effects on native protein/lipid or protein/ligand interactions, because anionic polymer might unspecifically interact with those components. Accordingly, **gentle yet efficient electroneutral polymers** would potentially enhance the stabilisation of notoriously challenging yet important drug targets that are highly prone to aggregation once extracted, such as class B G-protein coupled receptors.^{127,128}

On the other hand, electroneutral polymers or those with a reduced charge density facilitate or allow the use of specific applications that are hampered by polyanionic polymers. To name an example, surface plasmon resonance (SPR) spectroscopy enables quantitative membrane protein/ligand binding affinity and kinetic studies.¹²⁹ Thus far, SPR could only be used with an immobilised ligand whilst the protein-containing nanodisc was free in solution, as the adsorption of negatively charged nanodiscs on the anionic sensor chips was impeded due to Coulombic repulsions.¹³⁰ However, the immobilisation of nanodiscs containing membrane proteins would enable high-throughput screening for potential drug targets in the pharmaceutical industry. Electroneutral polymers such as DIBMA-SB or SMA(2:1)-SB are therefore promising candidates to overcome this bottleneck.

More specifically for the group of Prof. Dr. Sandro Keller, the promising SMA(2:1)-SB and DIBMA-SB copolymers will be further characterised. For instance, the lipid exchange behaviour among nanodiscs or the solubilisation efficiency towards various bacterial, plant, insect, or human cell membranes will be tackled in the near future. Furthermore, the group focuses on **additional DIBMA derivatives by modification of the maleic acid moiety**. This is particularly interesting, because, ideally, the benefits of DIBMA such as low UV absorbance or

mild effect on lipid acyl-chains can be preserved all by reducing its charge density and increasing its solubilisation efficiency. These derivatives carry either zwitterionic groups such as amino acids or neutral groups such as sugars attached to an open ring structure. This is in contrast with SMA(2:1)-SB and DIBMA-SB that carry the sulphobetaine group attached to a maleimide group (i.e., closed ring structure, Figure 1.4).

6. Conclusions

SMA(2:1), having an average S/MA molar ratio of 2:1, is thus far the most commonly used amphiphilic copolymer to extract and solubilise membrane proteins into native-like nanodiscs. Accordingly, an in-depth characterisation of SMA(2:1) nanodiscs was performed and quantitatively compared with those formed by SMA(3:1) and DIBMA. Furthermore, two alternative electroneutral polymers, termed SMA(2:1)-SB and DIBMA-SB, were designed from SMA(2:1) and DIBMA backbone modifications, respectively. The solubilisation behaviour and nanodisc properties formed by the existing and derivatised above-mentioned polymers were discussed and highlighted as follows:

- From a thermodynamic viewpoint, SMA(2:1) was found the most efficient solubiliser towards both model and *E.coli* membranes as compared with the more hydrophobic SMA(3:1) and the more hydrophilic DIBMA. This finding can be ascribed to the intrinsic polymer hydrophobicity: a favourable hydrophobicity, as reached in SMA(2:1), seems to be required to attain high membrane solubilisation efficiencies. Along this rationale, being more hydrophobic than their anionic counterparts, DIBMA-SB was more efficient in solubilising model membranes than DIBMA, whereas SMA(2:1)-SB and SMA(2:1) showed comparable efficiencies.
- The intrinsic polymer hydrophobicity is, to a certain extent, adjustable by solvent properties such as pH, ionic strength, or divalent cation concentrations. This is because they lead to (de)protonation, charge screening, or charge neutralisation of the polymers' carboxylate groups, thus affecting membrane affinities. Along these lines, electroneutral polymers are, by contrast, less susceptible to solvent changes.
- Membrane properties such as charge, thickness, or lateral pressure as caused by lipid unsaturation or protein content also have an impact on the polymers' solubilisation performance.
- The nanodisc size decreases with superior polymer/lipid ratios, and is thus, critically linked to the polymer solubilisation efficiency. It was shown that, at reduced solubilisation power, more polymer is required to efficiently encapsulate the lipid-bilayer core, thus leading to larger nanodisc diameters.
- Electroneutral polymers and DIBMA only had a gentle effect on the vesicle-like lipid-bilayer architecture, thus providing a near-native lipid environment for extracted

membrane proteins. High concentrations of SMA(2:1), however, affected the lipid acyl-chain order, underlining that the used polymer concentration for protein extraction and stabilisation is crucial.

- The *effective* SMALP and DIBMALP charge numbers amounted to $-(20-50)$, as evidenced by two complementary methods. Their *nominal* charge, however, is estimated to be an order of magnitude higher than their *effective* charge. This is because the latter either represents a local nanodisc charge or SMALPs/DIBMALPs that are partially screened by sodium ions.
- All polymer-bounded nanodiscs studied are colloiddally stable nano-assemblies, caused by their free hydration energies, which are largely independent of the nanodiscs' charge. Polyanionic nanodiscs formed by SMA(2:1) and DIBMA are additionally stabilised through Coulombic repulsions.
- SMA(2:1) nanodiscs are highly dynamic assemblies, as they rapidly exchange phospholipids by collisional transfer. On a time scale of seconds to minutes, lipid transfer kinetics among SMA(2:1) nanodiscs were shown to be faster than among DIPMALPs and slower than among SMA(3:1) nanodiscs. This finding can be readily explained by the difference in polymer hydrophobicity, and thus, nanodisc charge, accordingly tuning Coulombic repulsions among nanodiscs. This characteristic renders polymer nanodiscs promising tools for specific protein/lipid interaction studies.
- The “free” or excess SMA(2:1) fraction increases with elevated total polymer concentrations and seems to represent a polymer fraction that does not interact with the lipid membrane. It is plausible that this fraction is composed of short polymer chains with increased hydrophobicity and thus, reduced membrane affinity. In membrane-protein research, it is recommended to remove excess polymer as it might interfere with protein functional assays.
- The new electroneutral polymers provide an advantage over existing polymers regarding specific protein assays or experimental requirements, as demonstrated by cell-free protein production or protein/lipid interaction studies. Unspecific interactions of existing polyanionic polymers with lipids or proteins might mask native ones.

References

Note that this list does not include all references that appear within manuscripts.

1. Singer, S. J. & Nicolson, G. L. The fluid mosaic model of the structure of cell membranes. *Science* **175**, 720–731 (1972).
2. Nicolson, G. L. The fluid-mosaic model of membrane structure: still relevant to understanding the structure, function and dynamics of biological membranes after more than 40 years. *Biochim. Biophys. Acta, Biomembr.* **1838**, 1451–1466 (2014).
3. Watson, H. Biological membranes. *Essays Biochem.* **59**, 43–69 (2015).
4. Kuriyan, J., Konforti, B. & Wemmer, D. *The molecules of life: physical and chemical principles*. (Garland Science, 2012).
5. Casares, D., Escribá, P. V. & Rosselló, C. A. Membrane lipid composition: effect on membrane and organelle structure, function and compartmentalization and therapeutic avenues. *Int. J. Mol. Sci.* **20**, 2167 (2019).
6. Heimburg, T. *Thermal biophysics of membranes*. (Wiley, 2007).
7. Hankins, H. M., Baldrige, R. D., Xu, P. & Graham, T. R. Role of flippases, scramblases, and transfer proteins in phosphatidylserine subcellular distribution. *Traffic* **16**, 35–47 (2015).
8. Lodish, H. *et al. Molecular cell biology*. (W. H. Freeman, 2016).
9. Lemmon, M. A. Membrane recognition by phospholipid-binding domains. *Nat. Rev. Mol. Cell Biol.* **9**, 99–111 (2008).
10. Alberts, B. *et al. Molecular biology of the cell*. (Garland Science, 2002).
11. Schmidt, D., Jiang, Q. X. & MacKinnon, R. Phospholipids and the origin of cationic gating charges in voltage sensors. *Nature* **444**, 775–779 (2006).
12. Huang, C.-L., Feng, S. & Hilgemann, D. W. Direct activation of inward rectifier potassium channels by PIP₂ and its stabilization by Gβγ. *Nature* **391**, 803–806 (1998).
13. Fong, T. M. & McNamee, M. G. Correlation between acetylcholine receptor function and structural properties of membranes. *Biochemistry* **25**, 830–840 (1986).
14. Overington, J. P., Al-Lazikani, B. & Hopkins, A. L. How many drug targets are there? *Nat. Rev. Drug Discov.* **5**, 993–996 (2006).
15. Fiedler, S., Broecker, J. & Keller, S. Protein folding in membranes. *Cell. Mol. Life Sci.* **67**, 1779–1798 (2010).
16. Khao, J., Arce-Lopera, J., Sturgis, J. N. & Duneau, J. P. Structure of a protein-detergent complex: the balance between detergent cohesion and binding. *Eur. Biophys. J.* **40**, 1143–1155 (2011).
17. Zhou, H.-X. & Cross, T. A. Influences of membrane mimetic environments on membrane protein structures. *Annu Rev Biophys* **42**, 361–392 (2013).

18. Popot, J.-L. Amphipols, nanodiscs, and fluorinated surfactants: three nonconventional approaches to studying membrane proteins in aqueous solutions. *Annu. Rev. Biochem.* **79**, 737–775 (2010).
19. Frotscher, E. *et al.* A fluorinated detergent for membrane-protein applications. *Angew. Chemie Int. Ed.* **54**, 1–6 (2015).
20. Frisken, B. J., Asman, C. & Patty, P. J. Studies of vesicle extrusion. *Langmuir* **16**, 928–933 (2000).
21. Klingler, J., Vargas, C., Fiedler, S. & Keller, S. Preparation of ready-to-use small unilamellar phospholipid vesicles by ultrasonication with a beaker resonator. *Anal. Biochem.* **477**, 10–12 (2015).
22. Ciancaglini, P. *et al.* Proteoliposomes in nanobiotechnology. *Biophys. Rev.* **4**, 67–81 (2012).
23. Sanders, C. R. & Prosser, R. S. Bicelles: a model membrane system for all seasons? *Structure* **6**, 1227–1234 (1998).
24. Popot, J.-L. *Membrane proteins in aqueous solutions: from detergents to amphiphols.* (Springer, 2018).
25. Popot, J.-L. *et al.* Amphipols from A to Z. *Annu. Rev. Biophys.* **40**, 379–408 (2011).
26. Bayburt, T. H., Grinkova, Y. V. & Sligar, S. G. Self-assembly of discoidal phospholipid bilayer nanoparticles with membrane scaffold proteins. *Nano Lett.* **2**, 853–856 (2002).
27. Shih, A. Y., Arkhipov, A., Freddolino, P. L., Sligar, S. G. & Schulten, K. Assembly of lipids and proteins into lipoprotein particles. *J. Phys. Chem. B* **111**, 11095–11104 (2007).
28. Whorton, M. R. *et al.* A monomeric G protein-coupled receptor isolated in a high-density lipoprotein particle efficiently activates its G protein. *Proc. Natl. Acad. Sci. U. S. A.* **104**, 7682–7687 (2007).
29. Alami, M., Dalal, K., Lelj-Garolla, B., Sligar, S. G. & Duong, F. Nanodiscs unravel the interaction between the SecYEG channel and its cytosolic partner SecA. *EMBO J.* **26**, 1995–2004 (2007).
30. Tonge, S. R. & Tighe, B. J. Responsive hydrophobically associating polymers: a review of structure and properties. *Adv. Drug Deliv. Rev.* **53**, 109–122 (2001).
31. Knowles, T. J. *et al.* Membrane proteins solubilized intact in lipid containing nanoparticles bounded by styrene maleic acid copolymer. *J. Am. Chem. Soc.* **131**, 7484–7485 (2009).
32. Oluwole, A. O. *et al.* Solubilization of membrane proteins into functional lipid-bilayer nanodiscs using a diisobutylene/maleic acid copolymer. *Angew. Chemie Int. Ed.* **56**, 1919–1924 (2017).
33. Lee, S. C. *et al.* A method for detergent-free isolation of membrane proteins in their local lipid environment. *Nat. Protoc.* **11**, 1149–1162 (2016).
34. Dörr, J. M. *et al.* The styrene-maleic acid copolymer: a versatile tool in membrane research. *Eur. Biophys. J.* **45**, 3–21 (2016).

35. Orwick, M. C. *et al.* Detergent-free formation and physicochemical characterization of nanosized lipid-polymer complexes: lipodisq. *Angew. Chemie Int. Ed.* **51**, 4653–4657 (2012).
36. Overduin, M. & Esmaili, M. Native nanodiscs and the convergence of lipidomics, metabolomics, interactomics and proteomics. *Appl. Sci.* **9**, 1230 (2019).
37. Overduin, M. & Esmaili, M. Structures and interactions of transmembrane targets in native nanodiscs. *SLAS Discov.* **24**, 943–952 (2019).
38. Jenkins, A. D., Kratochvíl, P., Stepto, R. F. T. & Suter, U. W. Glossary of basic terms in polymer science. *Pure Appl. Chem.* **68**, 2287–2311 (1996).
39. Scheidelaar, S. *et al.* Effect of polymer composition and pH on membrane solubilization by styrene-maleic acid copolymers. *Biophys. J.* **111**, 1974–1986 (2016).
40. Scheidelaar, S. *et al.* Molecular model for the solubilization of membranes into nanodisks by styrene maleic acid copolymers. *Biophys. J.* **108**, 279–290 (2015).
41. Xue, M., Cheng, L., Faustino, I., Guo, W. & Marrink, S. J. Molecular mechanism of lipid nanodisk formation by styrene-maleic acid copolymers. *Biophys. J.* **115**, 494–502 (2018).
42. Orwick Rydmark, M. *et al.* Styrene maleic acid copolymer induces pores in biomembranes. *Soft Matter* **15**, 7934–7944 (2019).
43. Vargas, C., Cuevas Arenas, R., Frotscher, E. & Keller, S. Nanoparticle self-assembly in mixtures of phospholipids with styrene/maleic acid copolymers or fluorinated surfactants. *Nanoscale* **7**, 20685–20696 (2015).
44. Lichtenberg, D. Characterization of the solubilization of lipid bilayers by surfactants. *Biochim. Biophys. Acta, Biomembr.* **821**, 470–478 (1985).
45. Lichtenberg, D., Ahyayauch, H. & Goñi, F. M. The mechanism of detergent solubilization of lipid bilayers. *Biophys. J.* **105**, 289–299 (2013).
46. Zhang, R. *et al.* Characterizing the structure of lipodisq nanoparticles for membrane protein spectroscopic studies. *Biochim. Biophys. Acta* **1848**, 329–333 (2015).
47. Jamshad, M. *et al.* Structural analysis of a nanoparticle containing a lipid bilayer used for detergent-free extraction of membrane proteins. *Nano Res.* **8**, 774–789 (2015).
48. Kopf, A. H. *et al.* Factors influencing the solubilization of membrane proteins from *Escherichia coli* membranes by styrene–maleic acid copolymers. *Biochim. Biophys. Acta, Biomembr.* **1862**, 183125 (2020).
49. Cuevas Arenas, R., Klingler, J., Vargas, C. & Keller, S. Influence of lipid bilayer properties on nanodisc formation mediated by styrene/maleic acid copolymers. *Nanoscale* **8**, 15016–15026 (2016).
50. Swainsbury, D. J. K. *et al.* The effectiveness of styrene-maleic acid (SMA) copolymers for solubilisation of integral membrane proteins from SMA-accessible and SMA-resistant membranes. *Biochim. Biophys. Acta, Biomembr.* **1859**, 2133–2143 (2017).
51. Dominguez Pardo, J. J. *et al.* Solubilization of lipids and lipid phases by the styrene–

- maleic acid copolymer. *Eur. Biophys. J.* **46**, 91–101 (2017).
52. Paulin, S. *et al.* Surfactant-free purification of membrane protein complexes from bacteria: application to the staphylococcal penicillin-binding protein complex PBP2/PBP2a. *Nanotechnology* **25**, 285101 (2014).
 53. Swainsbury, D. J. K., Scheidelaar, S., Van Grondelle, R., Killian, J. A. & Jones, M. R. Bacterial reaction centers purified with styrene maleic acid copolymer retain native membrane functional properties and display enhanced stability. *Angew. Chemie Int. Ed.* **53**, 11803–11807 (2014).
 54. Dörr, J. M. *et al.* Detergent-free isolation, characterization, and functional reconstitution of a tetrameric K⁺ channel: the power of native nanodiscs. *Proc. Natl. Acad. Sci. U. S. A.* **111**, 18607–18612 (2014).
 55. Prabudiansyah, I., Kusters, I., Caforio, A. & Driessen, A. J. M. Characterization of the annular lipid shell of the Sec translocon. *Biochim. Biophys. Acta, Biomembr.* **1848**, 2050–2056 (2015).
 56. Komar, J. *et al.* Membrane protein insertion and assembly by the bacterial holo-Translocon SecYEG-SecDF-YajC-YidC. *Biochem. J.* **473**, 3341–3354 (2016).
 57. Jamshad, M. *et al.* G-protein coupled receptor solubilization and purification for biophysical analysis and functional studies, in the total absence of detergent. *Biosci. Rep.* **35**, (2015).
 58. Logez, C. *et al.* Detergent-free isolation of functional G protein-coupled receptors into nanometric lipid particles. *Biochemistry* **55**, 38–48 (2016).
 59. Smirnova, I. A. *et al.* Isolation of yeast complex IV in native lipid nanodiscs. *Biochim. Biophys. Acta, Biomembr.* **1858**, 2984–2992 (2016).
 60. Skaar, K., Korza, H. J., Tarry, M., Sekyrova, P. & Högbom, M. Expression and subcellular distribution of GFP-tagged human tetraspanin proteins in *saccharomyces cerevisiae*. *PLoS One* **10**, e0134041 (2015).
 61. Rehan, S., Paavilainen, V. O. & Jaakola, V.-P. Functional reconstitution of human equilibrative nucleoside transporter-1 into styrene maleic acid co-polymer lipid particles. *Biochim. Biophys. Acta, Biomembr.* **1859**, 1059–1065 (2017).
 62. Hardy, D., Bill, R. M., Rothnie, A. J. & Jawhari, A. Stabilization of human multidrug resistance protein 4 (MRP4/ABCC4) using novel solubilization agents. *SLAS Discov.* **24**, 1009–1017 (2019).
 63. Gulati, S. *et al.* Detergent-free purification of ABC (ATP-binding-cassette) transporters. *Biochem. J.* **461**, 269–278 (2014).
 64. Bell, A. J., Frankel, L. K. & Bricker, T. M. High yield non-detergent isolation of photosystem I-light-harvesting chlorophyll II membranes from spinach thylakoids: implications for the organization of the PS I antennae in higher plants. *J. Biol. Chem.* **290**, 18429–18437 (2015).
 65. Korotych, O., Mondal, J., Gattás-Asfura, K. M., Hendricks, J. & Bruce, B. D. Evaluation of commercially available styrene-co-maleic acid polymers for the extraction of

- membrane proteins from spinach chloroplast thylakoids. *Eur. Polym. J.* **114**, 485–500 (2019).
66. Dörr, J. M., van Coevorden-Hameete, M. H., Hoogenraad, C. C. & Killian, J. A. Solubilization of human cells by the styrene–maleic acid copolymer: insights from fluorescence microscopy. *Biochim. Biophys. Acta, Biomembr.* **1859**, 2155–2160 (2017).
 67. Sun, C. *et al.* Structure of the alternative complex III in a supercomplex with cytochrome oxidase. *Nature* **557**, 123–126 (2018).
 68. Bersch, B., Dörr, J. M., Hessel, A., Killian, J. A. & Schanda, P. Proton-detected solid-state NMR spectroscopy of a zinc diffusion facilitator protein in native nanodiscs. *Angew. Chemie Int. Ed.* **56**, 1–6 (2017).
 69. Broecker, J., Eger, B. T. & Ernst, O. P. Crystallography of membrane proteins mediated by polymer-bounded lipid nanodiscs. *Structure* **25**, 1–9 (2017).
 70. Hazell, G. *et al.* Evidence of lipid exchange in styrene maleic acid lipid particle (SMALP) nanodisc systems. *Langmuir* **32**, 11845–11853 (2016).
 71. Cuevas Arenas, R. *et al.* Fast collisional lipid transfer among polymer-bounded nanodiscs. *Sci. Rep.* **7**, 45875 (2017).
 72. Schmidt, V. & Sturgis, J. N. Modifying styrene-maleic acid co-polymer for studying lipid nanodiscs. *Biochim. Biophys. Acta, Biomembr.* **1860**, 777–783 (2018).
 73. Hall, S. C. L. *et al.* Adsorption of a styrene maleic acid (SMA) copolymer-stabilized phospholipid nanodisc on a solid-supported planar lipid bilayer. *J. Colloid Interface Sci.* **574**, 272–284 (2020).
 74. Oluwole, A. O. *et al.* Formation of lipid-bilayer nanodiscs by diisobutylene/maleic acid (DIBMA) copolymer. *Langmuir* **33**, 14378–14388 (2017).
 75. Gulamhussein, A. A., Uddin, R., Tighe, B. J., Poyner, D. R. & Rothnie, A. J. A comparison of SMA (styrene maleic acid) and DIBMA (di-isobutylene maleic acid) for membrane protein purification. *Biochim. Biophys. Acta, Biomembr.* **1862**, 183281 (2020).
 76. Adão, R. *et al.* DIBMA nanodiscs keep α -synuclein folded. *Biochim. Biophys. Acta, Biomembr.* **1862**, 183314 (2020).
 77. Esmaili, M. *et al.* Homogeneous nanodiscs of native membranes formed by stilbene–maleic-acid copolymers. *Nanoscale* **12**, 16705–16709 (2020).
 78. Lindhoud, S., Carvalho, V., Pronk, J. W. & Aubin-Tam, M.-E. SMA-SH: modified styrene-maleic acid copolymer for functionalization of lipid nanodiscs. *Biomacromolecules* **17**, 1516–1522 (2016).
 79. Hall, S. C. L. *et al.* An acid-compatible co-polymer for the solubilization of membranes and proteins into lipid bilayer-containing nanoparticles. *Nanoscale* **10**, 10609–10619 (2018).
 80. Ravula, T., Hardin, N. Z., Ramadugu, S. K., Cox, S. J. & Ramamoorthy, A. Formation of pH-resistant monodispersed polymer–lipid nanodiscs. *Angew. Chemie Int. Ed.* **57**, 1342–1345 (2018).

81. Ravula, T., Hardin, N. Z., Ramadugu, S. K. & Ramamoorthy, A. pH tunable and divalent metal ion tolerant polymer lipid nanodiscs. *Langmuir* **33**, 10655–10662 (2017).
82. Fiori, M. C., Jiang, Y., Altenberg, G. A. & Liang, H. Polymer-encased nanodiscs with improved buffer compatibility. *Sci. Rep.* **7**, 7432 (2017).
83. Fiori, M. C. *et al.* Extraction and reconstitution of membrane proteins into lipid nanodiscs encased by zwitterionic styrene-maleic amide copolymers. *Sci. Rep.* **10**, 9940 (2020).
84. Morrison, K. A. *et al.* Membrane protein extraction and purification using styrene-maleic acid (SMA) co-polymer: effect of variations in polymer structure. *Biochem. J.* **473**, 4349–4360 (2016).
85. <https://www.thermofisher.com/order/catalog/product/N360#/N360>.
86. Schmid, F.-X. Biological macromolecules: UV-visible spectrophotometry. *Encycl. Life Sci.* 1–4 (2001).
87. Ejima, D., Yumioka, R., Arakawa, T. & Tsumoto, K. Arginine as an effective additive in gel permeation chromatography. *J. Chromatogr. A* **1094**, 49–55 (2005).
88. Arakawa, T., Tsumoto, K., Nagase, K. & Ejima, D. The effects of arginine on protein binding and elution in hydrophobic interaction and ion-exchange chromatography. *Protein Expr. Purif.* **54**, 110–116 (2007).
89. Pellowe, G. A. *et al.* Capturing membrane protein ribosome nascent chain complexes in a native-like environment for co-translational studies. *Biochemistry* **59**, 2764–2775 (2020).
90. Nitzsche, R. & Simon, F. Bestimmung des Zetapotentials aus Messungen der elektrophetischen Mobilität. *Tech. Mess.* **64**, 106–113 (1997).
91. Debye, P. & Hückel, E. Zur Theorie der Elektrolyte. I. Gefrierpunktserniedrigung und verwandte Erscheinungen. *Phys. Z.* **24**, 185–206 (1923).
92. Gouy, L. G. Sur la constitution de la charge électrique à la surface d'un électrolyte. *J. Phys.* **9**, 457–468 (1910).
93. Gouy, G. Electrocapillarity function. *Ann. Phys.* **7**, 129–184 (1917).
94. Chapman, D. L. A contribution to the theory of electrocapillarity. *Philos. Mag.* **25**, 475–481 (1913).
95. Stern, O. Zur Theorie der elektrischen Doppelschicht. *Zeitschrift für Elektrochemie* **30**, 508–516 (1924).
96. Cosgrove, T. *Colloid science: principles, methods and applications*. (Wiley, 2010).
97. Bijarbooneh, F. H. *et al.* Aqueous colloidal stability evaluated by zeta potential measurement and resultant TiO₂ for superior photovoltaic performance. *J Am Ceram Soc* **96**, 2636–2643 (2013).
98. Ostolska, I. & Wiśniewska, M. Application of the zeta potential measurements to explanation of colloidal Cr₂O₃ stability mechanism in the presence of the ionic polyamino acids. *Colloid Polym Sci* **292**, 2453–2464 (2014).

99. Tanaka, M. *et al.* Effects of charged lipids on the physicochemical and biological properties of lipid-styrene maleic acid copolymer discoidal particles. *Biochim. Biophys. Acta, Biomembr.* **1862**, 183209 (2020).
100. Esmaili, M., Acevedo-Morantes, C., Wille, H. & Overduin, M. The effect of hydrophobic alkyl sidechains on size and solution behaviors of nanodiscs formed by alternating styrene maleamic copolymer. *Biochim. Biophys. Acta, Biomembr.* **1862**, 183360 (2020).
101. Bakalinsky, A. T. & Penner, M. H. Alcohol: properties and determination. in *Encyclopedia of Food Sciences and Nutrition* (Academic Press, 2003).
102. Gimpl, K., Klement, J. & Keller, S. Characterising protein/detergent complexes by triple-detection size-exclusion chromatography. *Biol. Proced. Online* **18**, 1–18 (2016).
103. Dong, M. W. HPLC instrumentation in pharmaceutical analysis: status, advances, and trends. in *Handbook of pharmaceutical analysis by HPLC: Separation science and technology* 47–75 (Academic Press, 2005).
104. Clarke, J. H. R. & Woodward, L. A. Raman spectrophotometric determination of the degrees of dissociation of methanesulphonic acid in aqueous solution at 25°C. *Trans. Faraday Soc.* **62**, 2226–2233 (1966).
105. Covington, A. K. & Thompson, R. Ionization of moderately strong acids in aqueous solution. Part III. Methane-, ethane-, and propanesulfonic acids at 25°C. *J. Solution Chem.* **3**, 603–617 (1974).
106. Jander, G., Jahr, K.-F., Schulze, G. & Simon, J. *Maßanalyse: Theorie und Praxis der Titrationen mit chemischen und physikalischen Indikationen.* (De Gruyter, 2009).
107. Lowe, A. B. & McCormick, C. L. Synthesis and solution properties of zwitterionic polymers. *Chem. Rev.* **102**, 4177–4189 (2002).
108. Woodfield, P. A., Zhu, Y., Pei, Y. & Roth, P. J. Hydrophobically modified sulfobetaine copolymers with tunable aqueous UCST through postpolymerization modification of poly(pentafluorophenyl acrylate). *Macromolecules* **47**, 750–762 (2014).
109. Raetz, C. R. H. & Dowhan, W. Biosynthesis and function of phospholipids in *Escherichia coli*. *J. Biol. Chem.* **265**, 1235–1238 (1990).
110. Danielczak, B., Meister, A. & Keller, S. Influence of Mg²⁺ and Ca²⁺ on nanodisc formation by diisobutylene/maleic acid (DIBMA) copolymer. *Chem. Phys. Lipids* **221**, 30–38 (2019).
111. Hanshaw, R. G., Stahelin, R. V. & Smith, B. D. Noncovalent keystone interactions controlling biomembrane structure. *Chemistry* **14**, 1690–1697 (2008).
112. Molnár, G., Fendrych, M. & Friml, J. Plasma membrane: negative attraction. *Nat. Plants* **2**, 16102 (2016).
113. Almgren, M. Mixed micelles and other structures in the solubilization of bilayer lipid membranes by surfactants. *Biochim. Biophys. Acta, Biomembr.* **1508**, 146–163 (2000).
114. Danielczak, B. & Keller, S. Collisional lipid exchange among DIBMA-encapsulated nanodiscs (DIBMALPs). *Eur. Polym. J.* **109**, 206–213 (2018).

115. Dukhin, A. S. & Goetz, P. J. *Characterization of liquids, nano- and microparticulates, and porous bodies using Ultrasound*. (Elsevier, 2002).
116. Waggett, F., Shafiq, M. D. & Bartlett, P. Failure of Debye-Hückel screening in low-charge colloidal suspensions. *Colloids Interfaces* **2**, 51 (2018).
117. Gambinossi, F., Mylon, S. E. & Ferri, J. K. Aggregation kinetics and colloidal stability of functionalized nanoparticles. *Adv. Colloid Interface Sci.* **222**, 332–349 (2015).
118. Israelachvili, J. N. *Intermolecular and surface forces*. (Academic Press, 2011).
119. Goldberg, R., Chai, L., Perkin, S., Kampf, N. & Klein, J. Breakdown of hydration repulsion between charged surfaces in aqueous Cs⁺ solutions. *Phys. Chem. Chem. Phys.* **10**, 4939–4945 (2008).
120. Comba, S. & Sethi, R. Stabilization of highly concentrated suspensions of iron nanoparticles using shear-thinning gels of xanthan gum. *Water Res.* **43**, 3717–3726 (2009).
121. Syrbe, A., Bauer, W. J. & Klostermeyer, H. Polymer science concepts in dairy systems – an overview of milk protein and food hydrocolloid interaction. *Int. Dairy J.* **8**, 179–193 (1998).
122. Nichols, J. W. Phospholipid transfer between phosphatidylcholine-taurocholate mixed micelles. *Biochemistry* **27**, 3925–3931 (1988).
123. Domínguez Pardo, J. J. *et al.* Membrane solubilization by styrene-maleic acid copolymers: delineating the role of polymer length. *Biophys. J.* **115**, 129–138 (2018).
124. Smyth, M. S. & Martin, J. H. J. X ray crystallography. *Mol Pathol* **53**, 8–14 (2000).
125. Wu, J., Lin, W., Wang, Z. & Chen, S. Investigation of the hydration of nonfouling material poly(sulfobetaine methacrylate) by low-field nuclear magnetic resonance. *Langmuir* **28**, 7436–7441 (2012).
126. Lemieux, M. J. & Overduin, M. Structure and function of proteins in membranes and nanodiscs. *Biochim. Biophys. Acta, Biomembr.* **1863**, 183445 (2021).
127. Hollenstein, K. *et al.* Insights into the structure of class B GPCRs. *Trends Pharmacol. Sci.* **35**, 12–22 (2014).
128. Bortolato, A. *et al.* Structure of class B GPCRs: new horizons for drug discovery. *Br. J. Pharmacol.* **171**, 3132–3145 (2014).
129. Patching, S. G. Surface plasmon resonance spectroscopy for characterisation of membrane protein-ligand interactions and its potential for drug discovery. *Biochim. Biophys. Acta, Biomembr.* **1838**, 43–55 (2014).
130. Luna, V. M. *et al.* Generation of membrane proteins in polymer-based lipoparticles as flow cytometry antigens. *Eur. Polym. J.* **109**, 483–488 (2018).

Abbreviations and Variables

A	Absorbance
ABC	ATP-binding cassette
CD	Circular dichroism
CV	Column volume
<i>d</i>	Hydrodynamic diameter
DDM	<i>n</i> -dodecyl- β -D-maltopyranoside
DIB	Diisobutylene
DIBMA	Diisobutylene/maleic acid
DIBMALP	DIBMA/lipid particle
DLS	Dynamic light scattering
DMPC	1,2-dimyristoyl- <i>sn</i> -glycero-3-phosphocholine
DSC	Differential scanning calorimetry
FRET	Förster resonance energy transfer
GPCR	G-protein coupled receptor
<i>I</i>	Ionic strength
LC	Liquid chromatography
LUV	Large unilamellar vesicles
MA	Maleic acid
MDS	Microfluidic diffusional sizing
M_n	Number-average molar mass
M_w	Mass-average molar mass
MS	Mass spectrometry
MSP	Membrane scaffold protein
NBD-PE	N-(7-nitrobenz-2-oxa-1,3-diazol-4-yl)-1,2-dihexadecanoyl- <i>sn</i> -glycero-3-phosphoethanolamine
nh	Anhydride
NMR	Nuclear magnetic resonance
POPC	1-palmitoyl-2-oleoyl- <i>sn</i> -glycero-3-phosphocholine
POPG	1-palmitoyl-2-oleoyl- <i>sn</i> -glycero-3-phospho-(1' rac-glycerol)
<i>R</i>	Polymer/lipid molar ratio

Rh-PE	N-(lissamine rhodamine B sulphonyl)-1,2-dihexadecanoyl- <i>sn</i> -glycero-3-phosphoethanolamine
S	Styrene
SAT	Saturation
SB	Sulphobetaine
SDS-PAGE	Sodium dodecyl sulphate polyacrylamide gel electrophoresis
SEC	Size exclusion chromatography
SMA	Styrene/maleic acid
SMALP	SMA/lipid particle
SOL	Solubilisation
SPR	Surface plasmon resonance
T	Temperature
TEM	Transmission electron microscopy
T_m	Main gel-to-liquid phase transition temperature
TR	Time-resolved
Tris	Tris(hydroxymethyl)aminomethane
UV	Ultraviolet
V	Elution volume
z	Effective nanodisc charge number
λ_{ex}	Excitation wavelength
$\rho(r)_{circ}$	Charge density at nanodisc belt
ζ	zeta-potential

Acknowledgements

I thank all the people who were involved in realising this thesis. In particular:

- Prof. Dr. Sandro Keller (Technische Universität Kaiserslautern, TUK) for giving me the opportunity to work in his lab, for his outstanding supervision and guidance during the past five years, and for the countless excellent discussions and advice;
- Prof. Dr. Martin van der Laan (Saarland University) for agreeing to act as second supervisor of this thesis, for the co-supervision within the IRTG 1830, and for fruitful discussions and advice throughout the years;
- Prof. Dr. Stefan Kins (TUK) for agreeing to act as chairman for the oral defense of this thesis;
- Prof. Dr. Heiko Heerklotz (University of Freiburg) for giving me the opportunity to perform zeta-potential measurements and field flow fractionation in his lab; Dr. Marie Markones and Dr. Martin Holzer for their dear support and advice on these techniques.
- Prof. Dr. Michael Overduin (University of Alberta) for the co-supervision within the IRTG 1830 and for giving me the opportunity to work in his lab for two months; Catharine Trieber, Jitendra Kumar, Cameron Smithers, and Paige Grant for their help and support with learning new techniques, and for funny times in and outside the lab.
- The collaboration partners PD Dr. Annette Meister (Martin-Luther-Universität Halle-Wittenberg) and Dr. Harald Kelm (TUK) for their continuous support with TEM images and ³¹P NMR measurements, respectively.
- Dr. Gabriele “Gabi” Amoroso for the excellent organisation of the IRTG 1830 and for continuous assistance on administrative issues;
- The IRTG 1830 for funding;
- All current and former members of the IRTG 1830 for fruitful discussions, interesting insights into various research areas, and lots of fun during IRTG colloquia and meetings. In particular, I thank Dr. Sabrina Marz and Anne Könnel for the resulting friendship;
- All current and former members of the “Molecular Biophysics” group—in particular, Simone Adkins, Michael Tope Agbadaola, Melike Aksu, Jasmin Baron, Dr. Jana Bröcker, Dr. Rodrigo Cuevas Arenas, Dr. Bartholomäus „Bartho“ Danielczak, Dr. Manabendra Das, Tim Diederichs, Dr. Sebastian Fiedler, Markus Fleisch, Dr. Erik Frotscher, David Glück, Lisa Hamsch, Moritz Häffner, Ina Heimann, Michaela Herrmann, Dirk Himbert, Jonas Höring, Kevin Janson, Felix Jung, Benjamin Klement, Jessica Klement, Johannes Klingler, Dr. Georg Krainer, Julia Lenz, Florian Mahler, Ogochukwu Patricia Mmeka, Duc Nguyen, Dr. Katharina “Katha” Niederprüm, Dr. Abraham Olusegun Oluwole, Kenechi Onyia, Dr. Eugenio Pérez Patallo, Jan Schatteburg, Ann-Cathrin Schlapp, Johannes Schnur, Moritz Smilde, Dr. Martin Textor, Dr. Carolyn Vargas, Pirkko Wenzel, Andreas

Werle-Rutter, Sophie Weyrauch, and Kai Zwara for the great work atmosphere and funny times in and outside the lab;

- Dr. Bartholomäus Danielczak, Dr. Katharina Niederprüm, Johannes Klingler, Florian Mahler, and Jonas Höring for their dear support throughout the years, the scientific and personal guidance, and excellent comments on the thesis;
- The TU-Nachwuchsring and the German Biophysical Society (DGfB) for funding attendances to conferences;
- My dear friends and family for their tireless and continuous support, especially my parents Edmée and Léon, my long-time life partner Dennis, and my very close friends Cindy and Julie.

Curriculum Vitae

Personal data

Name	Anne Grethen
Place of birth	Luxembourg, Luxembourg
Nationality	Luxembourgish

Employment

03.2016 – 09.2020	Technische Universität Kaiserslautern (TUK), Germany Research associate and PhD student in the group of Molecular Biophysics with Prof. Dr. Sandro Keller
-------------------	--

Education

Since 03.2016	International Research Training Group (IRTG) 1830, TUK, Germany Membership and second trainee spokesperson (2017–2019)
08.2019 – 10.2019	University of Alberta, Edmonton, Canada Research stay in the group of Prof. Dr. Michael Overduin
04.2010 – 12.2015	Technische Universität Kaiserslautern (TUK), Germany Diploma in Biophysics (final grade: 1.4) Diploma thesis in the group of Molecular Biophysics with Prof. Dr. Sandro Keller Title: Solubilization of OmpLA proteoliposomes with styrene/maleic acid copolymer
06.2009	Athénée de Luxembourg, 1ère C (general qualification for university entrance, comparable to the A-Level)

Conferences

04.2019	International SMALP Meeting 2019, Utrecht, The Netherlands <i>Poster presentation</i>
09.2018	Biennial Meeting of the German Biophysical Society, Düsseldorf, Germany <i>Poster presentation</i>
04.2018	International SMALP Meeting 2018: Overcoming Bottlenecks in Membrane Biology, Banff, Canada <i>Poster presentation</i>

- 04.2018 61st Annual Meeting of the Canadian Society for Molecular Biosciences: Membrane Proteins in Health and Disease, Banff, Canada
Poster presentation
- 03.2018 665. WE-Heraeus Seminar: Physical Approaches to Membrane Asymmetry, Physikzentrum Bad Honnef, Germany
Poster presentation: Best poster prize
- 03.2018 Membrane Section Meeting of the German Biophysical Society, Drübeck, Germany
Poster and short oral presentation
- 07.2017 19th International Union of Pure and Applied Biophysics (IUPAB) and 11th European Biophysical Societies' Association (EBSA) congress, Edinburgh, UK
Poster presentation, Travel grant obtained from the German Biophysical Society (DGfB)
- 05.2017 Bunsentagung 2017, Kaiserslautern, Germany
Oral presentation
- 11.2016 14th European Short Course: Principles and Applications of Time-resolved Fluorescence Spectroscopy", Berlin, Germany
No contribution
- 04.2016 Joint Meeting of the Membrane Sections of the French and German Biophysical Societies: Biophysics of Protein–Membrane Interactions: From Model Systems to Cells, Bad Herrenalb, Germany
Poster and short oral presentation

List of Publications

- Grethen A,* Glueck D,* Das M,* Mmeka OP, Pérez Patallo E, Meister M, Rajender R, Strate J, Kins S, Räschle M, Victor J, Etzkorn M, Köck Z, Bernhard F, Babalola JO, Vargas C, Keller S. Electroneutral amphiphilic copolymers forming lipid-bilayer nanodiscs for investigating membrane proteins. *In preparation*, **2021**.
- Ehsan M, Du Y, Mortensen JS, Hariharan P, Qu Q, Ghani L, Das M, Grethen A, Byrne B, Skiniotis G, Keller S, Loland CJ, Guan L, Kobilka BK, Chae PS. Self-assembly behaviors and application of terphenyl-cored trimaltosides for membrane protein study: impact of detergent hydrophobic group geometry on protein stability. *Chem. Eur. J.* **2019**, 25, 11545
- Grethen A; Glueck D; Keller S. Role of Coulombic Repulsion in Collisional Lipid Transfer Among SMA(2:1)-Bounded Nanodiscs. *J. Membr. Biol.* **2018**, 251, 443.
- Danielczak B, Grethen A, Vargas C, Keller S. Nanotechnologie für die Membranprotein-Forschung. *LABO* **2018**, 1-2/2018, 61.
- Grethen A; Oluwole AO; Danielczak B; Vargas C; Keller S. Formation of lipid-bilayer nanodiscs by styrene/maleic acid (2:1) copolymer. *Sci. Rep.* **2017**, 7, 11517.
- Vargas C, Frotscher E, Cuevas Arenas R; Grethen A; Keller S. Fluorierte Tenside und native Nanodiscs für die Membranproteinforschung. *Biospektrum* **2016**, 22, 140.

*shared first authorship

Zusammenfassung

Zur *in vitro* Funktions- und Strukturaufklärung müssen Membranproteine aus Zellmembranen extrahiert und in Membran-mimetischen Systemen stabilisiert werden. Amphiphile Kopolymere erreichten die letzten Jahre beachtliches Interesse, da sie Membranproteine mitsamt ihrer umgebenden Lipide aus komplexen Biomembranen ko-extrahieren und sogenannte Polymer-Nanodiscs bilden. Letztere enthalten somit eine native Lipiddoppelschicht, welche durch einen Polymerrand stabilisiert wird. Aus diesem Grund verleihen diese Membran-Mimetika den eingebetteten Membranproteinen eine erhöhte Stabilität im Vergleich zu herkömmlichen Detergens-Mizellen.

In dieser Arbeit wurde die Bildung von Nanodiscs mithilfe des meist benutzten Styrol-Maleinsäure-Kopolymers SMA(2:1) im Detail untersucht. Zu diesem Zweck wurde dessen Gleichgewichts-Solubilisierungseffizienz gegenüber Modell- und Biomembranen quantifiziert und mit dem hydrophoberen SMA(3:1) sowie dem hydrophileren Diisobuten-Maleinsäure-Kopolymer (DIBMA) verglichen. Es wurde gezeigt, dass SMA(2:1) aus thermodynamischer Sicht der effizienteste Solubilisierer ist in Bezug auf die Lipid- und Proteinextraktion. Lösungsmiteileigenschaften (pH-Wert, Ionenstärke) oder Membraneigenschaften (Seitendruck, Ladung oder Dicke) können die Solubilisierungseffizienz der Polymere allerdings in gewissem Maße beeinflussen. Zusätzlich wurde der Lipidtransfer zwischen SMA(2:1) Nanodiscs untersucht. Trotz ihrer hohen effektiven negativen Ladung tauschen diese Nanodiscs Phospholipide schneller untereinander aus als Vesikel oder Protein-Nanodiscs, was sie als hochdynamische Membran-mimetische Systeme auszeichnet.

Zudem wurden zwei alternative elektroneutrale Polymere vorgestellt. SMA(2:1)-SB und DIBMA-SB wurden durch Polymergrundgerüst-Modifikationen aus SMA(2:1) bzw. DIBMA hergestellt. Es wurde gezeigt, dass die derivatisierten Polymere Modell- und Biomembranen quantitativ solubilisieren und wie DIBMA nur einen geringen Einfluss auf die Integrität der Lipiddoppelschicht haben. DIBMA-SB solubilisiert Membranprotein-Komplexe unterschiedlicher Strukturklassen aus unterschiedlichen Zellmembranen. Hervorzuheben ist, dass die elektroneutralen Polymere für Protein/Lipid-Wechselwirkungsstudien zugänglich sind, im Gegensatz zu den anionischen Polymeren, welche unspezifische Wechselwirkungen eingehen. Zusammenfassend ermöglicht die eingehende Charakterisierung von Polymer-Nanodiscs deren Anpassung an spezifische experimentelle Anforderungen.

Eidesstattliche Erklärung

Hiermit erkläre ich, dass mir die Promotionsordnung des Fachbereichs Biologie der Technischen Universität Kaiserslautern in der derzeit gültigen Fassung bekannt ist. Ich versichere, dass ich die vorliegende Arbeit selbstständig verfasst, keine anderen als die angegebenen Quellen und Hilfsmittel verwendet, sowie die Ergebnisse anderer Mitarbeiter bzw. Autoren klar gekennzeichnet habe. Ich habe diese Dissertation oder Teile daraus keinem anderen Fachbereich als dem der Biologie der Technischen Universität Kaiserslautern vorgelegt und mich zu keinem früheren Zeitpunkt um den Doktorgrad beworben.

Anne Grethen

Kaiserslautern, Februar 2021